Seema Sen

Development of PVD-coated and nanostructured reactive multilayer films

Werkstofftechnik Aktuell

Schriftenreihe aus dem Fakultätsübergreifenden Institut für Werkstofftechnik (IWT) an der TU Ilmenau
Herausgegeben von Univ.-Prof. Dr. rer. nat. Peter Schaaf und Univ.-Prof. Dr.-Ing. Edda Rädlein

Band 19

Die vorliegende Schriftenreihe "Werkstofftechnik Aktuell" berichtet über aktuelle Forschungsergebnisse aus dem Institut für Werkstofftechnik (IWT) der TU Ilmenau. Die ausgewählten Texte spiegeln die breit gefächerten materialwissenschaftlichen und werkstofftechnischen Themen, die am IWT bearbeitet werden, wieder. Für weitere Informationen und Rückfragen können Sie sich gerne an das Institut (www.tu-ilmenau.de/wt) wenden oder das Institut persönlich besuchen. Über Ihre Anregungen, konstruktive Kritik und Ihre Kontaktaufnahme würden wir uns sehr freuen. Das IWT steht wissenschaftlichen Zusammenarbeiten stets aufgeschlossen gegenüber.

Development of PVD-coated and nanostructured reactive multilayer films

Seema Sen

Universitätsverlag Ilmenau
2018

Impressum

Bibliografische Information der Deutschen Nationalbibliothek
Die Deutsche Nationalbibliothek verzeichnet diese Publikation in der Deutschen Nationalbibliografie; detaillierte bibliografische Angaben sind im Internet über http://dnb.d-nb.de abrufbar.

Diese Arbeit hat der Fakultät für Elektrotechnik und Informationstechnik der Technischen Universität Ilmenau als Dissertation vorgelegen.

Tag der Einreichung:	14. November 2017
1. Gutachter:	Univ.-Prof. Dr. rer. nat. habil. Dr h.c. Peter Schaaf (Technische Universität Ilmenau)
2. Gutachter:	Univ.-Prof. Dr.-Ing. habil. Jean Pierre Bergmann (Technische Universität Ilmenau)
3. Gutachter:	Prof. Dr.-Ing. Markus K. Lake (Hochschule Niederrhein, Krefeld)
Tag der Verteidigung:	6. Juli 2018

Technische Universität Ilmenau/Universitätsbibliothek
Universitätsverlag Ilmenau
Postfach 10 05 65
98684 Ilmenau
http://www.tu-ilmenau.de/universitaetsverlag

readbox unipress
in der readbox publishing GmbH
Am Hawerkamp 31
48155 Münster
http://unipress.readbox.net

ISSN 1868-6532 (Druckausgabe)
ISBN 978-3-86360-189-8 (Druckausgabe)
URN urn:nbn:de:gbv:ilm1-2018000331

Cover Image:
Left: SEM image of freestanding ternary Ti/Si/Ti/Al reactive multilayer film. / Middle: Colored TEM image of Zr/Al binary reactive film. / Right: High speed photographic image of steady state reaction propagation in Ti/Si/Ti/Al reactive film (top) and unsteady propagation in Ti/3Al reactive film (bottom).

One never notices what has been done;

One can only see what remains to be done.

- Marie Curie

To my Parents and Avijit…

Danksagung

Ganz herzlich möchte ich mich bei Herrn Univ.-Prof. Dr. rer. nat. habil. Dr. h. c. Peter Schaaf, Leiter des Lehrstuhls für Fachgebiet Werkstoffe der Elektrotechnik der Technische Universität Ilmenau, für die Möglichkeit der Durchführung der Promotion bedanken. Vielen Dank für die wissenschaftliche Unterstützung, das Vertrauen und die Hilfsbereitschaft. Herrn Univ.-Prof. Dr.-Ing. habil. Jean Pierre Bergmann, Leiter des Lehrstuhls für Fachgebiet Fertigungstechnik der Technische Universität Ilmenau danke ich vielmals für die Übernahme des Gutachtens dieser Promotion und für die wertvollen Vorschläge. Ich möchte Herrn Prof. Dr.-Ing. Markus K. Lake, Leiter des Lehr- und Forschungsgebiets Produktionstechnik und Beschichtungsverfahren an der Hochschule Niederrhein für das entgegenbrachte große Vertrauen, die tatkräftige Unterstützung bei der Erstellung dieser Arbeit und intensive Betreuung danken. Ebenso danke ich Herrn Prof. Dr.-Ing. habil. Johannes Wilden für die vielen Diskussionen, die zur Qualität dieser Arbeit beigetragen haben. Mein Dank gilt auch Dr. Rolf Grieseler (Zentrum für Mikro- und Nanotechnologien, TU Ilmenau) und Dr. Andreas Mettenbörger (Lehrstuhl für Anorganische und Materialchemie, Universität zu Köln) für die Durchführung der XRD-Messungen und wertvollen Ergebnisdiskussionen der Phasenanalyse. Ich bedanke mich bei Herrn Prof. Dr.-Ing. Andreas Hoppermann, Dr. Henry Romanus und Frau Diana Rossberg für die Unterstützung im Rahmen der mikroskopischen Untersuchungen. Weiterhin möchte ich allen Kolleginnen, Kollegen und Mitarbeitern danken. Auch Frau Dr. Kathrina Knopf für die Unterstützung bei der Differential Scanning Kalorimetrie gedankt. Ich möchte allen meinen Studierenden danken, die durch ihre Master-, Bachelor- und Projektarbeiten in Teilen zu dieser Arbeit beitragen konnten. Ich möchte besonders Herr M. Babaei für die Probenbeschichtung sowie Frau Gao-Langels, Frau P. Bauzoubardis, Herr Arthur Desch und Herr Nikolai Desch für die Lötbeschichtung und das reaktives Fügen danken. Ich möchte auch Herrn Prof. Dr. Peter Färber und Herrn N. Kroppen für die Unterstützung bei des Stömungssimulation danken. Ferner danke ich den Herrn Peterhanwahr vom Sensotherm GmbH für seine wegweisenden Ratschläge für die Temperaturmessungen. Abschließend möchte ich meinem Mann Avijit Saha sowie meinen Eltern Khagendra

Mohan Sen, Sandha Rani Sen und Geschwister für die moralische Unterstützung danken. Sie haben mir in anstrengenden Zeiten Verständnis entgegengebracht und die erforderliche Kraft gegeben.

Kurzfassung

Als eine neue Klasse von energetischen Materialien speichern die reaktiven Multilagensysteme die chemische Energie. Sie setzen eine große Menge der Energie durch eine schnelle Reaktionspropagation nach einer Aktivierung in der Form von Wärme frei. Im Zusammenhang mit dem zunehmenden Potenzial in den hochmodernen Fügetechnologien und den anderen Industrieanwendungen finden solche Typen von reaktiven Mehrschichtensystemen große Aufmerksamkeit. Das hohe Interesse konzentriert sich auf die Anwendung der sehr schnellen und lokalisierten Energie Freisetzung. Die Kenntnisse über die Materialkombinationen und Morphologie spielt eine wichtige Rolle, um reaktive Mehrschichtensysteme mit entsprechenden Reaktionseigenschaften und Wärmemenge herzustellen. Im Mittelpunkt dieser Arbeit stehen daher die Entwicklung der Schichtweise abgeschiedenen reaktiven Multilagenschichten und die Charakterisierung der Reaktionseigenschaften. Die eingestellten Bereiche können wie folgt zusammengefasst werden:

- Die reaktiven Multilagenschichten von binären Ti-Al, Zr-Al und ternären Ti-Al-Si Kombinationen wurden mittels Magnetronsputtern-Deposition produziert, die zu der niedrigen - Medium oder hohen Energieklasse gehören.
- Die selbstverbreitenden Reaktionseigenschaften wurden in Bezug auf Wärme, Temperatur, Reaktionsgeschwindigkeit und Propagationsweisen charakterisiert.
- Herstellung der großflächigen freistehenden reaktiven Folien wurde aufgezeigt.

Für die Bestimmung der Reaktionswärme wurde die Standardbildungsenthalpie zu Beginn der Arbeit durch thermodynamische Simulationen mit Thermo-Calc 3.1 berechnet. Die Menge der Reaktionswärme hängt von der chemischen Zusammensetzung des Ti-Al-, Zr-Al- und Ti-Si Systems ab. Dann wurden Ti/Al, Zr/Al und Ti/Si/Ti/nAl Multilagenschichten für unterschiedliche Periodendicken, Molverhältnisse und Multischichtaufbau abgeschieden.

Die Ti/nAl (n = 1-3) reaktiven Multilagenschichten wurden mit verschiedenen Al-Molverhältnissen hergestellt. Die Reaktionsgeschwindigkeit änderte sich zwischen (0.68±0.4) m/s und (2.57±0.6) m/s. Die Reaktionstemperatur änderte sich im Bereich 1215-1298 °C. Die 1Ti/3Al Schicht zeigt auch eine instationäre Reaktionspropagation mit der Kräuselungsbandbildung. Außerdem wurden der Temperaturfluss und die chemische Vermischung in nanoskalige Schichten von 1Ti/1Al Zusammensetzung (für 20 nm Periodendicke) erstmals mittels Strömung Simulation berechnet. Die Ergebnisse zeigten, dass der Temperaturfluss viel schneller als das chemische Mischen während der fortschreitenden Reaktion ist.

Die 1Zr/1Al Schichten wurden mit der verschiedenen Periodendicken von 20 nm bis 55 nm untersucht. Die Reaktionsgeschwindigkeit und Reaktionstemperatur änderten sich im Bereich 0.23-1.22 m/s und 1581-1707 °C. Hier wurde auch die Oxidationsreaktion während der fortschreitenden Reaktion aufgezeigt.

Zum ersten Mal wurden ternäre Multilagenschichten von Ti, Si und Al-Reaktanten für verschiedene Schichtenanordnung (Si/Ti/Al/Si und Ti/Si/Ti/nAl, n = 1- 3) abgeschieden. Hier, Reaktionseigenschaften hängten von Schichtenanordnung und Al-Molverhältnissen ab. Für den Ti/Si/Ti/Al Schicht konnte eine maximale Reaktionspropagation von (9.2±2) m/s und eine Reaktionstemperatur von (1807±30) °C bestimmt werden. Danach wurden die vorgenannten ternären Folien erstmals in einem reaktiven Fügeprozess eingesetzt.

Für die Herstellung großflächiger freistehenden RMS, würde der Einfluss der Substratwerkstoffe in Hinblick auf der Ablöseverhalten nach der Beschichtung untersucht. Die Verwendung des Kupfersubstrats zeigt eine einfache und schnelle Weise, freistehende Folie zu produzieren. Diese Methode ermöglicht die Produktion von freistehenden 1Zr/1Al und 1Ti/1Si/1Ti/Al Folien mit der großen Fläche von 11 cm × 2 cm × 45 µm und 8 cm × 4 cm × 52 µm. Außerdem zeigt diese Arbeit einen verbesserten Herstellungsprozess mit der Skalierbarkeit und homogenen Mikrostrukturen von Multilagenschichten.

Die Untersuchungen in dieser Arbeit zeigen, dass die Zusammensetzung und Morphologie die Reaktionseigenschaften unmittelbar beeinflussen und bieten potenzielle Möglichkeiten als eine kontrollierbare Wärmequelle auf der Basis Ti/Al-, Zr/Al- und Ti/Si/Al RMS zur Verfügung stellen. Andererseits schließt

die Reaktion die Effekte der Oxidation und instationären Reaktionspropagation ein, die dabei hilfreich wären, die Reaktionskinetik zu verstehen. Die Ergebnisse in dieser Arbeit können als ein Beitrag zu einem Modell um ideale RMS in Bezug auf Reaktionseigenschaften zu entwickeln.

Abstract

As a new class of energetic materials, reactive multilayer systems store chemical energy. They release a large amount of energy in the form of heat by fast reaction propagation after activation. In connection with increasing potentiality in advanced joining technology and other industrial applications, such type of reactive multilayer systems pay attention. The high interests focus on the utilization of very fast and localized heat. The knowledge about material combination, morphology plays an important role to design reactive multilayer systems with an appropriate reaction propagation and heat release. Therefore, this research attributes the development of layer-by-layer-deposited planar reactive multilayer film and characterizing corresponding self-propagating reaction properties. The focused areas are summarized as follows:

- Reactive multilayer films of binary Ti-Al, Zr-Al and ternary Ti-Al-Si combinations were produced by Magnetron Sputter Ion Platting process, which belong to different energy classed reactive systems.
- The self-propagating exothermic reaction properties were characterized in terms of heat flow, temperature, reaction propagation velocity and propagation modes.
- The fabrication concept of freestanding foils with large surface was demonstrated.

In connection with the reaction heat, standard heat of formation was initially calculated by using Thermo-Calc 3.1 simulation. The amount of heat released has been influenced by the chemical compositions. Then Ti/Al, Zr/Al und Ti/Si/Ti/nAl reactive films were deposited for different bilayers, molar ratios and multilayer design.

The Ti/nAl (n = 1-3) reactive films with different Al-molar ratios were investigated. The reaction speed varies between (0.68±0.4) m/s and (2.57±0.6) m/s. The maximum reaction temperature varies in the range of 1215-1298 °C. The 1Ti/3Al film exhibits unsteady propagation with ripple band formation. Moreover, temperature flow and atomic mixing were characterized by using computational fluid dynamics simulation in 1Ti/1Al reactive foil for 20 nm bilayer thickness for the first time. The results show

that the temperature flow is much faster than the chemical mixing during an exothermic reaction.

Zr/Al reactive films with different bilayer thicknesses of 20-55 nm were deposited. Here, reaction speed and maximum temperature were found in the range of 0.23-1.22 m/s and 1581-1707 °C, respectively. Oxidation characteristic during a self-propagating reaction was also shown.

For the first time the ternary reactive films were investigated for two different multilayer design and Al- molar ratios (Si/Ti/Al/Si und Ti/Si/Ti/nAl, n = 1-3). Reaction properties depend on chemical compositions. For Ti/Si/Ti/Al reactive film, a maximum reaction propagation of (9.2±2) m/s and temperature (1807±30) °C was estimated. Then reactive joining was attempt first time by using this ternary film.

For the production of large-area freestanding RMS, the influence of the substrates with regard to the peel behavior was investigated. In that case, selection of a proper and cost effective substrate and developing synthesis methods are of great interest for large size films. The use of copper substrate shows a simple and efficient way to produce freestanding films. This work assures the production of 1Zr/1Al und 1Ti/1Si/1Ti/Al freestanding films with the size of ~ 11 cm × 2 cm × 45 µm und ~ 8 cm × 4 cm × 52 µm. Furthermore, this work shows an improved fabrication process of reactive films with scalability and uniform microstructure throughout the cross-section. Then reactive joining of steels was performed by using developed ternary reactive films.

The experimental results in this work predict composition and morphology dependent reaction properties and offer the potential use of Ti/Al-, Zr/Al- and Ti/Si/Ti/Al reactive films as controllable heat source due to their wide range of reaction properties. On the other hand, the reaction propagation includes the effects of oxidation and unsteady reaction, which will help to understand the reaction kinetics. The achieved results can be used as a contribution to model an ideal reactive multilayer film in terms of reaction properties.

Contents

1 Introduction

Reactive multilayer systems (RMS) in the form of layered structures or powder mixtures can store chemical energy and release a large amount of heat after self-propagating reaction. They mainly include the reactant systems of metal-nonmetal, metal-metal or metal-oxide or multicomponent [1-2]. Among them, nanoscale layer-by-layer deposited reactive multilayer film (RMF) pays a great deal of attention as an external heat source in joining applications [3], igniters [4] and airbag initiators [5]. RMFs are consisting of alternating multilayers of minimum two different types of reactants, which are capable of self-propagating reaction with an exothermic heat. Generally, two different reactant layers form a bilayer, whose thickness varies in the range of 10 to 300 nm and the total thickness is in the micrometer scale [6-7]. With an external electrical, thermal or mechanical ignition, RMFs react with a propagation velocity between 0.05 and 80 m/s and release a large amount of heat in the range of 25 to 105 kJ/mol [6-8]. Recently reported multilayer films are mostly two-component system, e.g. Nb/Si, Ni/Ti, Co/Al multilayer foils [9-11]. In this work, both binary and ternary reactive multilayer films of Ti, Al, Zr and Si reactants were developed. The graphical abstract of this scientific research considering the fundamental principle of self-propagating reaction in multilayer film has been presented in Fig. 1.1.

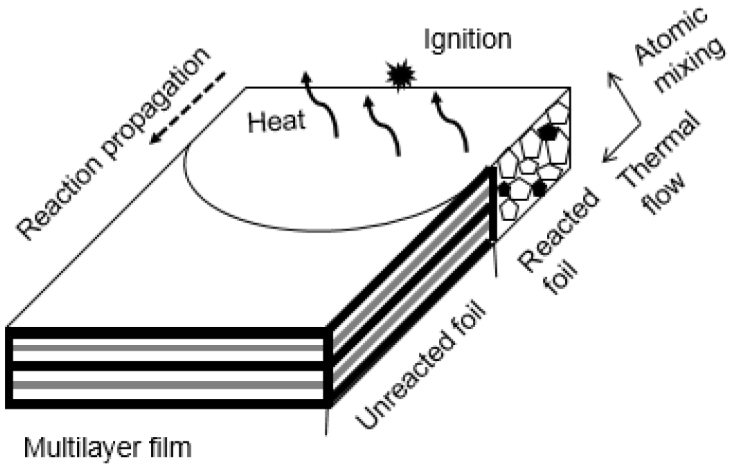

Figure 1.1: Fundamental principle of the self-propagating reaction in a reactive film.

In RMFs, once the self-propagating reaction begins, the faster atomic mixing takes place and increases the local temperature, which results in quick heat release. During this exothermic reaction, reaction speed indicates how fast the atomic mixing occurs to form reaction products. Here, reaction products are mainly intermetallic compounds or solid solutions. The type and amount of reaction products regulate the reaction heat and the maximum temperature. Therefore, the reaction velocity, heat release and reaction temperature are considered as self-propagating reaction properties in this work. In addition, the new concept of distinct atomic mixing interfaces in ternary RMFs will be introduced by changing multilayer arrangement besides controlling diffusion distance or molar ratios in the existing technologies. Detailed investigations of three types of RMFs and corresponding reaction properties will be beneficial in many application fields and future scientific studies.

Chapter 1 includes the introduction.

Chapter 2 focuses on the goals of this research.

Chapter 3 deals with the fundamentals of self-propagating reaction and the reactive film. Here, the most important technology for fabrication, ignition methods and potential applications will be discussed.

Chapter 4 includes the experimental method and equipment for reactive film deposition, characterization, heat flow, reaction temperature and velocity measurement.

Chapter 5 will focus on the thermodynamic simulation for calculating standard heat of formation (reaction heat) for three film systems and computational fluid dynamics (CFD) simulation for 1Ti/1Al reactive film.

Chapter 6 will focus on the binary Ti/Al reactive films highlighting the important features of microstructural morphology, reaction properties, propagation modes and their effect on reaction properties. Moreover, steady and unsteady propagation will be explained.

Chapter 7 will describe the bilayer thickness dependent reaction properties in binary Zr/Al reactive films. It will also highlight the oxidation effect on temperature profiles. Moreover, possible defects formation and changes of microstructural features after reaction have been also included.

Chapter 8 will introduce the ternary RMF of Ti-Si-Al systems for two multilayer arrangements and different Al-molar ratios of Si/Ti/Al/Si and Ti/Si/Ti/nAl (n = 1-3). Here, reaction properties will be characterized in all ternary films. This chapter will include distinguish features of controlling reaction heat, velocity and temperature by changing multilayer arrangements in spite of same reactants type.

Chapter 9 will include the comparison of reaction properties of developed films in terms of reaction heat, temperature and velocity. It will also highlight the characteristics of an ideal reactive film for joining application.

Chapter 10 will introduce on the most important factors of multilayer synthesis with a large surface area. It will also include our first attempt to use developed ternary film in the reactive joining.

Chapter 11 will conclude the summary of the developed reactive films and describe the further works for advanced technological needs.

2 Motivation and goals

The fields of energetic materials demand the development of new reactive films with extending reactant combinations and understanding their self-propagating reaction properties. Recently developed reactive films are mostly two-component systems [1, 6-11]. On the other hand, ternary multilayer combinations were hardly reported. Therefore, it is promising to improve the existing technologies by developing freestanding reactive films with large surface area and spreading the reaction characteristics. The overall idea was to develop new reactive films with a wide range of reaction properties to expand their potential uses. Therefore, this research focuses on the development of magnetron sputtered deposited reactive films having binary Ti-Al, Zr-Al and ternary Ti-Si-Ti-Al reactant combinations. Ti/Al and Zr/Al RMFs were deposited for different Al-molar ratios and bilayer thicknesses, respectively. For ternary RMFs, two types of layer designs of Ti/Si/Ti/Al/ and Si/Ti/Al/Si and different Al-molar ratios of 1Ti/1Si/1Ti/nAl (n = 1-3) were highlighted. The concept of such multilayer designs of pure reactants in ternary film was not reported before to our knowledge. Besides experiments, thermodynamic and numerical simulations were performed in this study. Here, standard reaction heat of phase formation was calculated by Thermo-Calc 3.1 simulation. Moreover, CFD simulation was used to characterize the temperature flow and reactant mixing during a self-propagating reaction in 1Ti/1Al RMF for a first time. This research contributes to develop new reactive foils with appropriate reaction properties. Moreover, this work can answer the following issues:

- How will reaction properties be influenced by reactant combinations, bilayer thickness, molar ratio, microstructural features in reactive multilayer films?
- How do different layer arrangements in ternary reactive films effect on reaction properties?
- How can a steady and unsteady reaction propagation be distinguished?
- How do reaction mode and oxidation state influence on reaction propagation?

- What characteristics should an ideal reactive multilayer film possess for joining?
- By what methods can be a freestanding uniform reactive film with large surface area scaled up?

3 State of the art

3.1 Self-propagating exothermic reaction

Self-propagating reaction is an important feature of reactive multilayer systems, as it releases a large amount of heat. The concept of self-propagating exothermic reaction was generated at first by Goldschmidt et al. 1898 [12] from a mixture of aluminum and iron oxide powders. After nearly 100 years, the self-propagating reaction was intensively discovered to form intermetallic compounds from the different types of powders mixtures composed of solid compacts of transition metals and B or C [13]. Then self-propagating reactions were observed in layered films of Rh/Si multilayers in the work of Floro et al. 1986 [14]. This reaction depends on the ability of the reactive systems to react in an exothermic way to form a combustion wave. The schematic representation of the propagation of a reaction wave in reactive multilayer film has been shown in Fig. 3.1 after [6]. After an ignition A and B multilayers react and a reaction front propagates to the unreacted zone. The reaction becomes self-sustaining if heat evolves in the reaction zone faster than it dissipates into the unreacted regions of the film [6-7, 13]. Within the reaction zone the reactant atoms of A and B diffuse perpendicular to the layers and the heat that is generated by their mixing diffuses parallel to the layers.

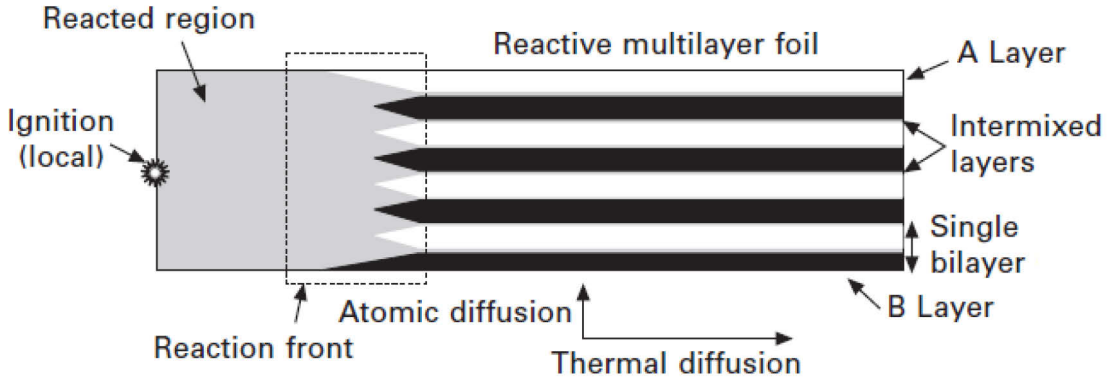

Figure 3.1: A schematic illustration of the reaction propagation from left to right in A/B multilayer film after Ref. [6]. Here, one A layer and one B layer form the bilayer and between reactants layer there presence an intermixed layer.

A large amount of quantified heat will be released due to formation of A_xB_y compound after local atomic intermixing of A and B reactants, which can be

transmitted to the adjacent components to fulfill the joining process and to supply heat for other industrial applications. A typical structure of the combustion reaction wave during a self-propagating reaction can be realized as presented in Fig. 3.2 according to the work of Merzhanov et al. [15]. The temperature profile shows a non-isothermic characteristic. Here temperature drops behind the maximum temperature maximum. This is because of the cooling of combustion products. This indicates the zone of higher temperature gradient. A warm-up (or pre-flame or preheating) zone is present before the reaction front. This zone is preparing for the chemical reaction, where there presence active heat transfers from the reaction zone. In this reaction zone, there presence an intense heat releases and weak heat exchange. The reaction velocities in the heat exchange zone and the heat release define the velocity and mode of the front propagation according to the modern theory of combustion wave propagation [16]. Generally, the size of the reaction zone is smaller than the preheating zone. However, the heat release depends on the reactive material systems and the final products.

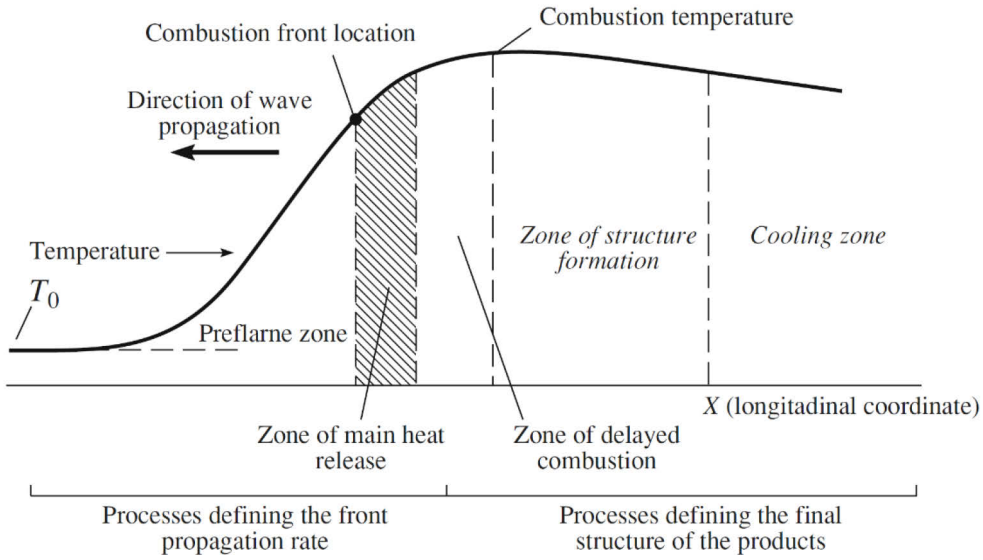

Figure 3.2: A typical structure of a combustion reaction wave in a reactive material system taken from Ref. [15].

3.2 Reactive material systems

Reactive material systems exhibit exothermic reaction heat and high adiabatic reaction temperature. Initially, the reactive systems included the powder mixtures. Generally, reactive systems include aluminides, silicide, carbides,

borides and thermites. However, for CuO_x/Al thermites, the reaction heat is about (151±35) kJ/mol with an adiabatic reaction temperature of 2846 K [17]. The drawbacks of the powder mixtures include the reduction of green density, particles agglomeration and the porosity in the reaction products. Reactive multilayer films can overcome those problems. Recently developed reactive systems include the layered multilayers of mostly binary components [6-11, 18]. A clear presentation of reaction heat and maximum adiabatic reaction temperature of different binary reactive systems can be summarized in Fig. 2. Based on the reaction heat, reactive systems can be classified into three energy classes of low (< 45 kJ/mol), medium (>45 kJ/mol, < 70 kJ/mol) and high (>70 kJ/mol) [19]. Among them one reactive film of Ni/Al was established commercially with a trade name NanoFoil® from Indium Corporation [20].The low energy classed reactive systems generally possess less reaction heat. Therefore, they are easy to handle and synthesize.

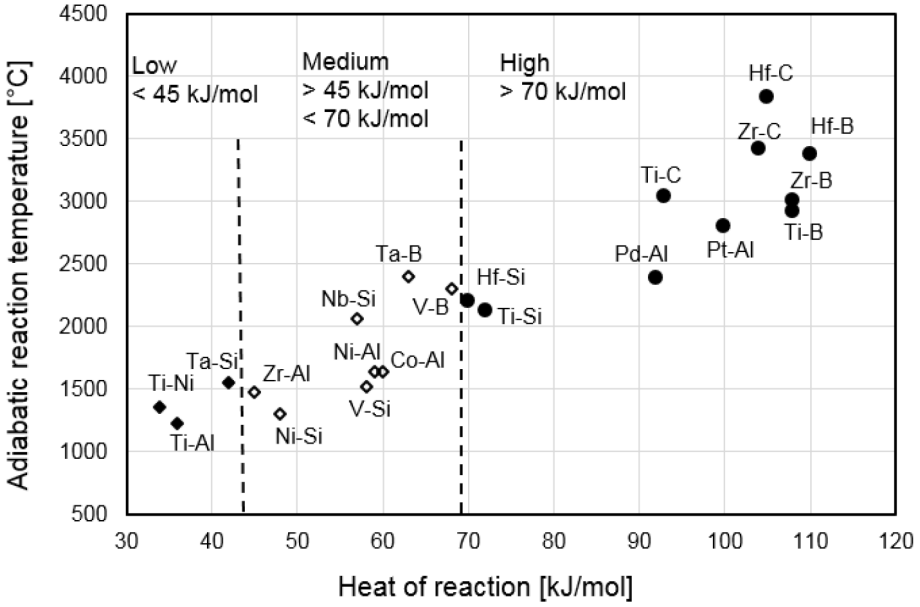

Figure 3.3: Heat of reaction vs. adiabatic reaction temperature for different binary reactive systems with energy classes (Data source: Refs. [21- 23]).

Nevertheless, low energy classed systems require higher activation energy input for activation. Sometimes they also require additional preheating to start the reaction. They can be applied to reactive joining, industrial and other applications where reduced amount of reaction heat is required. In contrast, high-energy class reactive systems are very active and require a less activation energy. The synthesis of such type of reactive systems can provide difficulties

of uncountable reactions. Generally, boride, silicide, carbide, some aluminides and thermites are belonging to this group. Compared to low and high, medium reactive systems are easy to handle and process. In this work, Ti/Al, Zr/Al and Ti/Si/Ti/Al RMFs from low and mainly medium energy classes were investigated having the motivation to expand their uses in joining, medical or other applications.

3.2.1 Nanoscale effects and diffusion phenomenon

In a multilayer film, nanoscale effects show promising thermo-physical effects such as reduction of melting temperature and high diffusion rates. As a consequent, it provides self-propagating exothermic reaction even at room temperature. It is based on the negative enthalpy between different reactants in multilayers to start a reaction after activation. The layered multilayer films exhibit size-dependent melting temperature. In that case, the melting temperature depressed, as observed for example in Pb/Ge multilayers [24]. This is because of the high interfacial energy per unit volume. The work of Rose et al. reported that the cohesive energy has a linear relation to the melting temperature and both the cohesive energy and the melting temperature describe the bond strength of materials [25]. By considering the cohesive energy of a nanomaterial as a function of surface and total atoms as mentioned [26], the melting temperature can be stated as follows:

$$\mathrm{T}_{mp} = \mathrm{T}_{mb}\left(1 - \frac{\mathrm{N}}{2n}\right) \qquad (1)$$

Here, T_{mp} and T_{mb} are the melting temperature of the nanomaterial and the bulk material. N and n indicate the surface atom and total atoms. N/n depends on the size and the shape of the nanomaterial. In case of nanofilm, the N/n was estimated to $4a/3h$ [26], where a and h indicate the atom diameter and thickness. Therefore, the melting temperature of a nanoscale film can be written as follows;

$$\mathrm{T}_{mp} = \mathrm{T}_{mb}\left(1 - \frac{2a}{3h}\right) \qquad (2)$$

On the other hand, diffusion phenomena in multilayer films are quite different from bulk materials due to very short length scales. The nanoscale elemental

layers form reaction products of mainly intermetallic after fast inter-diffusion. This happens due to high ratio of interfacial area to volume. However, the diffusion phenomena can be affected by coherency stress of distinct elemental layer as mentioned in Ref. [27-28].

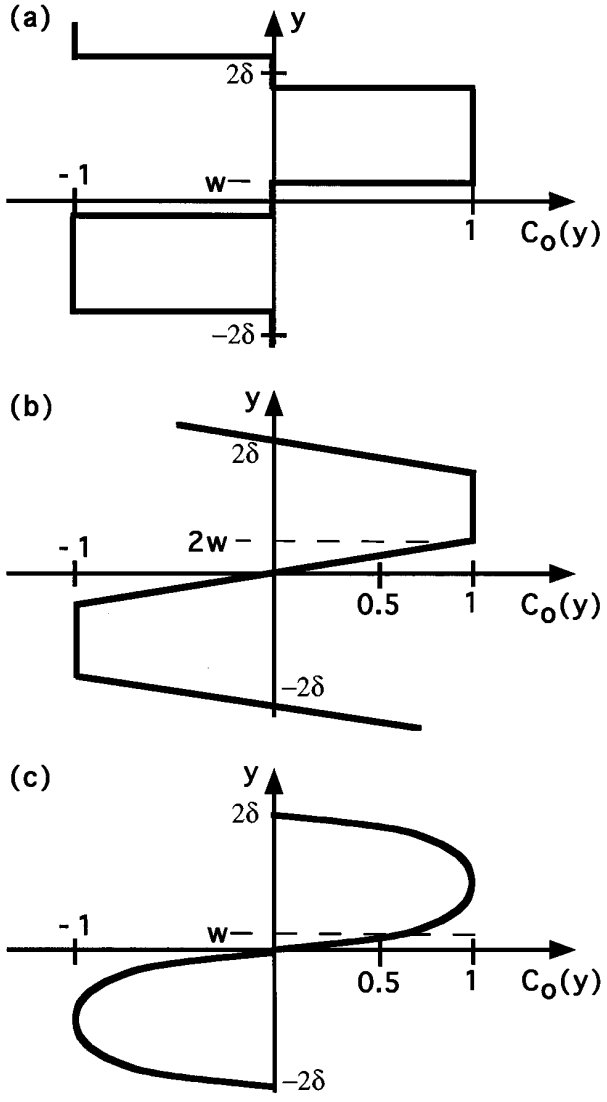

Figure 3.4: Composition profiles after premixing occurs during deposition process. Here, w indicates the premixing and δ indicates ¼ of bilayer thickness. Step premixing in which the composition profile only consists of pure reactants or the fully intermixed product (a); Linear premixing where the composition profile varies linearly between two reactant layers (b); Exponential premixing in which the quantity of each reactants increases or decreases (c) taken from Ref. [29].

Metastable phase can exist even without a self-propagating reaction in multilayer films. This phase forms due to premixing of elemental layers

during deposition or even long-term storage. This intermixed phase can be amorphous, solid solution and intermetallic compounds, which are thermodynamically favorable to exhibit. It is important to study the growth of intermixed products. As this intermixed product effects on atomic and thermal diffusion in multilayers.

The work of Mann et al. [29] indicate the presence of step, linear and exponential mixing of reactant mixing, as shown in Fig. 3.4 (a-c). In case of fully intermixed product formation, a profile can be similar to the step mixing and for a solid solution intermixed product, linear and exponential profiles can be estimated [29]. However, this premixed product can act as diffusion barrier, to reduce atomic diffusion and consequent reaction propagation.

3.2.2 Exothermic reaction properties and kinetics

The exothermic reaction properties of RMFs are mainly expressed in terms of reaction heat flow, reaction temperature and reaction velocity. On the other hand, reaction kinetics indicate how fast or slow a reaction propagates through a foil, what are the influencing factors to regulate the reaction properties for a given morphology and reactant combinations.

3.2.2.1 Reaction front velocity

Generally, reaction velocity shows how rapidly the distinct reactants diffuse together to form the reaction products. Here, the atomic mixing and temperature flow controls the reaction rate. The overall reaction propagation in reactive film with atomic mixing and heat flow was described at section 3.1. Here, the multilayer foil can be treated as a two-dimensional structure as the foil width is larger than the thickness and smaller than the length. Most of the analytical models of reaction propagation in the planar multilayers assume one dimensional atomic and thermal diffusion occurring normal and parallel to the multilayers [29-33]. According to this analytical model of reaction propagation as mentioned earlier by Mann et al. [29], the basic atomic diffusion equation is:

$$\frac{dC}{dt} - \vec{\nabla} \cdot (D\vec{\nabla}C) = 0 \qquad (3)$$

Where, C is the composition, t is the time and D is the coefficient of atomic diffusion (m^2/s). After expansion of dC/dt in terms of the partial derivatives of C with respect to t, x, y, and z, the atomic diffusion can be written as follows.

$$\frac{\partial C}{\partial t} + v_x \frac{\partial C}{\partial x} - \frac{\partial}{\partial y} D \frac{\partial C}{\partial y} - D \frac{\partial^2 C}{\partial y^2} = 0 \qquad (4)$$

Here, the reaction front mainly propagates in the x direction and thus the propagation terms in the y and z direction are set to zero. On the other hand, compositional change by the atomic mixing is considered in the y direction.

Therefore, the compositional term in z direction can be ignored. Here, the atomic diffusion coefficient can be derived from Arrhenius relation. The general equation for thermal transport as mentioned [29] is stated as:

$$C_p \rho \frac{dT}{dt} - C_p \rho \lambda \nabla^2 T = \frac{dQ}{dt} \qquad (5)$$

Here, dQ/dt indicates the heat generation rate. Cp and ρ are the average heat capacity and density of the material. λ indicates the thermal diffusion coefficient in m^2/s, T is the temperature and Q is the total heat in a unit volume of the multilayer system. After coupling Arrhenius atomic diffusion and thermal transport equation by expanding partial derivatives of dQ/dt and dT/dt, the combined equation can be written as follows:

$$C_p \rho \left(v_x \frac{dT}{dt} - \lambda \nabla^2 T \right) = v_x \frac{\partial \Delta(C)}{dx} \qquad (6)$$

Here, C is the composition and T is the temperature. Heat release (ΔC) is related to the rate at which composition C changes. The work of Armstrong and Koszykowski mentioned the equation 7 of the reaction velocity in multilayers [32].

$$v_x^2 = \frac{3A \exp(-E_a / RT_{max}) R \lambda^2 T_{max}^2}{\delta^2 E_a (T_{max} - T_0)} \qquad (7)$$

Where, E_a is the activation energy for atomic diffusion, R is the gas constant, δ is 1/4 of the bilayer thickness and A is an Arrhenius pre-factor. T_{max} and T_0

indicate the maximum and initial temperature during a steady-state propagation. Equation 7 shows the reaction velocity of the ideal multilayer without heat loss. In real conditions, the formation of premixed layer lowers the reaction heat. The work of Mann et al. 1997 [29] generalized reaction front velocity models developed by Armstrong and Koszykowski [32], which showed the linear and parabolic relation of the heat release and compositional changes as stated in equations 8 and 9. Here, K_n and α_n are Fourier eigenvalues and coefficients, respectively. The premixed region is incorporated with the term of K_n through the compositional variation in the premixed layer between two elemental layers.

$$v_x^2 = \left(\sum_{n=odd} K_n / \alpha_n^3 \right)^{-1} \frac{3\mathrm{A}\exp(-E_a/RT_{\max}) R\lambda^2 T_{\max}^2}{\delta^2 E_a (T_{\max} - T_0)} \tag{8}$$

$$v_x^2 = \left(\sum_{n=odd} K_n^2 / \alpha_n^2 \right)^{-1} \frac{3\mathrm{A}\exp(-E_a/RT_{\max}) R\lambda^2 T_{\max}^2}{\delta^2 E_a (T_{\max} - T_0)} \tag{9}$$

The work of Barbee and Weihs et al. 1996 developed an empirical model after considering the effect of premixed layer on reaction velocity [33]. In this case, a selectable propagating reaction front velocity of v can be expressed by equation 10.

$$v = \frac{K}{d^n}\left(1 - \frac{2w}{d}\right) \tag{10}$$

Here, w and d indicate the thickness of premixed zone and bilayer, respectively. K, n are the fitting parameters, where K indicates the energy release rate constant associated with mixing rate and thermal conductivity and describes the multilayer structure dependent heat release , which also dependent on other parameters such as density and heat capacity. According to Ref. [33], n is about 0.8 to 1.2 and K is in the range of about 100 to 20,000 mA°/sec, or 500 to 15,000 mA°/sec or 1,000 to 10,000 m A°/sec.

The reaction front velocities of recently reported reactive films are plotted in Fig. 3.5 after Refs. [34-42]. Here, reaction velocities less than 16 m/s correspond to the primary axis, whereas, high reaction velocities of Pt/Al, Ti/2B, Sc/Au and Y/Au films with blue dotted lines indicate the secondary axis. Initially, velocity increases with bilayers then decreases. All types of reactive films having bilayer thickness within 50 nm show maximum reaction

velocity due to optimum diffusion distance. Here, the overall reaction velocities of all reactive films vary within 0.1-100 m/s as a function bilayer thickness.

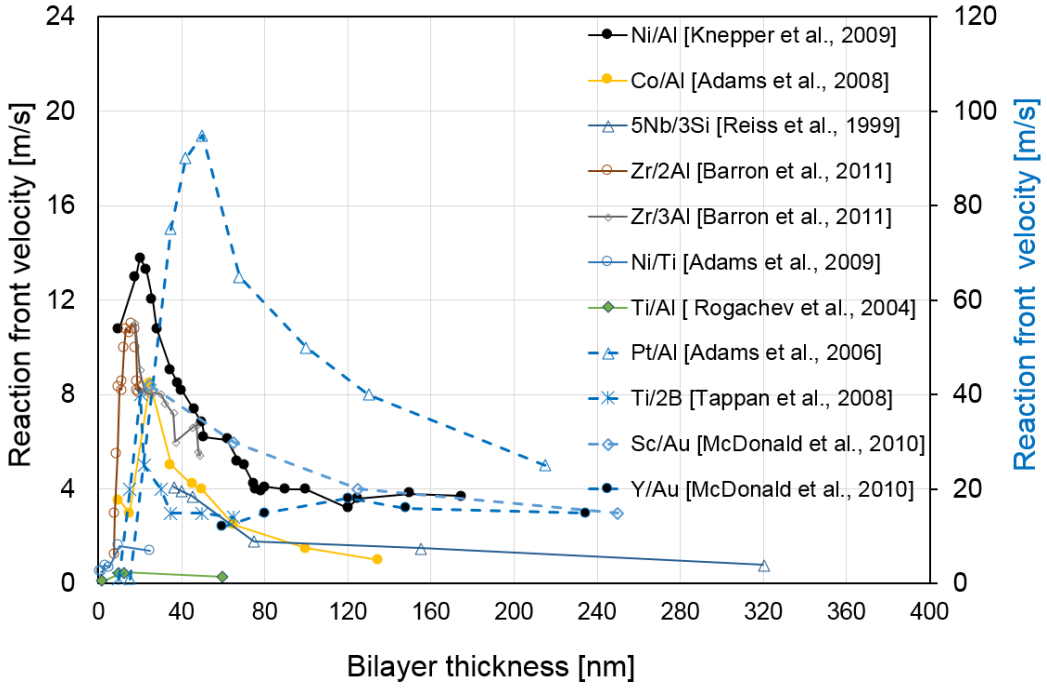

Figure 3.5: Reaction front velocity versus bilayer thickness plots for various multilayer foils. The multilayer films with medium and low reaction velocities less than 16 m/s correspond to the primary axis. Whereas, the velocity profiles of Pt/Al, Ti/2B, Sc/Au and Y/Au reactive films with blue dotted lines correspond the secondary axis. All measurements were conducted at room temperature and only for Ti/Al multilayer, it was 473 K. (Data source: Refs. [34-42]).

3.2.2.2 Reaction heat

Self-propagating reaction involves inherently the internal atomic mixing of reactants. The reaction heat depends on the types of reaction products form. A high amount of reaction products is expected for the increasing bilayer thickness and the total film thickness. In practice, the formation of premixed layer is unavoidable during deposition process, which also influences the heat release. However, the reaction heat can be quantified by using equation 11, which was derived elsewhere for step mixing of the pre-mixed zone in bilayers [15, 29, 43-45]. Here, ΔH_{form} and ΔH_{rxn} are the reaction heat without and with premixed layer, whereas w and d indicate the size of the premixed layer and bilayer thickness. For the formation of similar volume fraction of premixed

layer, reaction heat can be reduced pronouncedly for smaller bilayer thickness. However, the premixing layer thickness can vary through the films, as initially deposited reactant layers may exhibit higher premixing rate than the final layer as demonstrated [6].

$$\Delta H_{rxn} = \Delta H_{form}\left(1 - \frac{2w}{d}\right) \qquad (11)$$

The profile of premixed layer growth is an important factor to control the reaction heat. This premixing composition profile for a given multilayer film depends on the method to grow as mentioned in section 3.3.1 (Fig. 3.4). By considering the step composition profile of premixing zone, the dependency of reaction heat on bilayer in Al/Ni and Al/Monel reactive films has been shown in Fig. 3.6 after Ref. [29].

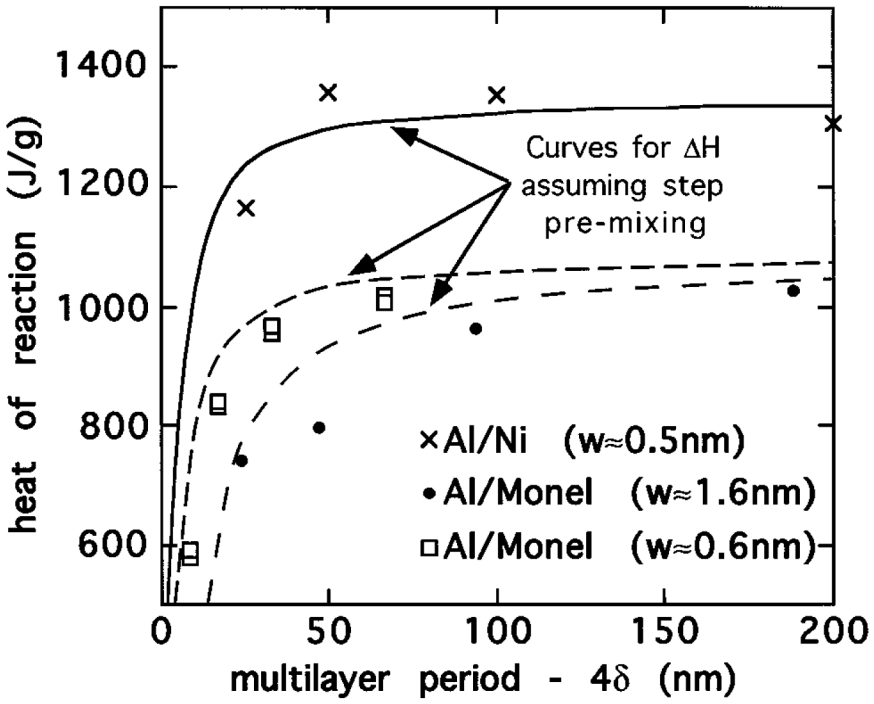

Figure 3.6: Heat of reaction versus bilayer thickness plots for Al/Ni and Al/Monel multilayer foils considering the step premixing after Ref. [29].

The type of premixed product is another important factor that can also quantify the reaction heat. The work of Gavens et al. 2000 [45] shows the reaction heat in Ni/Al reactive film for the similar intermetallic formation of Al_3Ni_2 in the premixed layer, which can be estimated by equation 12. In the case of formation of different reaction product (e.g. Al_9Ni_2) in the premixed layer, reaction heat can be quantified by equation 13 considering the atomic molar

ratio *V* of the reaction and premixed products. However, recent studies mostly used the simplification by assuming identical reaction products formation as that formed in premixed layer [43-45].

$$\Delta H_{rxn} = \Delta H_{Al_3Ni_2}\left(1 - \frac{2w}{d}\right) \quad (12)$$

$$\Delta H_{rxn} = \Delta H_{Al_3Ni_2} - \Delta H_{Al_9Ni_2}\left(\frac{2w}{d}\frac{V_{Al_3Ni_2}}{V_{Al_9Ni_2}}\right) \quad (13)$$

On the other hand, ternary multilayer film has dual bilayer thickness. The work of Knepper et al. 2009 [34] also quantified the total reaction heat for a dual bilayer film. By considering the equal volumes of reaction material for dual bilayer spacing of d_1 and d_2, the total heat can be expressed by equation 14.

$$\Delta H_{rxn} = \frac{1}{2}\Delta H_{form}\left[\left(1 - \frac{2w}{d_1}\right) + \left(1 - \frac{2w}{d_2}\right)\right] \quad (14)$$

The total reaction heat in a dual-bilayer foil follows a composite behavior and considers the average density of the interfaces. For simplicity, identical premixing thickness of *w* was considered for both bilayers. However, premixing layer thickness may vary depending on the reactants combinations.

3.2.2.3 Reaction temperature

During self-propagating reaction, reactants mixing will generate heat, which will increase the temperature. The reaction heat for the ideal composition profile can be expressed by equation 15 after Ref. [29]. Here, ΔH_o and T_{fo} indicate the reaction heat and maximum adiabatic temperature for the ideal composition profile without premixing. At adiabatic conditions, no heat loss occurs during self-propagating reaction.

$$\Delta H_0 = \rho C_p\left(T_{fo} - T_0\right) \quad (15)$$

The rate of heat generation has linear or parabolic relation to the rate at which the foil's composition has changed [29]. However, maximum adiabatic temperature (T_{fo}) is only achievable in case of no premixing layer and heat losses. In real condition, as-deposited premixing layer, reactants melting influence to loss the heat during a self-propagating reaction. The temperature

profiles presented in Fig 3.7 show an ideal reaction situation and the non-ideal situation with melting effects as mentioned in Ref. [29].

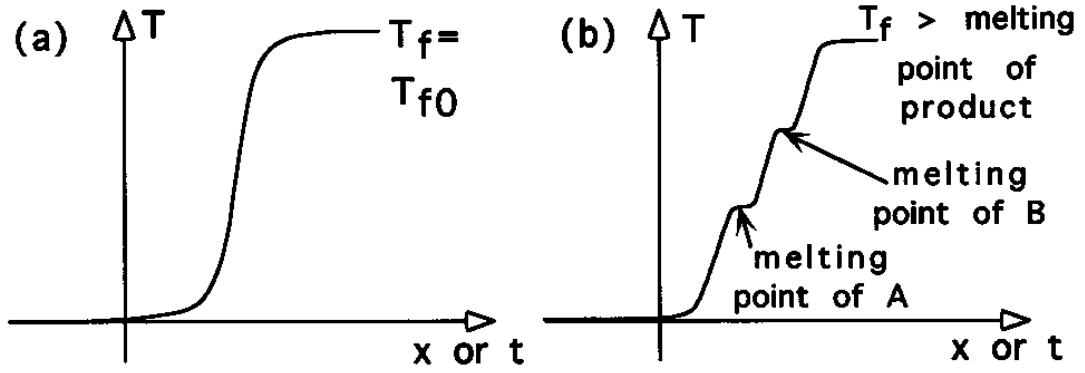

Figure 3.7: Temperature profile of a reaction front propagation having an ideal situation (a) and melting effect of the constituents (b) after Ref. [29]. Here, A, B are the reactants.

The reactant or constituent melting influences the maximum reaction temperature. If the melting point of final product is higher than the reaction constituent, it will have minor effect [29]. If melting temperatures are close together, it will influence on atomic mixing to have final products. On the other hand, reaction products can be solid or liquid, which also controls the reaction heat and consequent reaction temperature.

The reaction kinetics with an unsteady propagation can also effect on reaction temperature. The work of Reeves and Adams et al. [46] reported the large temperature variation near an instable reaction front in Co/Al reactive film, for an unsteady propagation. However, this mode introduced heat loss, reduced the reaction heat and final reaction temperature. On the other hand, secondary oxidation during a self-propagating reaction influence the reaction temperature. Recent studies show the high reaction temperature in Zr/Al multilayers with an oxidation effect compared to that of without oxidation [47]. However, the reaction kinetics influence the reaction propagation, heat flow and consequent average reaction temperature.

3.2.3 Manufacturing process

The common techniques to fabricate reactive films are the vapor deposition methods of sputtering and evaporation. Other fabrication techniques include the rolling and electrochemical deposition. Besides these methods, Atomic Layer Deposition method has recently developed. The overall manufacturing methods are described below.

3.2.3.1 Physical Vapor Deposition (PVD)

Sputter deposition is one of the most widely used PVD based techniques for reactive multilayers fabrication. Here, targets are the depositing material that one wishes to deposit. Different source and sample geometries can be utilized for sputter deposition including planar and non-planar multilayers fabrication. The recent work also reported the sputter-up or side-sputter deposition depending on the target and sample arrangements [36, 49]. In a co-deposition method, different targets are focused on the substrate simultaneously to deposit films. On the other hand, substrates are subjected to rotate over the sources and by full rotation, it produces two or more chemically distinct multilayers. Since last twenty years, the multilayers of Co/Al, Nb/Si, Nb/Al were manufactured by using magnetron sputter method [11, 36, 49]. An alternative approach to deposit multilayers is the evaporative (electron beam) method. The work of M. Kokonou et al. 2009 demonstrated the fabrication of Al/Ni reactive films by using electron gun evaporation method [50]. However, PVD method generates the chemically distinct layers and controllable layer thickness.

3.2.3.2 Cold rolling

Cold rolling is another fabrication method for multilayer films. Several investigations were performed previously to test whether this method can be extended to fabricate mostly metal/aluminum multilayers. The initial study of Battezzati et al. 1999 fabricated cold rolled Ni/Al multilayers with overall composition of Al50Ni50 [51]. The work of Sieber et al. 2001 developed the Ni/Al multilayer foils by using a fold and roll method [52]. The work of Qui et al. 2007 investigated also the exothermic reactions in the cold rolled Ni/Al

and Ti/Al multilayer foils and demonstrated the lower exothermic heat and slower reaction speed compared to that of vapor deposited films [53].

3.2.3.3 Electrodeposition

Electrodeposition process was first used in 1921 to fabricate Cu/Ni multilayers by using alternate deposition from two different electrolytes [54]. Two distinct methods of electrodeposition bath were reported, which are single-bath and dual-bath techniques. The single bath deposition uses a single electrolyte. Here, multilayers can be controlled by either potential or current. In the dual-bath techniques, the substrate is transferred between two different electrolytes and the layer is deposited alternately from each to build up the multilayer. The work of Celis et al. 1992 demonstrated the electrodeposited Cu/Ni multilayers fabricated by using the dual bath technique with sublayer thicknesses of 100, 25 and 5 nm [55]. However, electrodeposited multilayers rarely have precision microstructures. In spite of certain advantages over vapor deposition processes such as high deposition rate and low processing temperatures, the exothermic reaction characteristic of electrodeposited multilayers was not studied broadly [54-55]. Microstructural analysis of sputtered, rolled and electrodeposited multilayer films method has shown in Fig. 3.8. The sputtered Nb/Al multilayer film (d = 333 nm) [49] presented in Fig. 3.8 (a), shows uniform and controllable layer thickness. Fig. 3.8 (b) shows the cross section of a rolled Al/Ni multilayer film after Ref. [56]. The self-propagating reaction of cold rolled multilayer is not uniform, it reports a low amount of heat, and propagation velocity compared to PVD coated multilayer films [53]. This is because of larger bilayer thickness in micrometer scale, which shows higher diffusion distance.

In addition, it is difficult to fabricate uniform alternating layers by rolling process, although this method shows benefit as a cost effective fabrication method. Moreover, the work of Knepper et al. 2009 indicated the structural consistency of the sputtered Al/Ni multilayers compared to mechanically processed multilayers [56]. Fig. 3.8 (c) shows the electrodeposited Au/Co multilayer film after Ref. [57]. The work of Guan et al. 2007 demonstrated the fabrication of Au/Co multilayers (Au 200 nm / Co 800 nm) by using different pulse and current density [57]. However, the exothermic reaction in electrodeposited film was not widely reported.

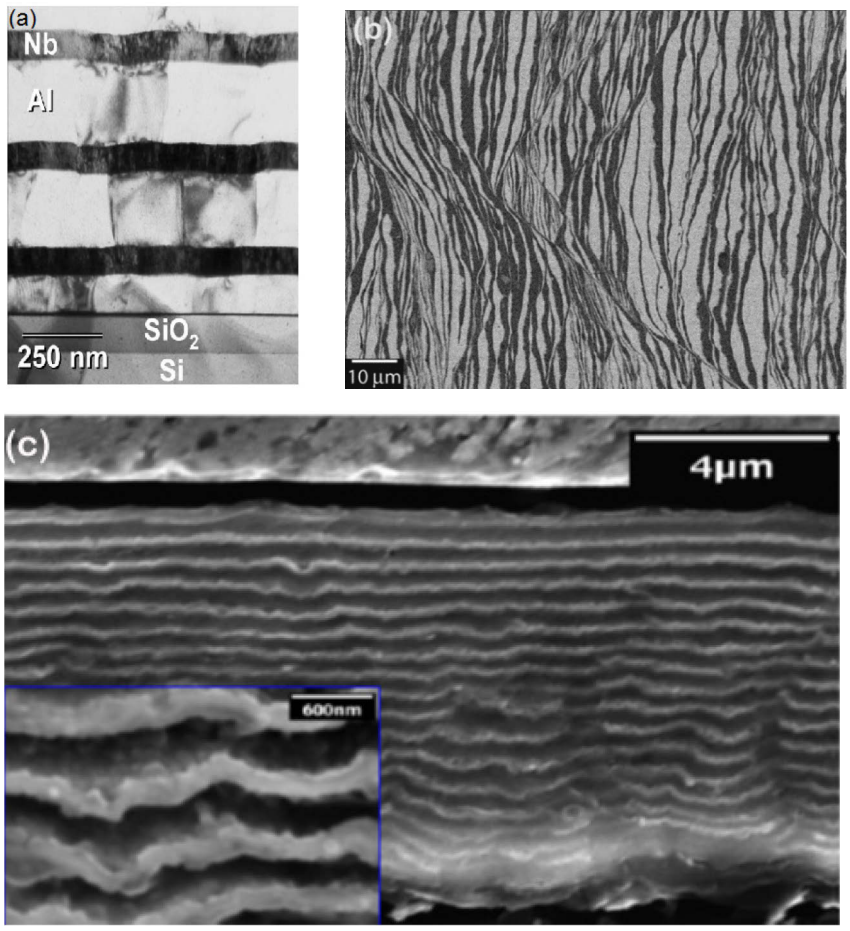

Figure 3.8: TEM image of the magnetron sputtered Nb/Al multilayer film (a) after Ref. [49]. SEM cross-section of cold rolled Al/Ni multilayer (b) after [56]. SEM image of an electrodeposited Au/Co multilayer (c) after Ref. [57].

3.2.3.4 Atomic Layer Deposition (ALD)

Recently, ALD process was demonstrated to fabricate reactive film [7]. This is mainly chemical precursor-based method, which deposits a given layer by self-terminating gas-solid reaction. Recent study of this method reported to deposit a single oxide layer onto Al nanoparticles [58-59] or to deposit alumina interfacial barrier layers within sputter-deposited CuO/Al thermite multilayers as diffusion barrier layer [60].

Concerning the reactive film fabrication, controlling the deposition parameter is an important factor to deposit distinct and uniform reactants layer. Here, PVD method offers an excellent multilayer and reactant spacing control compared to other methods, although rolling and electrodeposition methods

show lower production cost and high throughput. In this work, the magnetron sputtering method was used for depositing binary and ternary reactive films.

3.2.4 Ignition methods for multilayers

Reactive multilayer foils can be ignited at a discrete point or the whole foil. Generally, the energy requirements for ignition vary with activation methods. Common activation techniques include electrical spark, mechanical loading and laser irradiation as a point heating. Thermal heating is considered as global and point heating. The different ignition methods are as follows:

3.2.4.1 Laser ignition

Laser ignition is considered as a point heating without contact to activate reactive film. The work of Clevenger et al. 1990 first used the laser ignition to activate Ni/Si multilayer [61]. The recent studies of this ignition method demonstrate the threshold fluence, which depends on the multilayer design and microstructural features (e. g. bilayer, premixed zone) and laser beam parameter [61-63]. Picard et al. 2008 reported the laser threshold for Ni/Ti (low), Co/Al (medium) and Pt/Al (high) energy classed multilayers and found that higher enthalpy material pairs required smaller laser ignition fluence [62]. On the other hand, multilayer design and properties also influence on threshold fluences. Recent study indicated that Al capping layer (top layer) on Pt/Al multilayers required larger laser fluence to start a reaction than those having Pt capping layer due to the higher reflectance of Al [63]. It also demonstrated that smaller bilayer and the presence of a premixed zone in Pt/Al multilayer required higher laser fluences [62-63]. For activation of commercial nanofoil, the uses of YAG Laser, CO_2 Laser and IPG Laser were demonstrated [64].

3.2.4.2 Thermal heating

Thermal heating can be used as a point heating or global heating. A concentrated energy source of flame or filament corresponds the point heating. The work of Rogachev et al. 2004 used the tungsten filament for the initiation of exothermic reaction in Ti/Al multilayers [39]. By placing the multilayer on the hot plate, the exothermic reaction will be initiated, which

act as a global heating. By increasing hot plate temperature, the reaction will be examined [39, 65]. According to the work of Fritz et al. 2013 [65], reaction will not even start when they are heated to temperatures just 1 K below of the threshold ignition temperature (T_{ig}), which is stated in equation 16.

$$T_{ig} \propto \frac{{}^{E_A}/_{R}}{ln\left[\frac{2g\,\Delta H_{rxn} D_0 R T}{d\omega}\left(\frac{f}{m(1-m)}\right)\right]} \qquad (16)$$

The expression of ignition temperature considered the ignition volume, microstructure and physical material properties of the film [65]. This equation includes the variables of bilayer thickness (d), premixed zone (w), the atomic fraction of one of the reactants (m), the fractional concentration over which the product phase exists (f), the gas constant (R), and a geometrical term (g), activation energy (E_A), Arrhenius diffusion coefficient (D_0) and reaction heat (H_{rxn}). The absolute ignition temperature T_{ig} shows a logarithmic dependence on the bilayer thickness of each multilayer films.

3.2.4.3 Mechanical loading

Mechanical loading is another point ignition method that can be applied with a high strain rate. The work of Wickersham and Poole first reported the mechanical ignition in Zr/Si multilayer with a sharp tipped stylus [66]. Recent works demonstrated the uses of drop tubes [65-66], swinging lever arm device [65] and frictional testers [66] for mechanical ignition. The drop tube testing was performed using an impacter from greater height to the samples placed on the flat surface for Al based multilayers [65-67]. Here, the impact energy and height influence the ignition and the impact energy increases with bilayer. The work of Mason et al. 2013 used Asay shear impact experiment using a flat steel plunger to ignite the Ni/Al multilayer [68].

3.2.4.4 Electrical ignition

Electrical ignition includes the electrostatic discharge or direct current heating. The work of Ma et al.1990 first used an electrical spark to ignite Ni/Al multilayer film [69]. The electrical ignition was widely used to ignite Ni/Al, NiV/Al, Monel/Al, Nb/Si, Ti/Al and Ni/Ti multilayer foils [10, 36, 65-67]. This method included the threshold current densities required to ignite

foils. Recent studies show that this threshold current depends on the initial multilayer structures and their properties.

The work of Fritz et al. 2013 showed that the minimum current densities for activation vary with the contact area and film morphology, where reactive films with thicker bilayer and as-deposited premixed layer require higher current densities to start a reaction [65]. The electrical pulse ignition testing apparatus and mechanical loading of drop-tube and swinging-arm technique have been shown in Fig. 3.9 after Ref. [65]. However, the use of ignition methods depends on the accessibility and usability. In this work, we used an electrical activation method, which is less sensitive, simple and easy to handle for initiating the exothermic reaction in multilayer films.

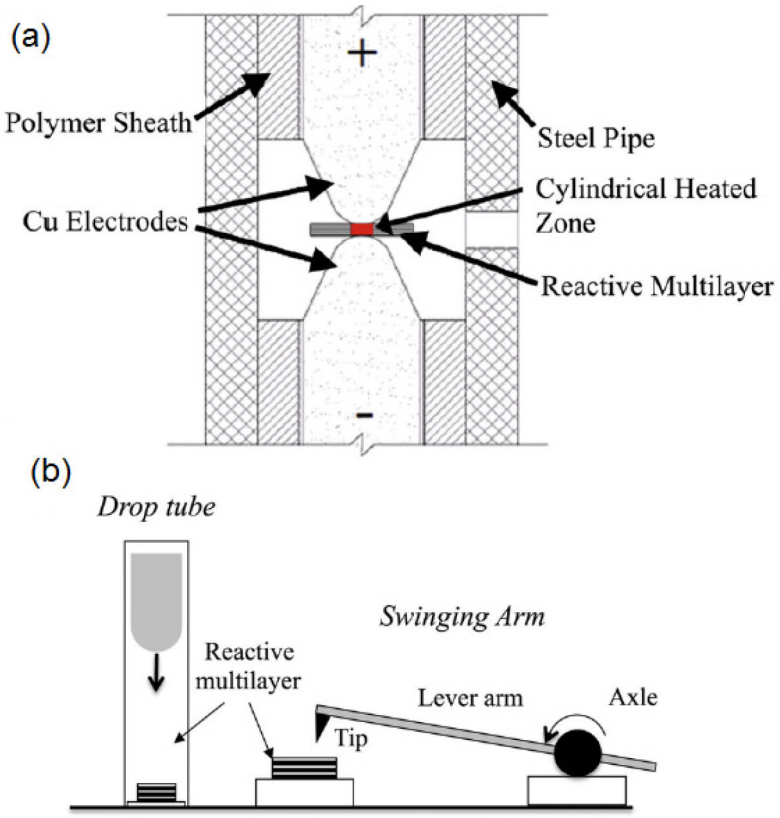

Figure 3.9: The electrical pulse ignition testing apparatus consisting of two copper electrodes (a) and a schematic representation of drop-tube and swinging-arm technique used for mechanical ignition testing (b) after Ref. [65].

3.2.5 Potential fields of application

3.2.5.1 Joining applications

The reactive joining (or nano-bonding) by using reactive films open up a lot of opportunities in the advanced joining technology in terms of quick and fast heat input. The conventional joining methods require a large amount of thermal flow or the use of high temperature furnaces, which result in introducing stress and structural distortion of the components. Therefore, the joining of heat sensitive materials or materials with different thermal expansion coefficients takes up the challenge. The reactive joining using quick and localized heat of reactive multilayer foils can solve this problem.

This reactive joining facility can be easily performed by stacking joint components with reactive films and melting layer arranged under pressure. After ignition, the reaction heat of reactive film melts the solders or brazes locally for short period by keeping the joint components cold at room temperature. This reactive joining is possible at any environments without disposal of detrimental gases or reaction products [70]. It is common to use multiple and simultaneous impulse of the reactive foils for large area bonding. For example, the target bonding by using commercial nanofoil is demonstrated in Fig. 3.10 after Ref. [70].

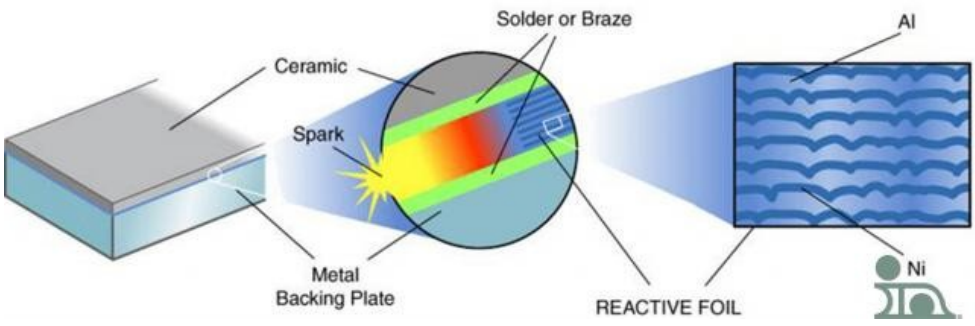

Figure 3.10: Ceramic sputter target bonding with backing plate using Ni/Al NanoFoil® as localized heat after Ref. [70].

The reactive joining by using localized heat of Ni/Al nanofoil was demonstrated to bond micro-electromechanical systems, sensitive polymers or organic substances, metals and ceramics in the recent studies [3, 8, 20, 70, 72-73]. In addition, diffusion bonding can also be performed by utilizing the diffusivity and reactivity of nanoscale reactive films. Recent studies

demonstrated the diffusion joining of TiAl intermetallic compounds by using Ti/Al and Ni/Al reactive films [73-75].

For dental applications, the joining of ceramic and metal pays attention due to brittle oxide layers, which cannot be readily controlled. The use of reactive joining can result in the sound metal-ceramic bonds with higher quality and longer life as mentioned [76 -77]. Moreover, this reactive joining shows benefits for small and large areas bonding at room temperature in the fields of lightweight construction, microsystem technology, precision engineering, automobile and aerospace applications.

3.2.5.2 Other fields of application

Reactive multilayer films are very promising as igniters to stimulate the neighboring energetic materials such as in the inflation of airbags [78-79], missiles and rockets [80]. Traditionally, the high energetic reactive systems are suitable for such as applications. Recently as igniters Ni/Al, CuO/Al reactive multilayers were reported [79, 81]. The uses of reactive films were also reported in defeating bio-agents [82], supplying heat source in thermal batteries [83].

The self-propagating reaction can be used for synthesis of intermetallic compounds, where conventional methods show sometimes difficulties. On the other hand, intermetallic compounds are very promising for high temperature applications due to higher corrosion and oxidation resistant. In this case, by choosing the molar ratios and bilayer size, the specific intermetallic compounds are to be synthesized after self-propagating reaction. Recent studies reported the synthesis of beta-NiAl, gamma-TiAl, beta-RuAl intermetallic compounds from Ni/Al, Ti/Al and Ru/Al multilayers, respectively [84-85].

4 Materials and experimental methods

This chapter describes the fabrication method to deposit nanoscale reactive films and the concept to make film freestanding. The analytical techniques to characterize the films and the experimental set up to evaluate reaction heat, temperature and velocity are summarized. The computational simulation has been included.

4.1 Selection of reactant combinations for RMFs

In this work, binary Ti-Al, Zr-Al and ternary Ti-Al-Si combinations were highlighted, which are belonging to different energy classed reactive material systems. Ti/Al and Zr/Al reactive films were investigated for different Al-molar ratios and bilayer thicknesses. On the other hand, multilayer design and Al-molar ratios were controlled to design ternary Ti-Si-Al combination. The overall focus concentrates on the development of reactive films with a wide range of reaction properties in order to expand their applicability. These reactive films offer lots of scope as localized heat source. The structure and morphology dependent quantified reaction heat and reaction properties of RMFs show the great advantage to design such films. In regard to quantified and fast heat supply, the joining areas of automobile and aviation, electronics and energy sectors will be beneficial. These developed RMFs also offer potential applications in medical and other industrial fields.

4.2 Magnetron Sputter Ion Plating (MSIP) method

The reactive foils were deposited by using MSIP by arranging the 4 targets by an alternating manner in DC powered PVD machine (CC 800/8 HI). Here, 99.99 % pure Ti, Zr, Al and Si targets were used to deposit films. The MSIP deposition facility has been shown in Fig. 4.1. Throughout the deposition, four targets were simultaneously sputtered on the rotating substrate. Here, 100 µm thick copper foil was used as a substrate and alternating multilayers were deposited on it with a side sputter configuration. In all multilayer films, Al layer was deposited as last top layer.

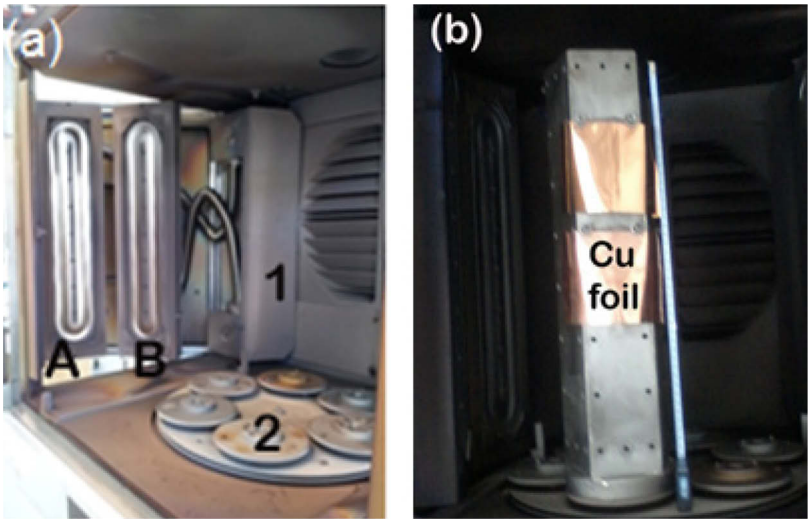

Figure 4.1: Magnetron Sputter Ion Platting (PVD, CC 800/8 HI) equipment for multilayer deposition (a). Here, A, B indicate the alternating target arrangement, 1 and 2 indicate the vacuum chamber and the rotating table for substrate. Substrate holder with Cu foil (b).

Initially, targets were pre-sputtered prior to the deposition in order to reduce the chance of oxygen and other impurities in the multilayer film, which may have previously oxidized or poisoned. The substrate was etched by using argon ion etching after evacuation. Here, highly pure (99.9999 %) ionized argon with a flow rate of 50 mln (milliliter normal per minute) was introduced to ensure oxide free and active substrate surface for multilayer deposition. During deposition, the base pressure was set to 9 mPa. Moreover, the ultra-high pure argon was used with a flow rate of 185-230 mln as process gas. A shield plate was introduced in order to avoid the mixing of atomic fluxes. Initially, multilayers were deposited on the cooled substrate. A thermometer was inserted in the MSIP facility for temperature measurement. Here, the maximum chilled temperature of 100±20 °C was noticed during the deposition.

Generally, the overall deposition rate of a PVD film can be controlled by adjusting the power, gas flow, deposition time and distance. But to adjust the reactant layer thickness of multilayer, variable target powers or rotation speeds can be used as demonstrated in Refs. [6-7, 11]. In this work, different target powers were used by keeping a constant substrate rotation, target-substrate distance and gas flow rate. The overall deposition conditions for different RMFs are also listed in table 4.1. Here, RMFs were fabricated by

using different target powers at a constant substrate rotation of 1.2 rpm and substrate-target distance of 12 cm.

Table 4.1: Deposition conditions for different RMFs synthesis in MSIP method. Here, mln stands for milliliter normal per minute. All films were deposited on Cu substrate.

Reactant combinations	Deposition pressure [Pa]	Ar flow rate [mln]	Target power [kW]	Variables
1Ti/1Al	0.47	185	1/0.5	Al-molar ratio
1Ti/2Al			1/1	
1Ti/3Al			1/1.5	
1Zr/1Al	0.53	230	0.650 – 3.300	Bilayer
1Si/1Ti/1Al/1Ti	0.5-0.48	185	1.2/1/0.6/1	Multilayer arrangement
1Ti/1Si/1Ti/1Al			1/1.2/1/0.6	
1Ti/1Si/1Ti/2Al			1/1.2/1/1.1	Al-molar ratio
1Ti/1Si/1Ti/3Al			1/1.2/1/1.6	

The composition of reactive film can be determined by relative thickness and atomic density of reactants, (e. g. RMF contains equal reactant layer thickness for 50/50 composition with equal density) as mentioned in Refs. [10, 29]. The ratio of reactant layer thicknesses was chosen to achieve an equiatomic stoichiometry and different molar ratios. Different molar ratios and bilayer thicknesses were deposited for Ti/Al and Zr/Al reactive films, correspondingly. Whereas, ternary films were constructed with two different multilayer designs and Al-molar ratios of Si/Ti/Al/Si and Ti/Si/Ti/nAl (n = 1-3). The details of large size film synthesis will be discussed in section 10.1.

4.3 Synthesis of freestanding RMFs

The sputtered deposition of RMFs always requires the use of substrates. On the other hand, the joining and other industrial applications demand the freestanding reactive films. Therefore, the selection of substrate plays an important role in regard to peel behavior. Initially, two substrates were considered with the purpose of making films freestanding. The first substrate was the Cu electroplated stainless steel. Here, Cu layer with the thickness of

approx. 20-50 µm was electrodeposited on steel. The second substrate was 100 µm thick Cu foil. For Ti/Al RMFs, Ti was chosen as first layer. Therefore, it is important to analyze the microstructural feature of this first layer, which influences on overall multilayer growth. Fig. 4.2 shows SEM micrographs of MSIP coated Ti layer on two different types of substrates. It shows that the Ti layer on Cu foil has the fine microstructure than that of the substrate of Cu-coated steel. The high thermal conductivity of Cu foil helps to build fine microstructure, which has shown in Fig. 4.2 (b). Therefore, Cu foil was used as substrate for further RMFs deposition.

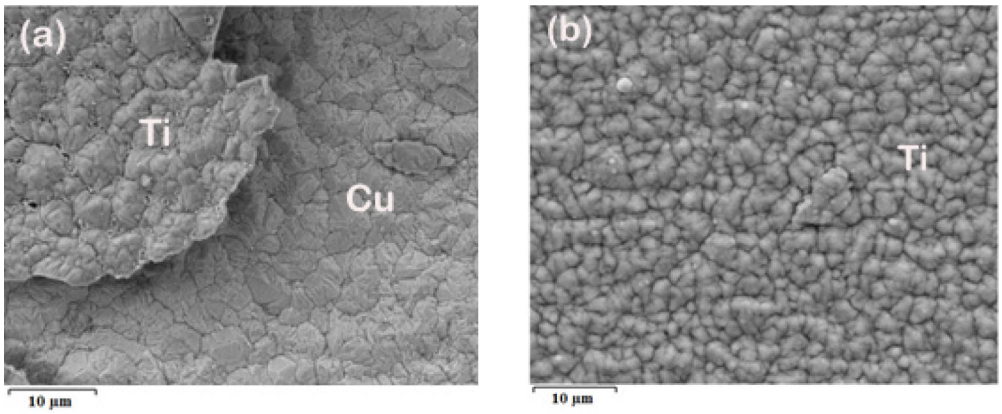

Figure 4.2: SEM micrographs of sputter deposited Ti layer on substrate-1 (Cu electrodeposited stainless steel) (a) and substrate-2 (100 µm thick Cu foil) (b).

After deposition, RMFs were cut and then immersed in the etching solution to make freestanding. The selective copper etching method has shown in Fig. 4.3 (a). This etching was done at room temperature in a solution of nitric acid and purified water, containing three different types of solution concentration. These three compositions are only 65 % Con. HNO_3, 1:1 and 1:2 mixture of acid 65 % Con. HNO_3 and purified water. During the etching process, the reaction products of copper nitrate turn the color of the green solution. Precautions should be taken to perform this process in the laboratory ventilation hoods in order to filter the fume of NO_2. Then freestanding films were carefully rinsed with water and left to dry. The thin film was detached from the substrate quickly and completely after 5 to 30 min depends on the concentration of the etching solution. For concentrated solution, dissolution rate is very high, but foils have the tendency to break and bend in order to compensate the internal stress. For 1:1 mixture, we achieved the satisfactory conditions. Normally, for lower film thickness the effect of internal stress is more. Therefore, the multilayer foils can break and become flakes. For higher

foil thickness more than 5-6 μm, foils have less possibility to bend, which is also shown in Fig. 4.3 (b). In addition, during the handling, freestanding films require special care due to brittleness. In regard to freestanding films, the use of Cu foil indicates several advantages, which are as follows:

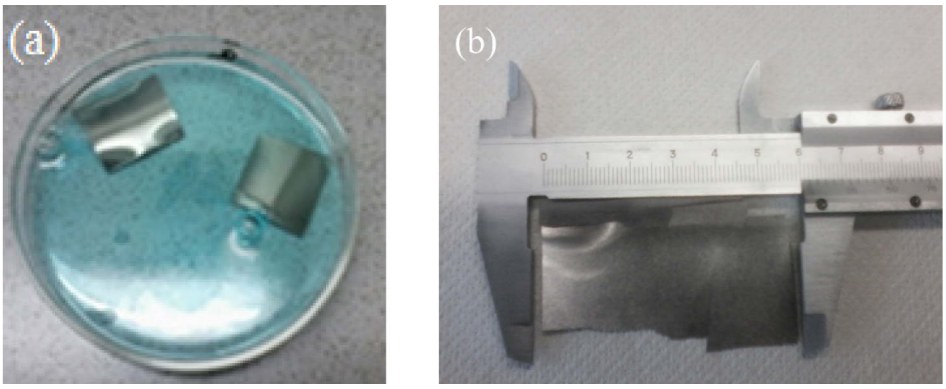

Figure 4.3: Methodology of freestanding multilayer foils synthesis. Dissolution of Cu in a nitric acid solution (a) and freestanding Zr/Al RMF (l = 10 μm) (b).

The major aspect is the heat sink nature of the copper substrate. The reactive film technology often faces the problem of as-deposited premixing layer and overheating, which reduce the heat release and reaction propagation of RMFs. Cu substrate with high thermal conductivity can reduce these problems. It is also expected that, such substrate will be beneficial to produce the high energetic RMFs, where premixing is mostly accounted.

Secondly, the use of copper substrate ensures the quick and complete separation of the foil from the substrate, which can be beneficial for the scaling up of multilayer production. All types of PVD films, which are not affected by the etching solution and don't build any low temperature constituents with Cu, can be synthesized by this method. This work also ensures the fabrication of freestanding Ti, TiN and Ti/TiN films besides Ti/Al, Zr/Al and Ti/Si/Ti/Al RMFs. The use of this method also shows the flexibility to produce freestanding particles, foils and flakes. Another important aspect is that Cu is cheap and no additional coating process of substrate is required to make film freestanding.

4.4 Characterization techniques

4.4.1 Microstructural analysis

The microstructural features of as-deposited and reacted RMFs were investigated by using Scanning Electron Microscope (SEM), Transmission Electron Microscope (TEM) and Atomic Force Microscope (AFM). SEM (Zeiss DSM 982) at an operating voltage of 15 kV equipped with an energy dispersive spectrometer (EDS) was used. Oxford instruments microanalysis with Aztec materials characterization system was conducted for quantitative image analysis. For electronics microscope, freestanding flake-type RMFs were attached to the Al-SEM sample stubs, which have been presented in Fig. 4.4 (a). Fig. 4.4 (b) shows the sample preparation using focused ion beam (FIB).

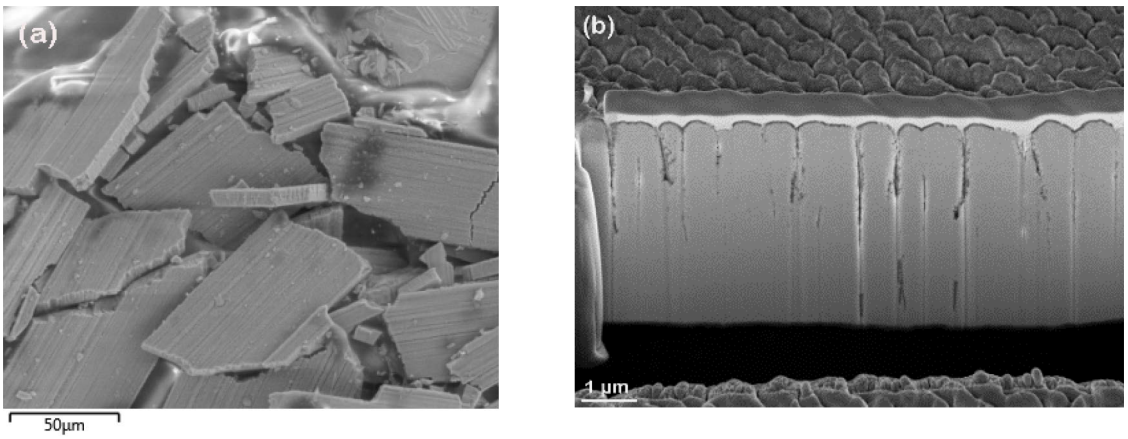

Figure 4.4: SEM image of freestanding RMFs as particles glued in Al stubs (a), RMF sample preparation with FIB/SEM sample (b).

4.4.2 Phase identification by XRD

X-ray powder diffraction (XRD) was used for phase identification after fast self-propagating reaction. Generally, X-ray diffraction is based on constructive interference of monochromatic X-rays, which are generated by a cathode ray tube, filtered to produce monochromatic radiation, collimated to concentrate, and directed toward the sample. The interaction of the incident rays with the sample produces diffracted ray when conditions satisfy Bragg's Law. This law relates the wavelength of electromagnetic radiation to the diffraction angle and the lattice spacing of a crystalline sample. Then

diffracted X-rays are detected and analyzed. By scanning the crystalline sample through a range of 2θ angles, all possible diffraction directions can be attained. Here, reacted films in the form of flakes were examined by using X-ray diffraction (XRD D 5000 Theta-Theta Bruker) using Cu K_α radiation (at TU Ilmenau). The diffraction patterns were analyzed in the range of 20°-100° to identify crystalline phases by using Bruker Diffrac. Eva. software tool. The reacted Zr/Al RMFs ignited in argon, were characterized by using X-ray diffractometer (STOE-STADI MP) vertical system working in transmission mode equipped with a linear PSD detector using Mo Kα (λ=0.70930 nm) radiation (at Department of Chemistry, University of Cologne). Phase analysis and quantification were carried out using WinXPOW Software (v. 3.0.2.1, STOE&Cie GmbH). The influence of chemical composition, molar ratios and bilayer thickness on the formation of reaction products were investigated by this characterization process.

4.5 Electrical resistivity measurement

In this work, electrical ignition was used to initiate the self-propagating reaction. Therefore, the characteristic of resistivity is very important for understanding how well those reactive films allow electric currents to flow through it. Therefore, electrical resistivity was examined. A simple two-wire resistance measurement facility equipped with a digital multimeter (Keithely 2000) was used for measuring the resistivity. This multimeter works with the maximum current flow 3 amperes and voltage difference of 230 volts. The electrical resistance of multilayer films was estimated for the measurement area of 1 cm × 1 cm. By incorporating film thickness and measurement area, electrical resistivity was estimated. This measurement will be helpful to understand the flow of electric current of a given composition of reactive film.

4.6 Differential scanning calorimetry

Differential scanning calorimetry (DSC) is another characterizing tool to analyze the heat flow during a slow reaction of reactive film. The calorimetric study of reaction in multilayer films is being developed having the focus on increment of signal to noise ratio by considering adequate sample mass, film thickness and heating rate [15, 86, 119]. In this work, we used freestanding reactive films for DSC (TA Instruments Q2000) analysis to record the heat

flow and phase transformation temperatures. In each DSC run, a small amount (~ 2 to 8 mg) of freestanding foil in the form of flakes was placed in an aluminum crucible, which was closed with a lid. The sample was heated from 100 °C to 550 °C at different heating rates of 5-40 K/min in the flowing nitrogen atmosphere. The DSC facility was initially calibrated. The universal TA instrument software was used to evaluate temperatures of phase change. The second heating run was performed in order to confirm the complete phase transformation in the first run, which also acted as a baseline. The transformation heat was measured by integrating the net heat flow with respect to time. DSC traces were limited to a maximum temperature of 550 °C and therefore, reactions beyond this temperature were not included. Therefore, the DSC analysis is primarily considered for qualitative analysis.

4.7 Measurement of reaction propagation and temperature

After an electrical ignition of RMF, the reaction propagation and temperature were measured at the same time. The overall experimental setup has been shown in Fig 4.5. Initially, freestanding films with the dimension of approx. 3-5 cm × 1 cm placed on a ceramic plate and then activated by applying 3-21 V electrical ignition connecting with the DC power supply equipment. Please note that, due to such freestanding films and performing the reaction on ceramic block, the heat loss is also considered to be minimal. The model of two corner ignition has been reported to start the reaction in multilayer films [87]. Here, one side and two side ignitions were performed. During self-propagating reaction, the propagation was recorded by using a high speed video camera (Kenyce high speed microscope VW9000) in the range of 2000-10000 frames per second. All tests were performed in air at room temperature without preheating the freestanding foils and reaction propagation is monitored in plain view. The reaction propagation was recorded and then the reaction front velocity was measured from the time variant captured high speed photographic images.

Simultaneously, reaction temperature was measured by using two-color pyrometer (also ratio pyrometer) in the short infrared wavelengths. Recent study reported the use of two- color pyrometer for temperature measurement for unknown emissivity [88]. The major advantages of this method are that

non-contact temperature measurement and also it does not require the emission properties of films. On the other hand, the measurement is quick.

In this work, two different pyrometers were used at different temperature ranges. A two-color pyrometer (Metis MQ22, 350-1300 °C) was used from Sensotherm GmbH, which has the spectral range of 1.45-1.8 µm with response time less than 0,002-10 ms. Another one is the two-color pyrometer (Metis HQ22, 700-2300 °C) in a high speed mode, which can be used for more than 25000 measurements per second. It has short infrared wavelengths within the spectral range of 1.45-1.8 µm. Initially, the pyrometer was calibrated and temperatures were estimated to be accurate within ± 80 °C. The spot size has been maintained of 1-2 mm. The spot was focused at the top view of the reactive film. Due to pyrometer specification, no initial preheating temperature will be characterized. However, the temperature measurement will be significant to characterize the T-t profile and to estimate the maximum reaction temperature.

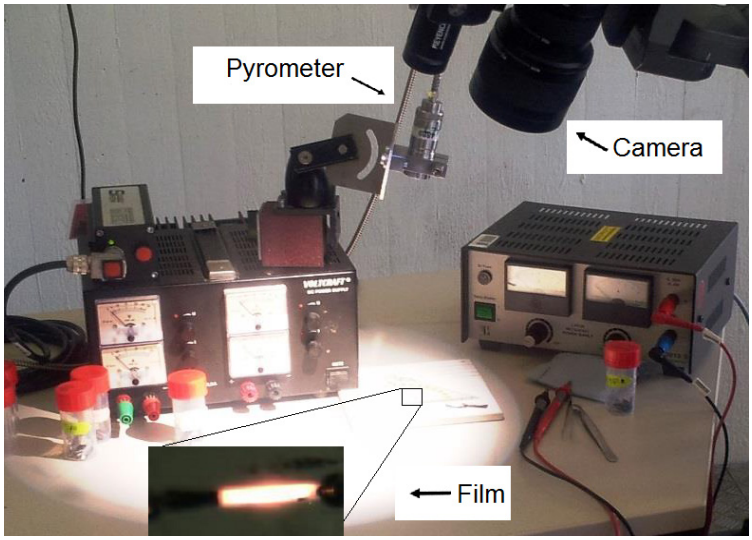

Figure 4.5: Experimental set up for investigation of reaction propagation and temperature measurement by using high speed camera and two-color pyrometer.

4.8 Reactive joining process

In this work, reactive joining of stainless steel components was investigated by using commercial Ni/Al nanofoil (from Indium Corporation) and developed Ti/Si/Ti/Al ternary reactive film. For joining with commercial nanofoil, two different types of melting layers of only Sn and Ni-coated Sn were electrodeposited on the cleaned steel components. The reactive joining

of steels with ternary film was attempted by considering only Sn melting layer. Here, the Sn layer with a thickness of 12-18 µm was electrodeposited on the stainless steels specimen. In case of Ni coated Sn melting layer, Sn and Ni layer have the thickness of 10 µm and 6 µm, respectively. The sample has the dimension of 5 cm × 2 cm × 0.5 cm. Then the melting layer was coated with the area of 1 cm × 2 cm, which indicated the joint area. Reactive films slightly larger than the size of bonded area were sandwiched between the components under pressure.

The reactive joining process has been well developed [70]. The schematic representation of reactive joining has been shown in Fig. 4.6. This reactive joining includes the following steps; (1) Introducing reactive films between joined components coated or arranged with melting layers. (2) Applying uniaxial compressive load to the joint assembly in order to build uniform contact. The choice of the pressure depends on the types of the components to be joined. (3) Ignition of reactive film for providing heat for joining within milliseconds. (4) Cooling and then elimination of the compressive load. (5) Removal of the joint assembly and inspection.

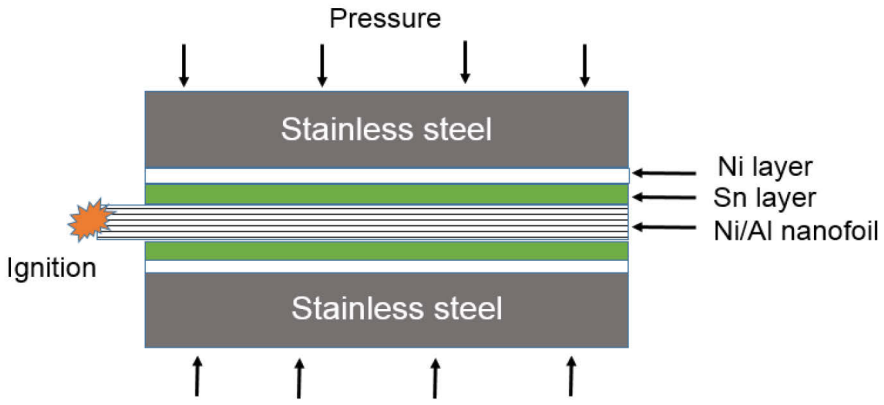

Figure 4.6: Schematic representation of the cross-section of reactive joint of steels using Ni/Al nanofoil.

4.9 Thermodynamic and numerical CFD simulation

In this work, the standard enthalpy of formation (reaction heat) of Ti-Al, Zr-Al and Ti-Si systems were calculated by using CALPHAD (Calculation of Phase Diagrams) based Thermo-Calc 3.1 simulation. Here, Thermo-Calc binary (TC Bin) database was used to calculate standard enthalpy of formation of different stable phases of these binary systems at standard conditions of

25 °C and 1 bar. Computational fluid dynamic (CFD) simulation was used to characterize the steady state exothermic reaction in Ti/Al film. Here, the governing equations were solved using the finite volume methodology (FVM) applying Ansys CFD Fluent numerical code. The computational domain has discretized using block structured body fitted grids and linear interpolation scheme. The temperature flow and reactant mixing in 20 nm domain of 1Ti/1Al films during self-propagating reaction were numerically simulated. The overall characterization techniques in this work are summarized in table 4.2. The typical material characterization techniques include the methodology for experimental analysis and simulation.

Table 4.2: Summary of all used experimental techniques and equipment.

Characteristics	**Technique**	**Equipment**
Microstructural analysis	SEM	Zeiss DSM 982
	TEM	Philips TECNAI
Surface topography	AFM	XE7 Park systems
Chemical composition	EDX-SEM	Zeiss DSM 982
Crystallographic phase identification	XRD	XRD D5000 Theta-Theta Brucker, X-ray diffractometer (STOE-STADI MP)
Transformation heat flow and phase change temperature	DSC	TA Instruments Q2000
Resistivity	Two-wire method	Keithely multimeter 2000
Reaction propagation	High speed camera	Keyence high speed microscope VW9000
Reaction temperature	Two-color pyrometer	Metis MQ22 (350-1300 °C) Metis HQ22 (700-2300 °C)
Standard heat of formation	Thermo-Calc	Thermo-Calc 3.1 (CALPHAD)
Temperature flow and reactant mixing	CFD	Ansys CFD (FVM)

Results and Discussions

5 Simulation

5.1 Thermodynamic simulation

Thermo-Calc simulation was used to simulate the reaction heat of all stable phases of different reactant combinations and then chemical compositions of multilayer film were selected for the deposition. Here, the CALPHAD method was used to analyze the phase equilibria and thermochemical properties of a multicomponent system. The basis of this method is to minimize the Gibbs free enthalpy. For the calculation of phase equilibria in a multicomponent system, the minimization of the total Gibbs energy (G) of all the phases will take place in equilibrium, which can be expressed as:

$$G = \sum_{i=1}^{p} n_i \, G_i^{\varphi} = minimum \qquad (17)$$

Here, n_i is the number of moles, and G_i^{φ} indicates the Gibbs energy of phase i. The thermodynamic description of a system, requires the assignment of thermodynamic functions for each phase. The CALPHAD method employs a variety of models to describe the temperature, pressure, and concentration dependencies of the free-energy functions of various phases. The total Gibbs enthalpy of a system has been described in details in Refs. [89-90], which can be expressed as:

$$G^{\varphi} = G_T^{\varphi}(T,x) + G_p^{\varphi}(p,T,x) + G_m^{\varphi}\left(T_c, \beta_0, T, x\right) \qquad (18)$$

In this equation, $G_T^{\varphi}(T,x)$ is the contribution to the Gibbs energy by the temperature (T) and the composition (x), $G_p^{\varphi}(p,T,x)$ is the contribution of pressure (p), and $G_m^{\varphi}\left(T_c, \beta_0, T, x\right)$ is the magnetic contribution of the Curie temperature (T_C) and the average magnetic moment per atom (β_0). By applying the mathematical model containing adjustable parameters, the free Gibbs enthalpy of an ideal solution, non-ideal and excess energy can be estimated. This will give the information of the phase diagram, as well as the thermodynamic properties of all the phases and the system entirely. In addition, the CALPHAD method represents the thermodynamic properties for various phases which predicts properties of multicomponent systems by accounting the crystallography, bond type, order-disorder transitions and

magnetic properties. Here, the calculated enthalpy of formation of different phases of this work was compared with available literatures.

5.1.1 Ti-Al binary system

In this work, Thermo-Calc calculated Ti-Al equilibrium phase diagram and the enthalpy of formation of Ti-Al system were shown in Fig. 5.1 (a-b). The enthalpy of formation of all stable phases in this system differs between -35 kJ/mol and -41 kJ/mol. The Ti-rich phases are TiAl, Ti_3Al, which have wide composition range. The Al-rich phases are Al_2Ti, $Al_{11}Ti_5$ and Al_3Ti. In this work, simulated enthalpy of formation of the stable phases of Ti-Al binary systems are summarized in table 5.1 and compared with the available literatures as stated in the work of Nassik et al., 2003 [91] and Kubaschewski et. al., 1955 [92]. Here, ($-\Delta H$) indicates the exothermic heat (reaction heat or heat of formation or enthalpy of formation). The calorimetric study of Nassik et al. 2003, showed the higher reaction heat for the phase formation of $TiAl_3$ [91]. This work shows a high reaction heat of -40 kJ/mol for the formation of TiAl and Al_2Ti intermetallics.

5.1.2 Zr-Al binary system

The reaction heat of all stable intermetallic compounds in Zr-Al system was also calculated by using Thermo-Calc 3.1 simulation. Fig. 5.2 (a) shows the equilibrium Zr-Al phase diagram. Fig. 5.2 (b) shows that Zr-Al system has a large number of intermetallic compounds mainly with narrow composition range. There are eight intermetallic compounds with the reaction heat higher than -33 kJ/mol. The Zr-rich compounds are $AlZr_2$, Al_3Zr_5, Al_2Zr_3 and Al_4Zr_5. The Al-rich side of the phase diagram shows the intermetallic phases of AlZr, Al_3Zr_2, Al_2Zr and Al_3Zr. The reaction heats of all stable phases of Zr-Al system differ in the range of -33 kJ/mol and -47 kJ/mol. Mostly, the Al-rich or equal molar fraction intermetallic compounds show the higher reaction heat than Zr-rich compounds. In this work, a high reaction heat of -46.97 kJ/mol was found for Al_3Zr_2 intermetallic. Recent studies reported the higher reaction heat for the formation of Al_2Zr and Al_3Zr_2 phases as mentioned in Refs. [91-97]. Here, table 5.1 summarized a comparative study of reaction heat of different stable phases in Zr-Al binary system.

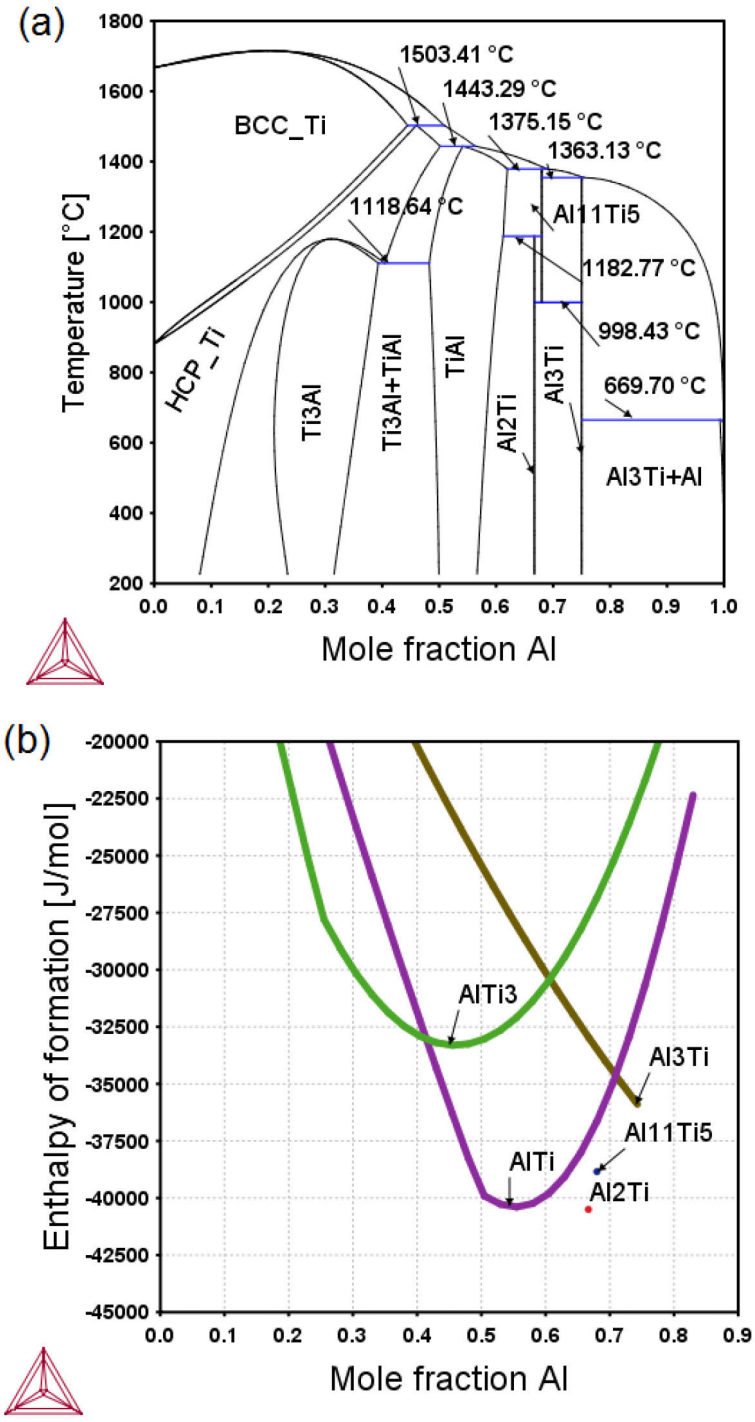

Figure 5.1: Thermo-Calc 3.1 calculated equilibrium Ti-Al phase diagramm (a) and enthalpy of formation of different phases in Ti-Al system (b). [This work].

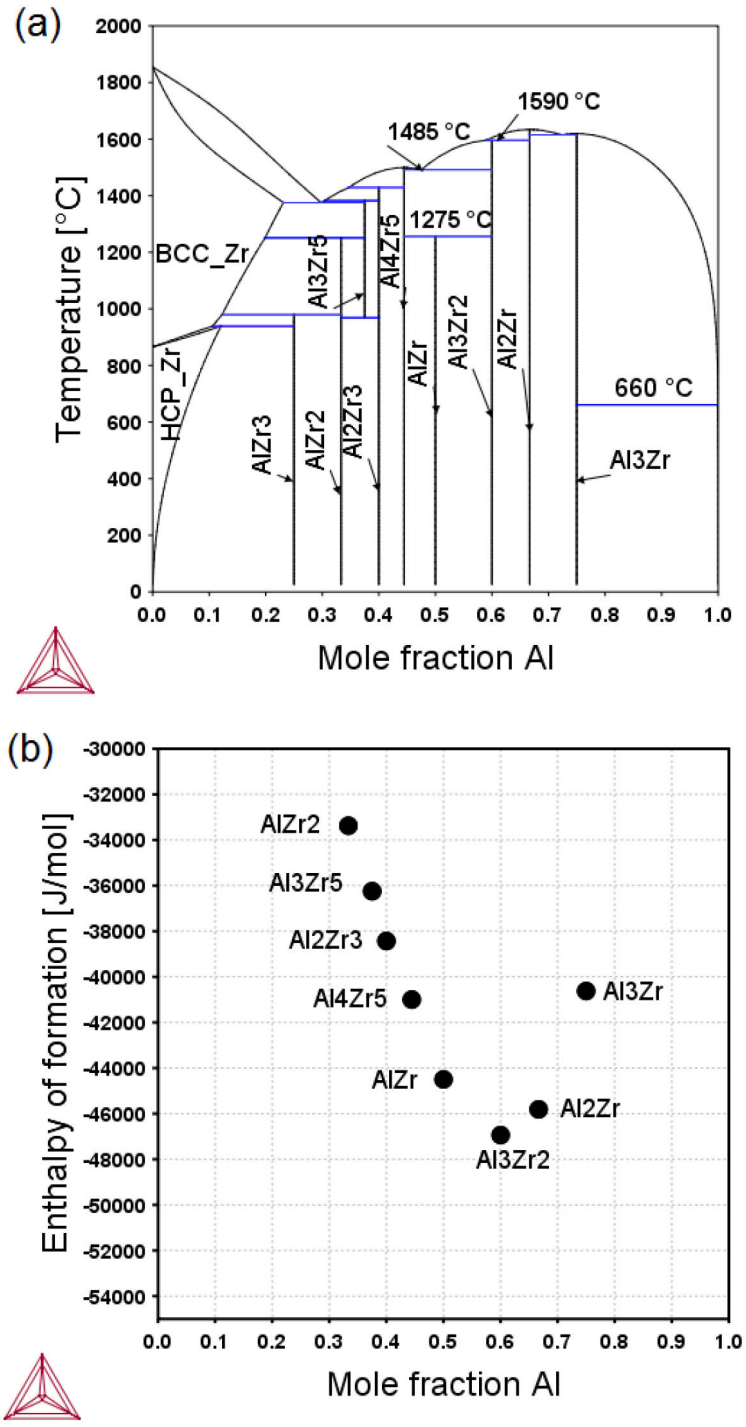

Figure 5.2: Thermo-Calc 3.1 calculated equilibrium Zr-Al phase diagram (a) and enthalpy of formation of different phases in Zr-Al system (b). [This work].

5.1.3 Ti-Si binary system

The thermodynamic calculation of equilibrium Ti-Si phase diagram and standard enthalpy of formation have been shown in Fig. 5.3 (a-b). In this binary system, five stable phases with enthalpy of formation between -50 kJ/mol and -80 kJ/mol have been noticed, which are presented in Fig 5.3 (b). The Ti-rich intermetallic phases are $SiTi_3$ (-50.30 kJ/mol), Si_3Ti_5 (-74.03 kJ/mol) and Si_4Ti_5 (-79.40 kJ/mol). The SiTi phase has an enthalpy of formation -77.42 kJ/mol. The Si-rich phase is Si_2Ti, which has the enthalpy of formation in the range of -58.32 kJ/mol. The simulated results of this work were compared with the work of Schlesinger et al. 1990 [105] and also listed in table 5.1.

A high reaction heat was noticed for the formation of Si_4Ti_5 phase in this work. The intermetallic compound of Si_2Ti (Si mole fraction = 0.67) shows relatively lower reaction heat. Generally, two poly types may exist for Si_2Ti phase, which are C54 (face center orthorhombic lattice) and C49 (base center orthorhombic lattice) phase and many investigations suggested the initial formation of metastable C49 phase, which transform to C54 phase [106].

In case of ternary Ti/Si/Ti/Al and Si/Ti/Al/Si films, distinct atomic mixing interfaces of Ti-Si, Al-Si and Ti-Al are to be accounted. In that case, the intermetallic formation of binary systems needs to be considered. For Al-Si binary system, this simulation estimates the standard reaction heat of 1.6 kJ/mol for (0.12) Si mole fraction. The intermetallics of Ti-Al system presented in section 5.1.1 should be considered in this ternary system. In case of multiple intermetallics formation, types and volume fraction of these phases control the overall reaction heat of reactive films.

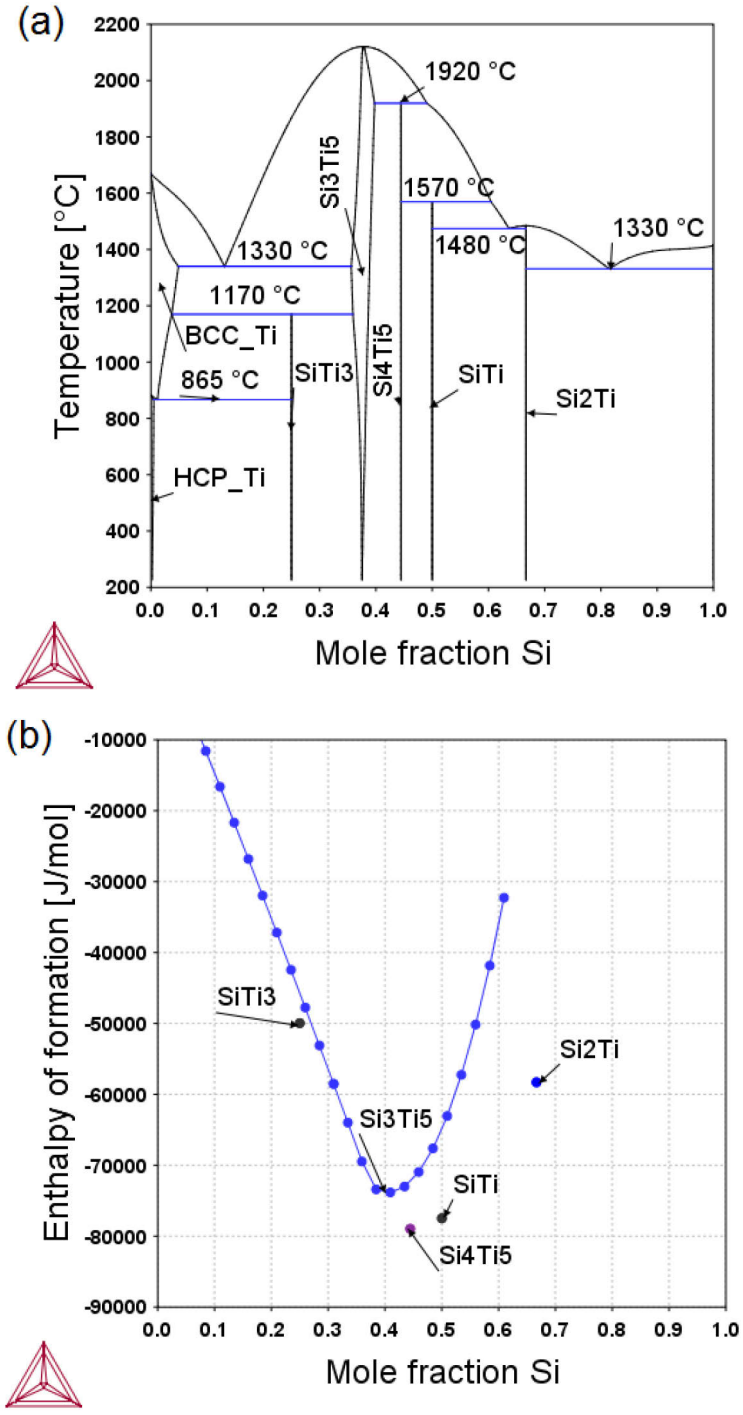

Figure 5.3: Thermo-Calc 3.1 calculated equilibrium Ti-Si phase diagram (a) and reaction heat of different phases of Ti-Si binary system (b). [This work].

Table 5.1: Thermo-Calc 3.1 calculated enthalpy of formation (-ΔH) of different phases in Ti-Al, Zr-Al and Ti-Si binary systems.

Ti-Al				
Phases	**Al - mole fraction**	**Crystal structure [94-96]**	**-ΔH (kJ/mol) [This work]**	**-ΔH (kJ/mol) Lit. [Ref.]**
$AlTi_3$	0.30	Hexagonal, D019	-30.03	-25±2.1 [91-93]
AlTi	0.54	Tetragonal, L10	-40.36	-35.1±0.5 [91]
Al_2Ti	0.66	Tetragonal	-40.48	-37.1±0.9 [91]
$Al_{11}Ti_5$	0.68	D023	-38.82	-
Al_3Ti	0.74	Tetragonal, D022	-35.59	-39.2±1.8 [95]

Zr-Al				
Phases	**Al - mole fraction**	**Crystal structure [Ref.]**	**-ΔH (kJ/mol) [This work]**	**-ΔH (kJ/mol) Ref. [97-98]**
$AlZr_2$	0.33	Hexagonal [99-100]	-33.49	-
Al_3Zr_5	0.37	Hexagonal [101], Tetragonal [99]	-36.29	48±4
Al_2Zr_3	0.40	Tetragonal [99,102]	-38.29	49±4
Al_4Zr_5	0.44	-	-41.05	52±4
AlZr	0.50	Orthorhombic BCr-type [103]	-44.49	53±4
Al_3Zr_2	0.60	Orthorhombic BCr-type [99]	-46.97	55±4
Al_2Zr	0.67	C14, $MgZn_2$ [99]	-45.82	54±4
Al_3Zr	0.75	D023[104]	-40.69	49±4

Ti-Si				
Phases of Ti-Si system	**Si - mole fraction**	**Crystal Structure Ref. [107]**	**Enthalpy of formation, -ΔH (kJ/mol) [This work]**	**Literature, Ref. [105] ΔH (kJ/mol)**
$SiTi_3$	0.25	Tetragonal	-50.30	-53
Si_3Ti_5	0.41	Hexagonal	-74.03	-72
Si_4Ti_5	0.45	Tetragonal	-79.4	-81
SiTi	0.50	Orthorhombic	-77.42	-79
Si_2Ti	0.67	Orthorhombic	-58.32	-57

5.2 Computational Fluid Dynamics (CFD)

5.2.1 Numerical modelling

For the first time, CFD simulation was used to characterize the self-propagating reaction in nanoscale Ti/Al RMF. Here, the governing equations (mass, momentum and energy) were solved by using the finite volume methodology (FVM) applying Ansys CFD Fluent numerical code [108]. Fig. 5.4 shows the Ti/Al reactive film with 1:1 molar ratio and corresponding solution domain with a dimension of 20 nm × 100 nm. The computational domain was discretized using block structured body fitted grids and linear interpolation scheme. The number of elements, element size in x and y direction are 50000, 0.2 nm and 0.2 nm, respectively. For the spatial discretization of mixing and validation, the time step of 10^{-10} sec was considered for maximum 20 iterations. The boundary conditions of two dimensional solution domain are also shown in Fig. 5.4.

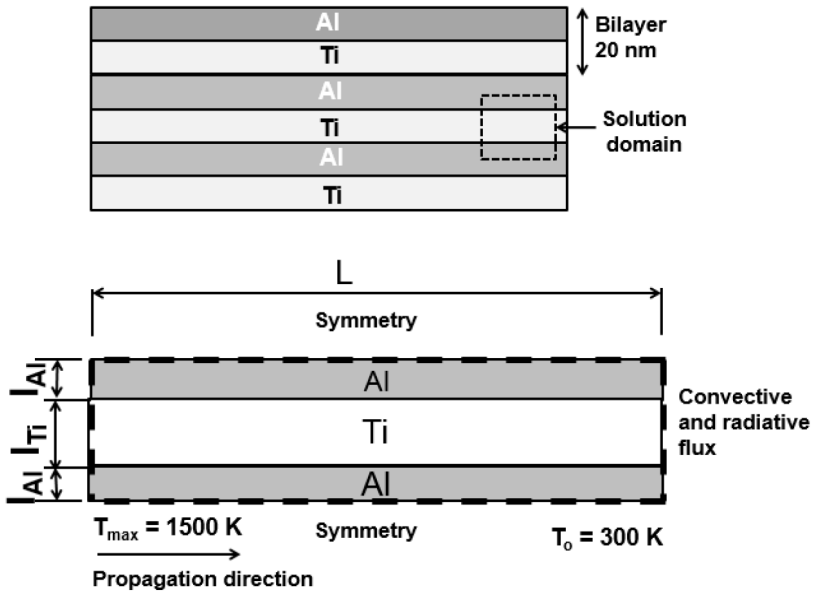

Figure 5.4: Schematic representation of the 1Ti/1Al reactive film with 20 nm bilayer and corresponding CFD solution domain with boundary conditions. Here, L= 100 nm, I_{Ti} = 10 nm, I_{Al} = 5 nm.

These boundary conditions are as follows:

(1) An adiabatic boundary condition exists on the inlet side. Initially, reactive foil is at room temperature (T_0 = 300 K). The foil was activated on the inlet side. After activation, the reaction temperature reached to the maximum temperature of T_{max} = 1500 K. Then the reaction front propagates opposite to the adiabatic boundary wall.

(2) The convective and radiative heat fluxes were considered at the outlet side.

(3) On upper and lower sides of the solution domain, a symmetry condition exists.

In this CFD simulation, the numerical formulation to describe the self-propagating reaction in Ti/Al RMF is based on the following assumptions:

(1) The time dependent thermal flow and species transport were considered in the two dimensional flow, as the thickness of foil is very small compared to the width and length.

(2) The melting of reactants or reaction products is neglected.

(3) The effects of intermixing region and unsteady reaction propagation were ignored.

(4) Here, overall physical properties of 1Ti/1Al film (density, thermal conductivity and specific heat) are assumed to be dependent on the composition.

(5) The atomic diffusion is represented by a single binary diffusion coefficient. Here, the thermally activated atomic diffusivity can be assumed to follow the Arrhenius equation.

$$D = D_0 \exp\left(\frac{-E_a}{RT}\right) \tag{19}$$

Where, E_a is the activation energy, T is the absolute temperature and R is the universal gas constant and D_0 is the Arrhenius pre-exponent. Here, the Arrhenius pre exponent factor, $D_0 = 2.5\times10^{-8}$ m^2s^{-1} and activation energy, E_a = 94.4 kJ/mol were used according to the work of Grieseler [109], which showed an appropriate diffusion phenomena of layered Ti-Al system with molar ratio of 1:1.

The diffusion flux arises due to concentration and temperature gradient according to Fick's law. The mass balance equation for titanium species transport is as follows;

$$\frac{\partial}{\partial t}(\rho C_{Ti}) + \nabla.(\rho \vec{v} C_{Ti}) = -\nabla \cdot J_{Ti} \tag{20}$$

$$J_{Ti} = -\rho D C_{Ti} \tag{21}$$

Where, C_{Ti} is the concentration of Titanium, ρ is the density and D is the diffusion coefficient. Here, species concentration from atomic mixing is conserved in the scalar field of $C(x, y, t)$. The concentration is initially defined $C = 1$ for Ti and $C = 0$ for Al. Here, physical properties of density (ρ), thermal conductivity (λ) and the specific heat (Cp) in the control volume are obtained as.

$$\begin{aligned} \rho &= \rho_{\mathrm{Ti}} \mathrm{C} + \rho_{\mathrm{Al}} (1 - \mathrm{C}) \\ \lambda &= \lambda_{\mathrm{Ti}} \mathrm{C} + \lambda_{\mathrm{Al}} (1 - \mathrm{C}) \\ C_p &= C_{p_{Ti}} \mathrm{C} + C_{P_{Al}} (1 - \mathrm{C}) \end{aligned} \tag{22}$$

For 1Ti/1Al RMF, used physical properties are: density, ρ_{Al} = 2700 kg/m^3, ρ_{Ti} = 4500 kg/m^3; specific heat $C_{p(Al)}$ = 897 J/KgK, $C_{p(Ti)}$ = 523 J/KgK and thermal conductivity λ_{Al} = 236 W/mK, λ_{Ti} = 22 W/mK [110]. The heat generation rate is assumed to be proportional to the rate at which the composition changes. A similar approach was demonstrated successfully in the work of Raic` et al. [111]. Here, a linear relationship between energy (Q) released by exothermic reaction and the concentration has been considered, which is closer to the real condition [45].

$$Q(C) = -\rho c_p (T_{max} - T_0) C \qquad (23)$$

Here, T_{max} and T_o indicate the maximum adiabatic reaction temperature and initial temperature. Thermo-Calc simulated reaction heat of 40 kJ/mol was considered to be released during the reaction in this work. Moreover, the second order upwind scheme was used for the spatial discretization of diffusive terms.

5.2.2 Concentration profile during reaction

The atomic mixing during a self-propagating reaction in 1Ti/1Al reactive foil was characterized by using numerical CFD simulation. The simulated concentration fields have been illustrated in Fig. 5.5. Initially, 1Ti/1Al foil has 100 % Ti (red) and 100 % Al (blue) layers with thickness of 10 nm and 5 nm respectively. Fig. 5.5 shows that the contour plots of concentration profile of Ti in mass fraction at different time of activation. After 0.1 ns of activation, there presence no reactant mixing. With increasing time to 1 ns, atomic mixing rate is still very low. It illustrates a low atomic mixing till 10 ns after activation. At the time of 0.1 µs, the atomic mixing occurs, which completes at the time of 1 µs. This result shows that atomic mixing rate varies with time of activation at the perpendicular of multilayers.

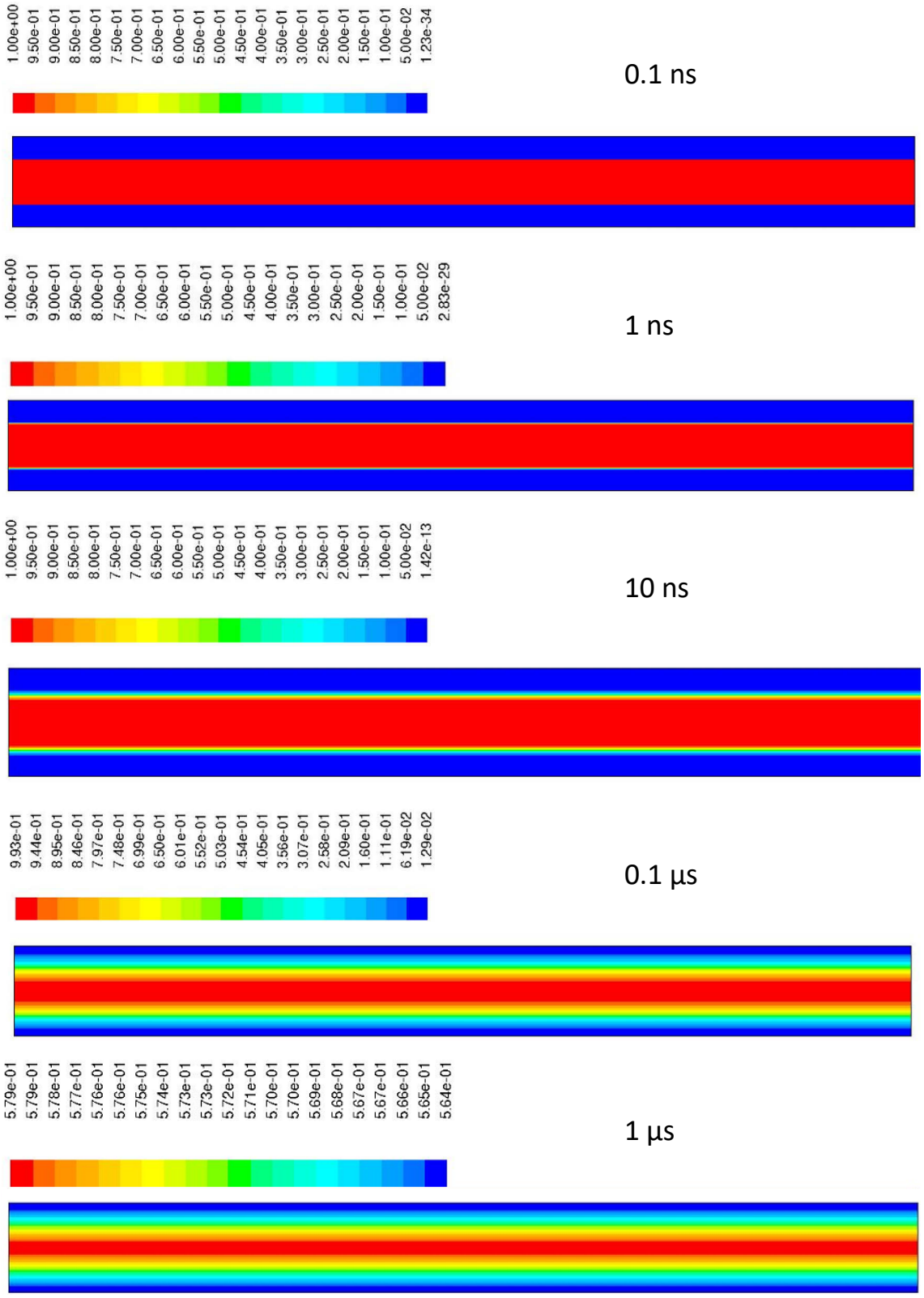

Figure 5.5: Initially 1Ti/1Al multilayer has 100 % and 0 % Ti content with red and blue color. Contour plots of concentration profile (mass fraction of Ti) at different time after activation.

During the self-propagating reaction, the concentration fields of reactant layer change by intermixing. It mainly starts to change at the interface of two elemental layers due to concentration gradient. With time variation, species transport changes. Here, the important fact is the diffusion coefficient D, as mentioned in equation (19). It varies with the temperature and increases as the temperature increases. However, the diffusion coefficient is kept constant due to less availability of data in this simulation.

The concentration profile of Ti, changes within 0.1 ns to 1 μs of activation. The result shows that the reactant layers mix fully after 1μs of activation. Please note that, this simulation corresponds the ideal conditions of atomic mixing in Ti/Al multilayers without the effects of premixing layer and heat loss.

5.2.3 Simulated temperature flow during exothermic reaction

The contour plots of temperature distribution during a self-propagating reaction are shown in Fig. 5.6. Temperature profile varies within time of activation. The thermal transportation changes in the axial direction of the multilayers. The inlet side was activated, where the maximum temperature of 1500 K was reached. The contour plots presented in Fig. 5.6 clearly show the time dependent temperature flow from maximum to the minimum temperature. Temperature flows from the inlet to outlet direction. After 0.1 ns of activation, the temperature flows to the outlet side, where the temperature reaches to 1090 °C. At the time of 0.1μs, 100 nm long domain has a homogeneous temperature of 1500 °C.

To get additional inside into these results, temperature distribution within 100 nm long domain at different time was plotted in Fig 5.7. Within a very short period of 0.001 ns, temperature starts to proceed to the outlet side. For the time of 0.1 ns, the outlet side has still 300 K. For the time of 0.06 ns after activation, the temperature fields spread out from the 100 nm solution domain. After comparing this result with the recent studies, we find the time dependent temperature distribution in the reaction zone and preheating zone, which shows a good agreement with Refs. [111-112].

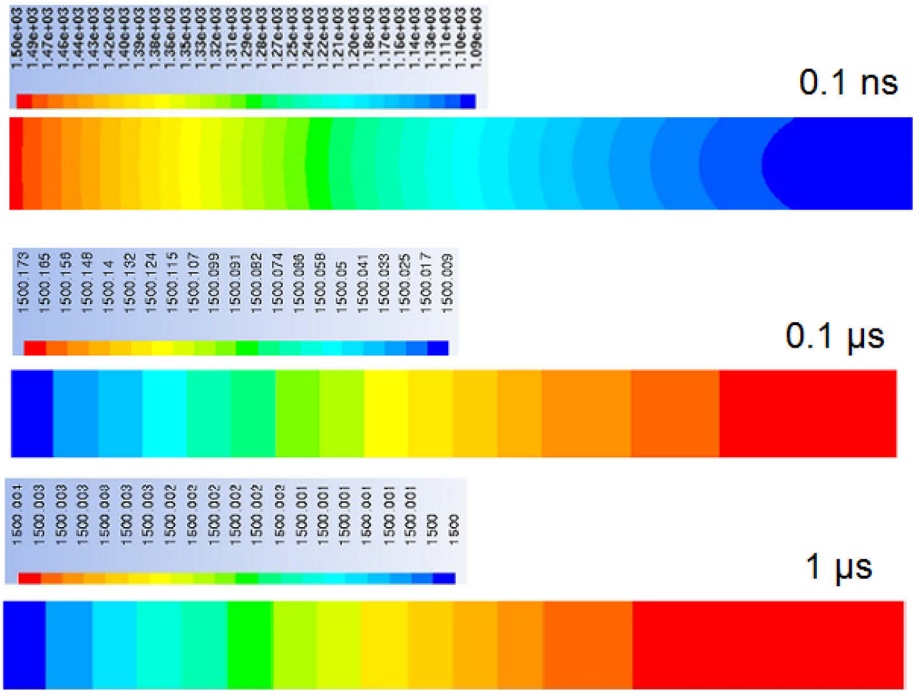

Figure 5.6: Contours plots of temperature distribution at different time after activation.

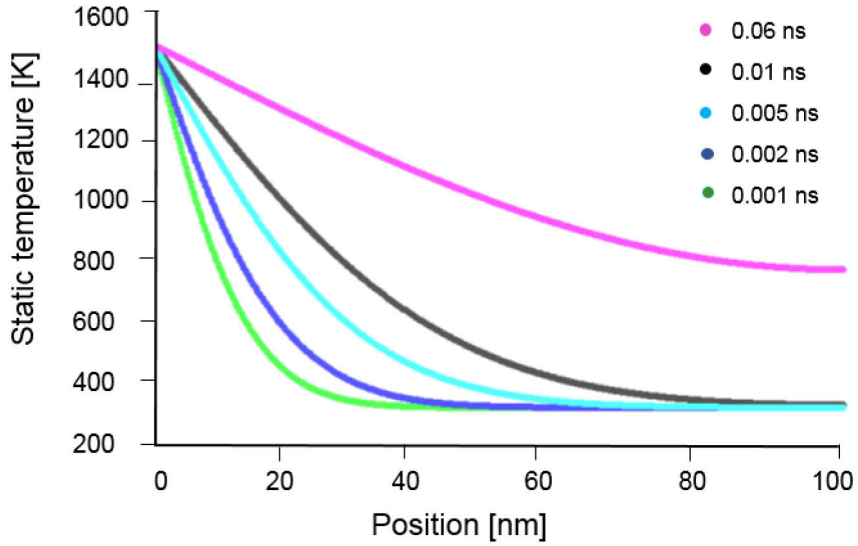

Figure 5.7: Temperature flow as a function of propagation distance after different time of activation. Here, propagation distance is about 100 nm in x direction according to the solution domain.

This CFD simulation results show the faster temperature transport than the atomic mixing. The temperature flow is essentially unidirectional, which is mostly taken in the axial direction. The species profile occurs in the perpendicular direction of layers due to a concentration gradient. This

simulated concentration profile shows a good agreement with Refs. [29, 45], where the atomic diffusion was modelled as a one-dimensional phenomenon in the normal direction to the layers. However, the influences of the premixed layer, microstructural morphology of multilayer and the heat loss were ignored in this simulation. To optimize the reaction performance of RMFs, it is necessary to have a good understanding of the nanoscale reaction propagation in regard to temperature flow and concentration profile. This simulation work will also be beneficial to understand the reaction kinetics in the nanoscale reaction zone.

6 Ti/Al reactive multilayer film

6.1 Synthesis of Ti/Al RMFs with different molar ratios

As a low energy classed reactive system, Ti/Al RMF was investigated. The Thermo-Calc simulated results in Ti-Al binary system, presented at section 5.1.1, show the composition dependent reaction heat of different phases. Therefore, three different types of Al-molar ratios of 1Ti/ nAl (n =1, 2, 3) having compositions of 1Ti/1Al, 1Ti/2Al and 1Ti/3Al were investigate in this work. The equilibrium phase diagram and corresponding film compositions are shown in Fig. 6.1. Here, we focus to understand the role of different Al molar ratios on the formation of reaction products, heat flows and reaction propagation. The deposition parameters were also listed in table 4.1 at section 4.2. The Ti/Al RMFs have the layer sequence of Cu-substrate /Ti/Al/Ti/…./Al with approx. 185 periods. Then, the reaction properties of freestanding Ti/nAl films were characterized in terms of heat flow, reaction temperature and propagation velocity.

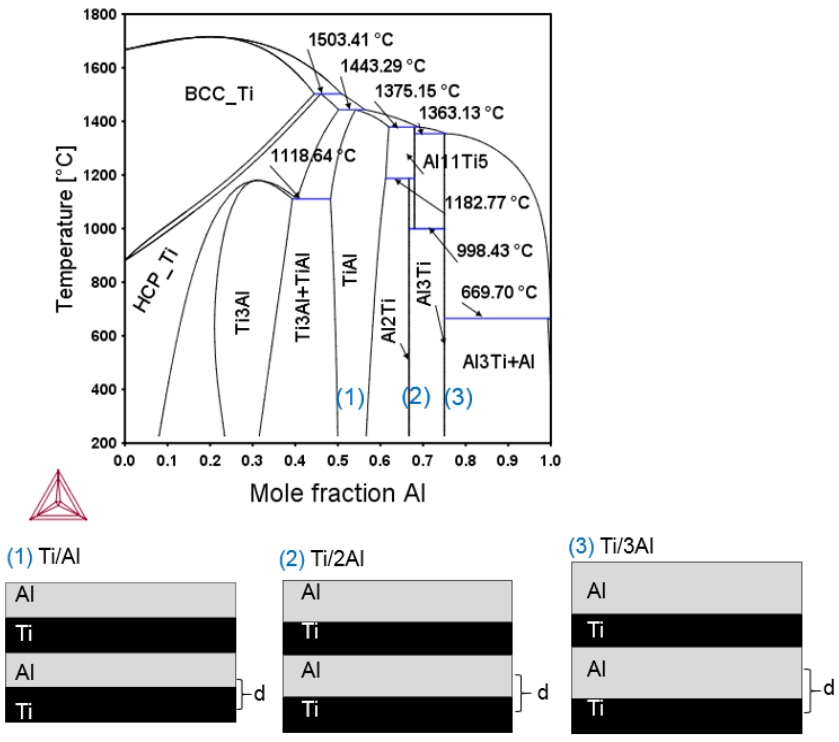

Figure 6.1: Selection of Ti/Al RMFs with different Al-molar ratios having compositions of (1) Ti/Al, (2) Ti/2Al and (3) Ti/3Al in the Ti-Al phase diagram.

6.2 Microstructural analysis of as-deposited RMFs

The as-deposited freestanding Ti/nAl foils were characterized. The quantitative image analysis shows that 1Ti/1Al, 1Ti/2Al and 1Ti/3Al films have the constant thickness of 10 nm Ti layer with 10 nm, 18 nm and 27 nm Al layer, respectively. The EDX –SEM analysis shows the compositions of 54 at. %, 67 at. % and 77 at. % Al in 1Ti/1Al, 1Ti/2Al and 1Ti/3Al multilayer foils. The overall film thicknesses vary in the range of 3.5-7 μm. The cross-sectional SEM image of Ti/3Al film, presented in Fig. 6.2 (a) exhibits the fine columnar microstructure. The column width varies in the range of (580±110) nm. In each columnar structure, there is a coherency of individual elemental layers of Ti and Al, which is visible in Fig. 6.2 (b). It demonstrates the alternating sequence of bright 27 nm Al and dark 10 nm Ti layers in the columnar grain. The microstructural analysis also suggests the presence of pores to some extent for higher Al content foils.

Then, the microstructural morphology of deposited film was correlated with the structure zone Thornton model as mentioned [113-114]. The columnar grains were grown in the competitive way with a V-shaped structure in Ti/nAl film. The microstructural morphology may fit to the zone-T (transition zone). The use of Copper substrate is expected to provide the cooling effect and helps to avoid overheating during film growth. The bright field TEM images of 1Ti/3Al film presented in Fig. 6.2 (c-d), show the alternating Al and Ti layer with controlled thickness. The high-resolution TEM image presented in Fig. 6.2 (d) shows a portion of intermixing zone (w) having approx.1-2 nm thickness between Ti and Al layers.

The development of film morphology of the sputter-deposited multilayers proposed an important aspect to understand the microstructure dependent reaction properties in regard to the zone microstructure. Normally, the film morphology having high temperature zone structure (e. g. Zone-3 as mentioned in Refs. [113-114]) shows higher diffusion possibilities. In this case, the formation of intermixing layer would be pronounced, which may decrease the reaction heat. On the other hand, very low temperature zone (zone-1) with higher defects concentration, pores, rough surface and larger grain gaps can influence negatively on reaction properties. In this case, microstructure morphology of zone-T or Zone-2 in RMFs can reduce the

formation of premixing layer, which is expected to regulate the reaction propagation positively.

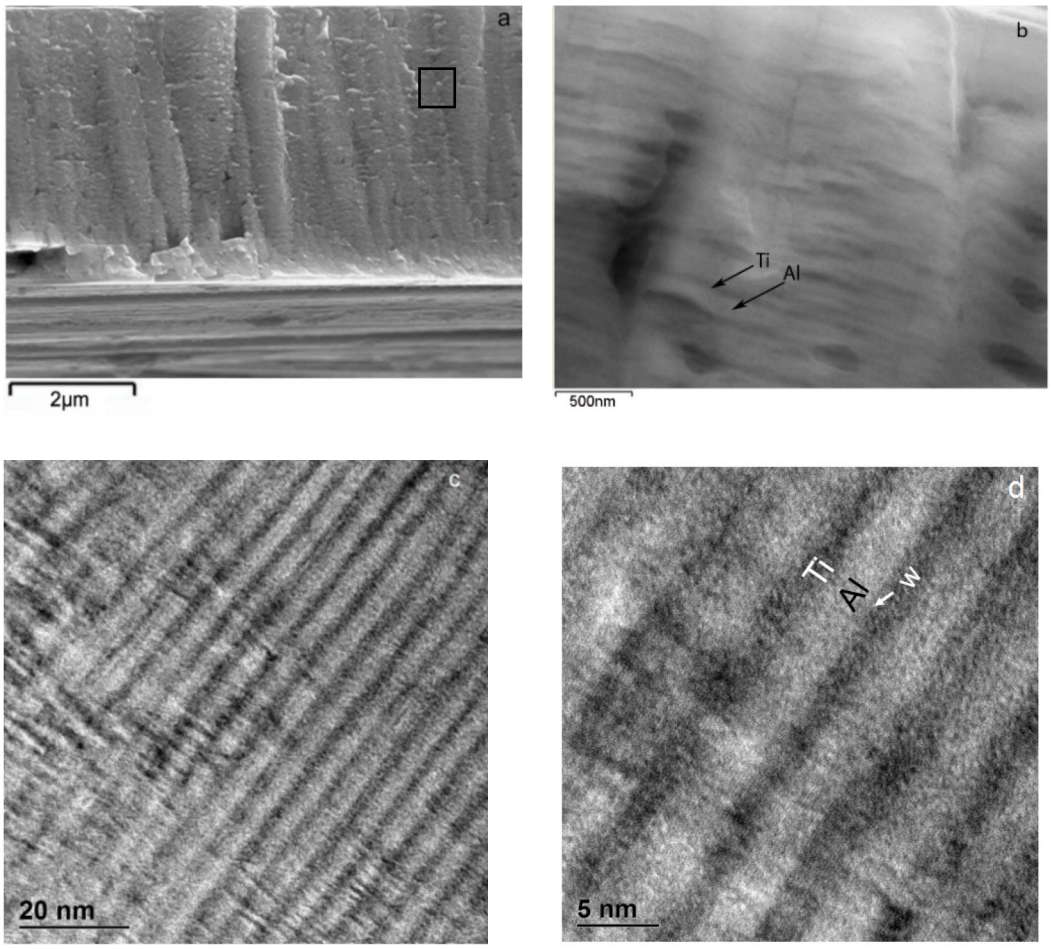

Figure 6.2: Cross-sectional SEM image of as-deposited freestanding 1Ti/3Al film (a). Alternating Al and Ti layers in each columnar microstructure in 1Ti/3Al film (d = 37 nm) (b). High resolution bright field TEM images of Ti/3Al films having controlled Ti and Al reactants layers (c, d). Here, w indicates the premixing layer.

6.3 Reaction products identification by XRD

The phase formation in reacted Ti/Al films was investigated by XRD analysis by using XRD D5000 Theta-Theta Brucker. During an exothermic reaction, the reaction kinetics in multilayer films by slow and fast heating rate can provide different reaction products. The recent works as demonstrated in Refs. [69, 115], show that the phase formation upon slow heating in the Ni-Al system is different as the phase formed during self-propagating reaction. The similar approach has been also mentioned by the work of Van Heerden

et al. to show the different phase formation in case of quenched reaction front compared to those formed during un-arrested reaction front [116]. Therefore, in this work we evaluate the reaction products just after a fast self-propagating reaction. The freestanding films without preheating were placed on the ceramic block and then ignited by using an electrical ignition in air. Therefore, the heat loss is also considered minimal, which assures a real condition of application.

Fig. 6.3 exhibits the XRD patterns (Y-offset) of reacted Ti/Al RMFs after a fast self-propagating reaction in air. The reaction products of $TiAl_3$ (Orthorhombic) and $TiAl_2$ (Orthorhombic) intermetallic compounds have been noticed. It may presence a very small amount of Ti. On the other hand, XRD patterns may include some peaks of impurities or oxides of reactants or products.

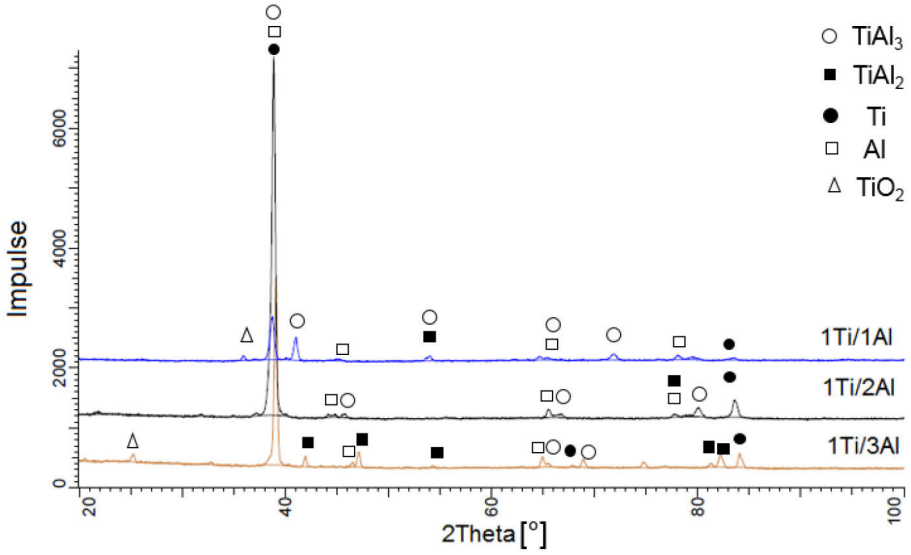

Figure 6.3: XRD diffractograms of Ti/Al RMFs for various molar ratios. Here, reflexes are marked according to Ref. [117].

Here, all compositions of Ti/Al RMFs show similar types of intermetallic compounds, which are mainly Al-rich. With increasing Al-molar ratios in Ti/Al RMFs, the amount of intermetallic increases. However, for the 1Ti/1Al composition, no expected reaction product of TiAl intermetallic was found. On the other hand, cooled freestanding films were ignited in air by an electrical spark. The available research shows the formation of different reaction products of Ti_3Al, TiAl and $TiAl_3$ for different molar ratios of

uniformly preheated Ti/Al films ignited by hot filament in vacuum as mentioned Ref. [118].

In contrast, our results show the formation of Al-rich intermetallic compounds of $TiAl_3$ and $TiAl_2$ as reaction products after a fast self-propagating reaction. Possibly, oxidation, the allotropic phase transformation of Ti and the presence of premixing zone may influence the final products. However, besides film compositions, ignition method and reaction environment are expected to influence on phase formation.

6.4 Exothermic reaction properties of Ti/Al RMFs

6.4.1 Transformation heat and phase change temperature by DSC

The DSC analysis of the freestanding 1Ti/1Al, 1Ti/2Al and 1Ti/3Al films was investigated and compared. The DSC plots are shown in Fig. 6.4 (a-c). In the first run, Ti/Al RMFs were heated in a range of 100 °C - 550 °C. After cooling at room temperature, the sample was heated again to 550 °C in the second run. The plots of second heating run are also shown in Fig. 6.4 (a) by y-offsett, which confirms the complete phase transformation during the first heating run.

In Fig. 6.4 (a), the intense exothermic peak was found in the temperature range of 420 °C - 480 °C. 1Ti/1Al foil shows three exothermic peaks at (300±10) °C, (470±5) °C and (498±10) °C. Here, the exothermic peaks broaden. For the 1Ti/2Al foil, the exothermic peaks are found at the temperatures of (264±5) °C, (303±5) °C and (472±15) °C. The 1Ti/3Al foil shows exothermic peaks at the temperatures of (425±20) °C and (467±5) °C. The DSC plots also may presence small endothermic peaks. The transformation heat flows are found in the range of (86±10) J/g, (152±15) J/g and (240±8) J/g in 1Ti/1Al, 1Ti/2Al and 1Ti/3Al RMFs, respectively.

Please note that these DSC traces are limited to the maximum temperature of 550 °C and reactions beyond this temperature were not included. Therefore, this transformation heat can not be quantified as total reaction heat. Fig. 6.4 (b) exhibits DSC traces of Ti/Al reactive films at a heating rate of 40 K/min. With increasing the heating rate, peak height increases.

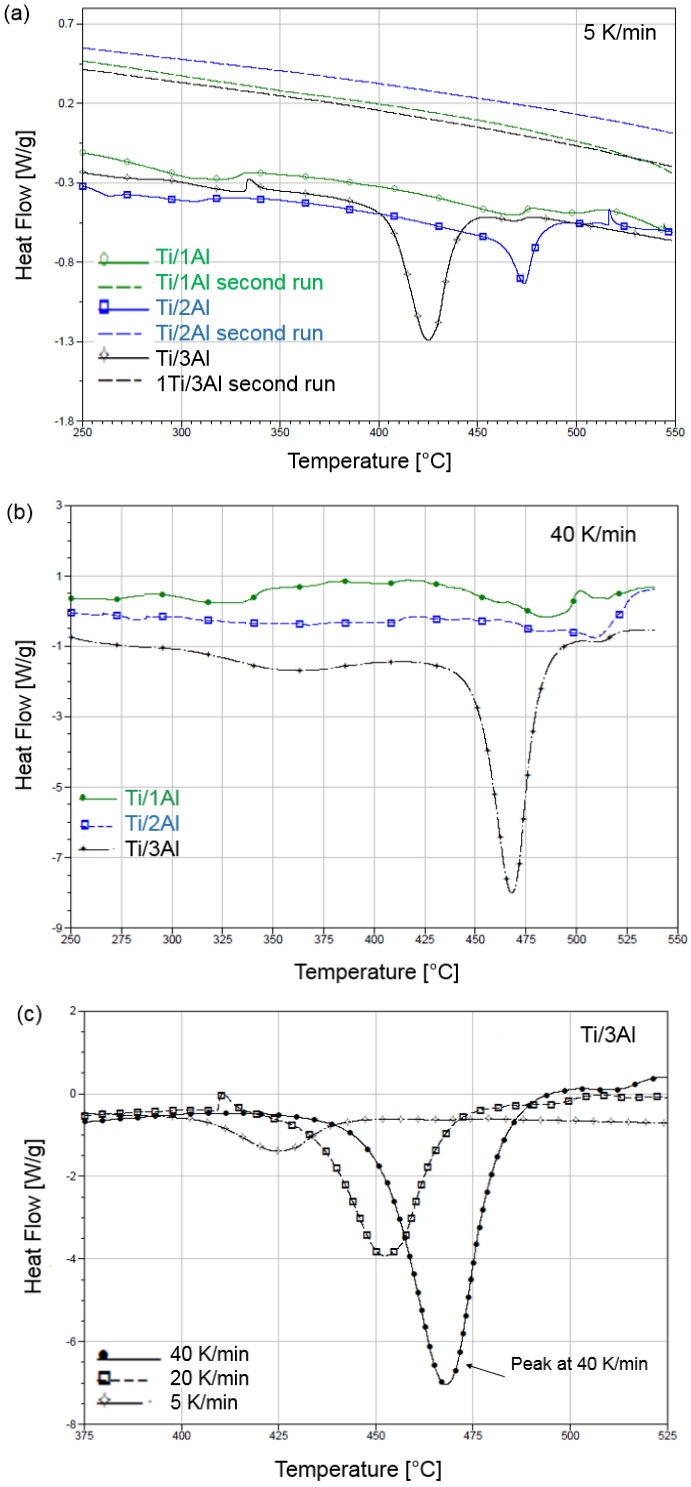

Figure 6.4: DSC traces of all Ti/nAl RMFs at heating rate of 5 K/min (a), 40 K/min (b). DSC traces of Ti/3Al RMFs at different heating rates (c).

Fig. 6.4 (c) shows that exothermic peaks of 1Ti/3Al reactive film shift to a relatively higher temperature and it increases the power signal with increased heating rate. In 1Ti/3Al reactive films, the transformation heat increases from (240±8) J/g to (530±5) J/g with increasing heating rate up to 550 °C. As the premixed layer effects more pronouncely on shorter bilayer, the transformation heat is reduced in RMS with lower bilayer thickness compared to 1Ti/3Al RMFs.

This result shows a similar approach as mentioned in Refs. [119-120]. However, DSC heat flow depends on the reaction mechanism, kinetics and reaction products as mentioned in Refs. [118,121]. Consequently, film morphology can also influence on the phase change temperature and heat release. Recent studies of DSC analyis shows the higher amount of reaction heat in Ni/Al multilayer foils for increasing bilayer thickness [15, 34, 45].

However, this result can be treated as qualitative analysis of Ti/Al films for different compositions. Further works should be performed to adjust the experimental papameters, film thickness and morphology in order to get even higher power signal.

6.4.2 Reaction front velocity of Ti/Al RMFs

The high-speed photographic images of a reaction front propagation with time variation are shown in Fig. 6.5. Here, a stable reaction front propagates through the RMF with a yellow color glow. The reaction front propagates fully through the films within approximately 20 to 35 milliseconds depending on different molar ratios of Ti/Al RMFs. As freestanding Ti/Al RMFs were placed on ceramic plate and self-propagating reaction was investigated at the un-arrested reaction front condition. Therefore, the heat lose is considered to be minimal.

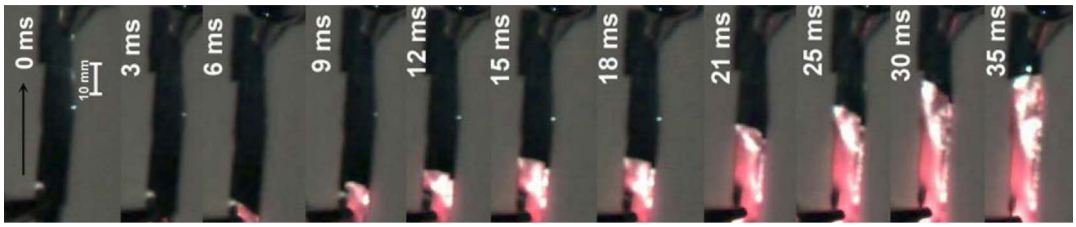

Figure 6.5: High-speed photographic images of a steady state wave front propagation in 1Ti/3Al RMF. Sample was ignited at 9 V electrical spark in air. This foil has bilayer thickness of 37 nm and total thickness of approx. 7 µm.

Moreover, the different ignition potentials were used to study the influences on the reaction speed and propagation manner. Velocity has been measured from the high speed photographic images of a single wave front captured in a top view after applying electrical ignitions in air. Multiple tests were performed to determine the average reaction front velocity at 3 V, 9 V, 15 V and 21 V ignitions.

The reaction front velocity of Ti/Al RMFs, presented in Fig. 6.6, illustrates the dependency on input ignition potentials. The reaction front velocities of Ti/Al films vary between (0.68±0.4) m/s and (2.57±0.6) m/s depending on the ignition potentials and molar ratios. Velocity was measured from a single reaction wave front.

At lower ignition potential of 3 V, all films show lower reaction velocity. For 1Ti/1Al composition, the reaction speed increases until 9 V and then decreases at higher potential. It is believed that at higher ignition potential, films can be overheated and the reaction front can quench due to foil deformation. The reaction front velocity of 1Ti/2Al composition is found nearly constant. The high conductivity and moderate diffusion distance of atom mixing of this film type exhibits nearly constant reaction velocity. With increasing ignition potentials, the reaction velocity of 1Ti/3Al RMF increases and then decreases. The possible reason is that the higher energy input exceeds the critical energy required for reaction front propagation. The current flows in this film heat the system, which enhances the atomic mixing and increases the reaction propagation.

Furthermore, 1Ti/3Al reactive foils show both steady and unsteady reaction propagation. A low reaction velocity was found for this foil type mainly at higher ignition potentials due to unsteady propagation. More details of the unsteady reaction propagation will be discussed in the section 6.4.5. After ignition at different potentials, a single wave front mainly passes through the film. Many authors indicate the dependency of the reaction speed on the periodic layers and for higher periodic layer, the reaction speed decreases [29, 45, 122].

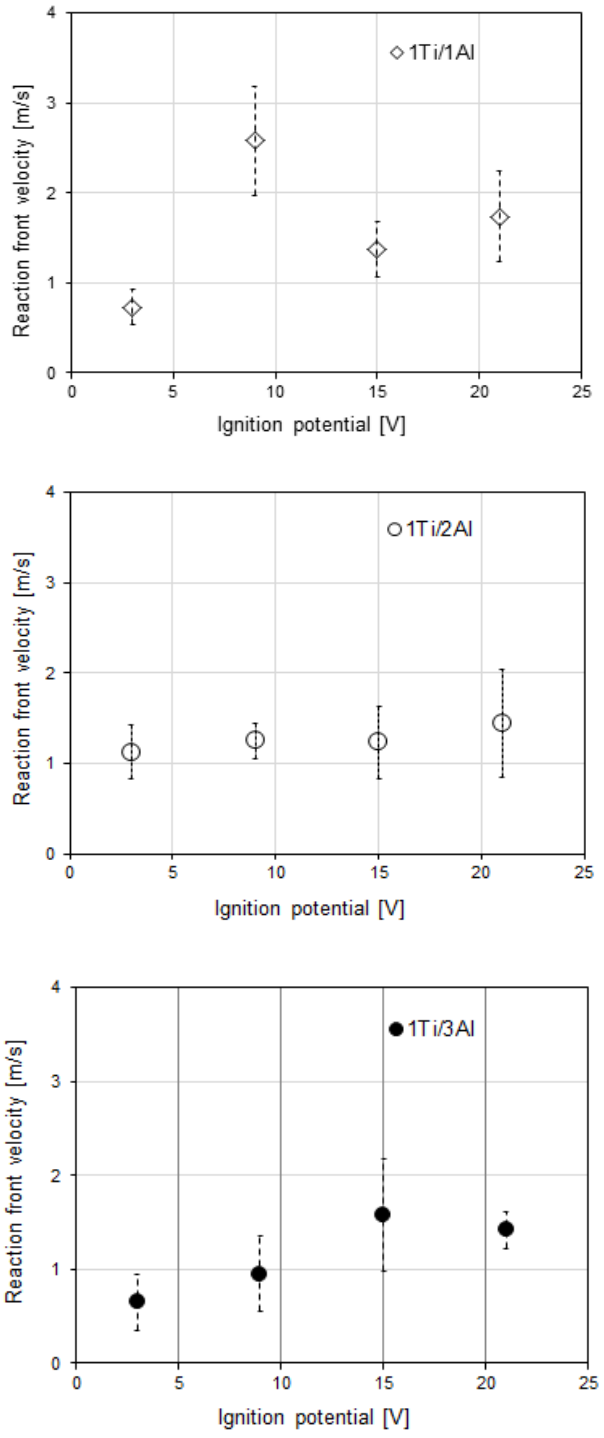

Figure 6.6: Reaction front velocity plots in all Ti/Al films at different ignition potentials in air.

Compared to the recent studies, this work shows the dependency of the reaction velocity on molar ratios and input potentials. Please note that here one or two side ignition methods don't have the influence on the reaction velocity. It is expected that, this mode can act as both point and global heating, which reduces the delay to start the reaction. In all cases, a single wave front was mainly noticed and compared. The average reaction front velocities of Ti/Al RMFs, corresponding film morphology and resistivity are also listed in table 6.1.

However, one exception of propagation characteristic was noticed in 1Ti/3Al reactive films. For such a composition, the dual reaction front was also observed mainly at higher ignition potentials in a few trials, which has been shown in Fig. 6.7. Here, two wave fronts from opposite corner propagate through the 1Ti/3Al film. The higher conductivity of this composition exceeds to the critical ignition conditions and thus it can be heated quickly, which results in the dual reaction front.

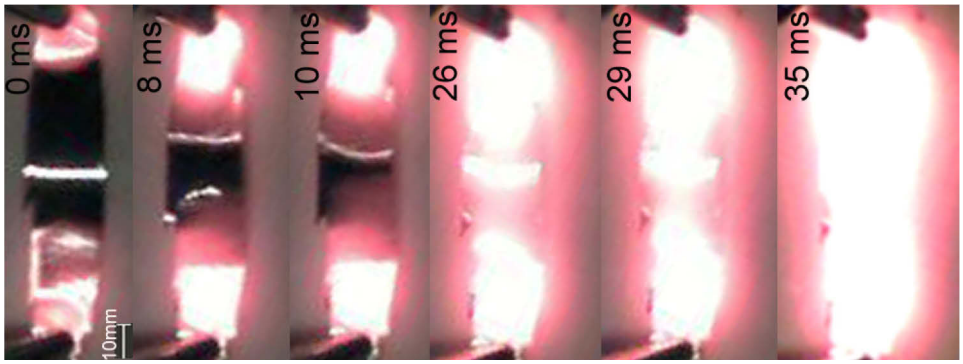

Figure 6.7: High-speed photographic images of a dual reaction wave front propagation in 1Ti/3Al reactive film at 15 V electrical spark. Here, reaction time is relative to the first image.

A similar approach of computational model was mentioned in Ref. [87] for dual front in Ni/Al multilayer. When two combustion fronts from opposite direction met each other, can create hot spot with the higher temperature. According to the combustion theory as demonstrated in Ref. [123], the stored enthalpy in the preheating zones of the colliding reaction waves shows the higher brightness. On the other hand, the brightness profiles of the combustion wave indicate the thermal structure during self-propagating reaction. However, the concept of dual combustion fronts can extend their usability.

In this work, we found the dependency of the reaction propagation on ignition potentials for different molar ratios of Ti/Al films. Too low ignition potential provides poor reaction propagation. On the other hand, too high potential includes higher costs and enhances also unstable reaction propagation. At 9 V ignition, all films exhibit the steady state single wave front propagation with appropriate velocity. Therefore, electrical spark of 9 V can be considered as an optimal potential for exothermic reaction in Ti/Al reactive foils.

Table 6.1: Film morphology, resistivity and reaction propagation in all Ti/Al RMFs.

Morphology	**1Ti/1Al**	**1Ti/2Al**	**1Ti/3Al**
Layer [nm]	10/10	10/18	10/27
No. of periods	185	185	185
Composition (at. % Al)	54	67	77
Electrical resistivity [mΩ.cm]	1.08±0.2	0.75±0.1	0.36±0.1
Propagation mode	Steady	Steady	Steady, unsteady
Reaction front velocity [m/s]			
3 V	0.73±0.2	1.15±0.4	0.68± 0.4
9 V	2.57±0.6	1.25±0.3	0.95±0.5
15 V	1.38±0.3	1.24±0.5	1.60±0.7
21 V	1.83±0.6	1.47±0.7	1.58±0.3

6.4.3 Reaction temperature evaluation

The reaction temperature of Ti/Al RMFs during the self-propagating reaction was recorded by using two-color pyrometer (Metis MQ22). The reaction temperature-time (T-t) profiles for the steady state reaction at 9 V spark are shown in Fig. 6.8. A typical reaction T-t profile of 1Ti/1Al composition, presented in Fig. 6.8 (a), has mainly two sections. In the section-1, the

temperature increases to the maximum temperature (T_{max}) and then drops at section-2.

In Fig. 6.8 (b), the reaction temperatures of the steady propagation in all Ti/Al foils increase sharply to the maximum temperature, which are in the range of 1150 °C and 1260 °C. Here, maximum reaction temperatures of all Ti/Al films are lower than the melting temperature of *Ti* (T_m = 1668 °C) and much higher than the melting temperature of *Al* (T_m = 660 °C). The section-1 at T-t profile indicates the time for preheating and the exothermic reaction. The fast atomic mixing increases the reaction temperature to the maximum reaction temperature, where mostly the reaction products form. In case of liquid or solid-liquid state of reaction products at maximum temperature, final products form during cooling cycle at section-2.

During an exothermic reaction, the reaction proceeds at the narrow zone near the maximum temperature. According to the layer model as mentioned in Ref. [124], the sharp or inclined increment of the heating curve in the temperature profile determines the size of the reaction and preheating heating zone. Here, T-t profiles show a high preheating rate of 1Ti/3Al RMF due to higher conductivity. On the other hand, relatively slower preheating was observed for the 1Ti/1Al foil due to inclined heating curve. Here, it is expected that premixing layer in RMF with smaller bilayer thickness reduces the atomic mixing rate.

During self-propagating reaction, the heat transfer between reaction zone and preheating zone influences on the reaction temperature. In case of premixing layer, thermal diffusivity will be reduced. On the other hand, the allotropic endothermic phase transformation of Ti can also influence on maximum reaction temperature.

Moreover, the shape of the T-t profile exhibits several characteristics during reaction propagation. For instances, the thermal structures indicate the reactant or product melting and formation of reaction products as mentioned [29]. The melting of Al layer can regulate the heat losses during the temperature increment cycle at section-1.

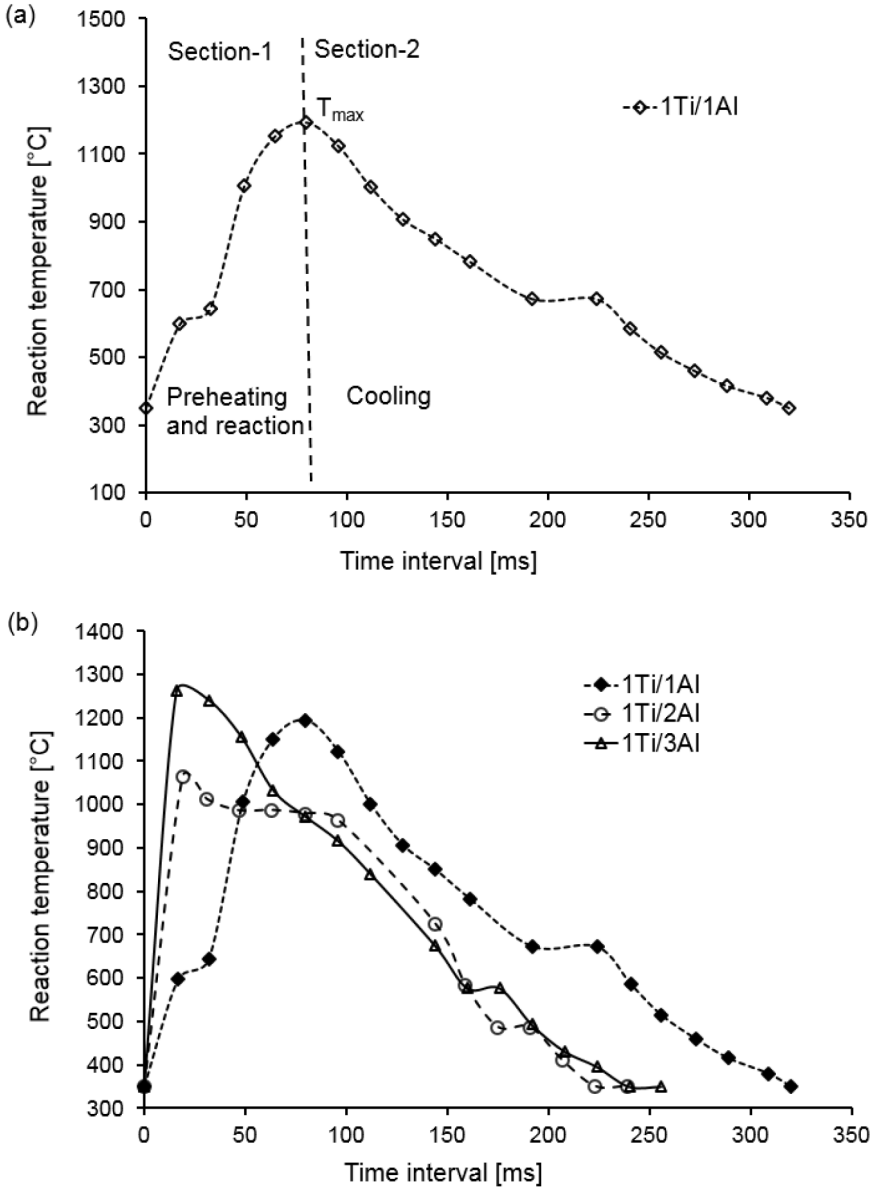

Figure 6.8: Typical reaction temperature-time (T-t) profile of 1Ti/1Al RMF (a). T-t profiles of all 1Ti/nAl RMFs in air (b) measured by two color pyrometer (Metis MQ 22).

Please note that T-t profile can differ depending on the types of reaction products. In particularly, the temperature profile of 1Ti/2Al RMF presented in Fig. 6. 8 (b), exhibits the isothermal section at (1000±15) °C just after to reaching maximum temperature, which is expected to correspond the isothermal eutectoid transformation for the formation of $TiAl_2$ and $TiAl_3$ reaction products. In the cooling cycle, the temperature plateau at (620±50) °C is visible, which is expected to correspond the formation of $TiAl_3$+Al. Moreover, the foil compositions, periodic thickness and reaction constituents influence the temperature profile and the reaction temperature.

On the Other hand, the maximum reaction temperatures were also measured by using two color pyrometer (HQ22) in a high speed mode. Due to collecting more data points in case of high-speed mode, the maximum temperatures are also found relatively high. But the T-t profiles have similar characteristics. Here, the average maximum reaction temperatures of (1298±189) °C, (1213±120) °C and (1215±105) °C were found in 1Ti/1Al, 1Ti/2Al and 1Ti/3Al reactive films, respectively. The maximum temperatures measured by two types of pyrometers at 9 V electrical ignition are listed in table 6.2.

Table 6.2: Maximum reaction temperature (T_{max}) in all Ti/Al RMFs measured by two different two-color pyrometers (MQ22 and high speed-HQ22).

Composition	Avg. T_{max} measured by MQ22 [°C]	Avg. T_{max} measured by HQ22 [°C]
1Ti/1Al	1192±85	1292±189
1Ti/2Al	1151±105	1213±120
1Ti/3Al	1260±32	1215±105

6.4.4 High temperature oxidation during self-propagating reaction

In this work, oxidation behavior was observed in air having a representative T-t profile. The representative temperature profile of Ti/2Al films with an oxidation characteristic is presented in Fig. 6.9. It shows the temperature plateau after reaching to the maximum reaction temperature. It remains in delay for approx. (70±30) milliseconds at high reaction temperature of (1280 ± 50) °C before cooling. Whereas, without oxidation effect, Ti/Al films cool quickly after reaching to the maximum temperature. However, this plot shows both oxidation and non-oxidation characteristics in 1Ti/2Al reactive films in air. However, temperature profile with oxidation has lower slope, which slows down the preheating rate compared to that of without significant oxidation. It is expected that previously formed oxides during storage or oxide formation in the heating cycle to some extent during intermetallic formation slow down the preheating rate, which results in lower slope in the temperature increment cycle.

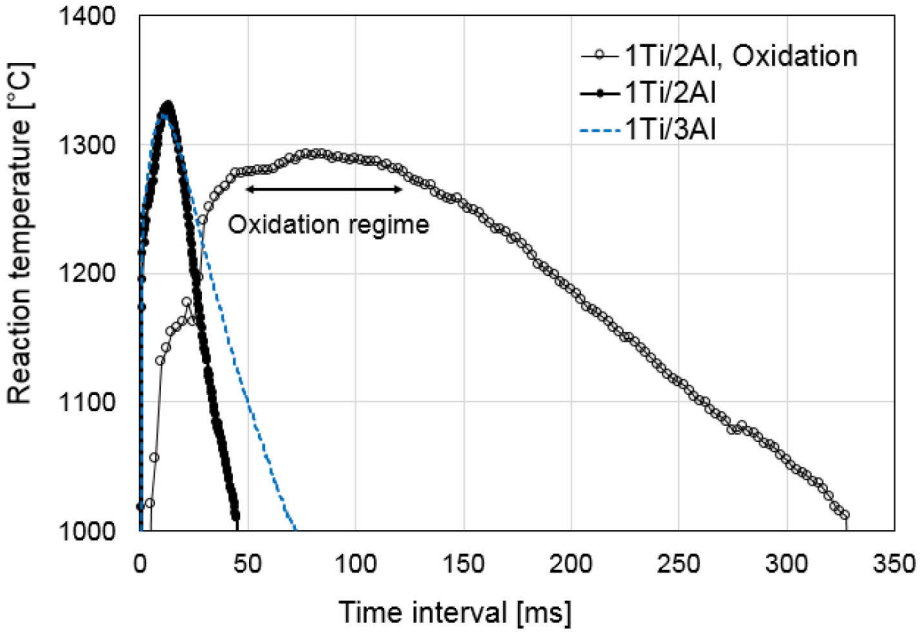

Figure 6.9: T-t profiles of Ti/Al RMFs without and with significant oxidation effect.

However, in this work no room temperature oxidation was focused. The oxidation characteristics with cooling delay at maximum temperature incorporate also a diffusion control process. Here, the dissociation of intermetallic compound and formation of oxides are expected to extend the cooling delay. However, oxide formation of reactants is energetically preferable according to the Ellingham diagram [125]. Normally, metallic films are to be oxidized to some extent, when they were ignited in air. It may have no significant influence, unless it effects on reaction propagation and temperature profile.

The oxidation effect would be considered significant, when it intensely influences on reaction properties. The recent studies show the positive effects of oxidation on reaction heat and temperature in Zr/Al multilayer films ignited in air [126] and also this oxidation can be avoided by igniting these films in vacuum [126-127]. As the characteristic temperature profile of oxidation includes the temperature plateau, therefore, the diffusion phenomenon of oxide growth is also very interesting. The Wagner theory of oxide growth is associated with diffusion controlled process, where the oxidization rate is affected by the oxygen partial pressure and temperature [128]. Here, the diffusion process is also followed by Fick's first law and diffusion flux can be stated as mentioned [129].

$$J_1 = -D.\frac{\Delta C}{\Delta x} = D.\left(\frac{C_2 - C_1}{\Delta x}\right) \quad (24)$$

In this equation, J and D indicate the diffusion flux and diffusion coefficient. C_2 and C_1 are the concentration of the diffusing components within scale Δx. During fast exothermic reaction, this oxidation occurs after formation of reaction products. Therefore, a high diffusion distance it is expected for the oxidation reaction compared to that of intermetallic formation. On the other hand, the volume increment of the oxides can be explained by the Pilling Bedworth (PB) ratios from oxide and metal volume [130]. The formation of sluggish constituents (reactant/product melts or eutectoid or peritectoid components) during exothermic reaction can enhance the oxidation possibility at higher temperature.

Finally, the oxidation plays an important role during a self-propagating reaction by delaying cooling. Therefore, the oxide formation can be interesting in terms of their applications. The application fields that require longer period of localized heat, oxidation effect with temperature plateau could be beneficial. However, during storage the room temperature oxidation of these nanoscale films can be avoided by using additional coatings or melting layers directly on the reactive films.

6.4.5 Reaction propagation mode and its effects on reaction properties

In this work, two types of reaction propagation modes were noticed in Ti/3Al RMF. The steady state reaction mode has intense bright glow as shown in Fig. 6.10 (a). After reaction, the visual appearance of the foil surface is nearly smooth. Here, reacted films retain nearly their shape and texture after reaction. Here, a small amount of deformation can be also noticeable. Another mode is the unsteady reaction propagation without too intense glow. Here, unsteady propagation was found in Ti/3Al RMF mainly for high ignition potentials of 15 - 21 V electrical spark. Specially, the formation of ripple band was observed for unsteady propagation in 1Ti/3Al RMF, which is presented Fig. 6.10 (b). Here, wave like band structures form with a definite interval texture, which have been shown in Fig. 6.10 (c-d). The macroscopic band structure has approx. 160 µm width.

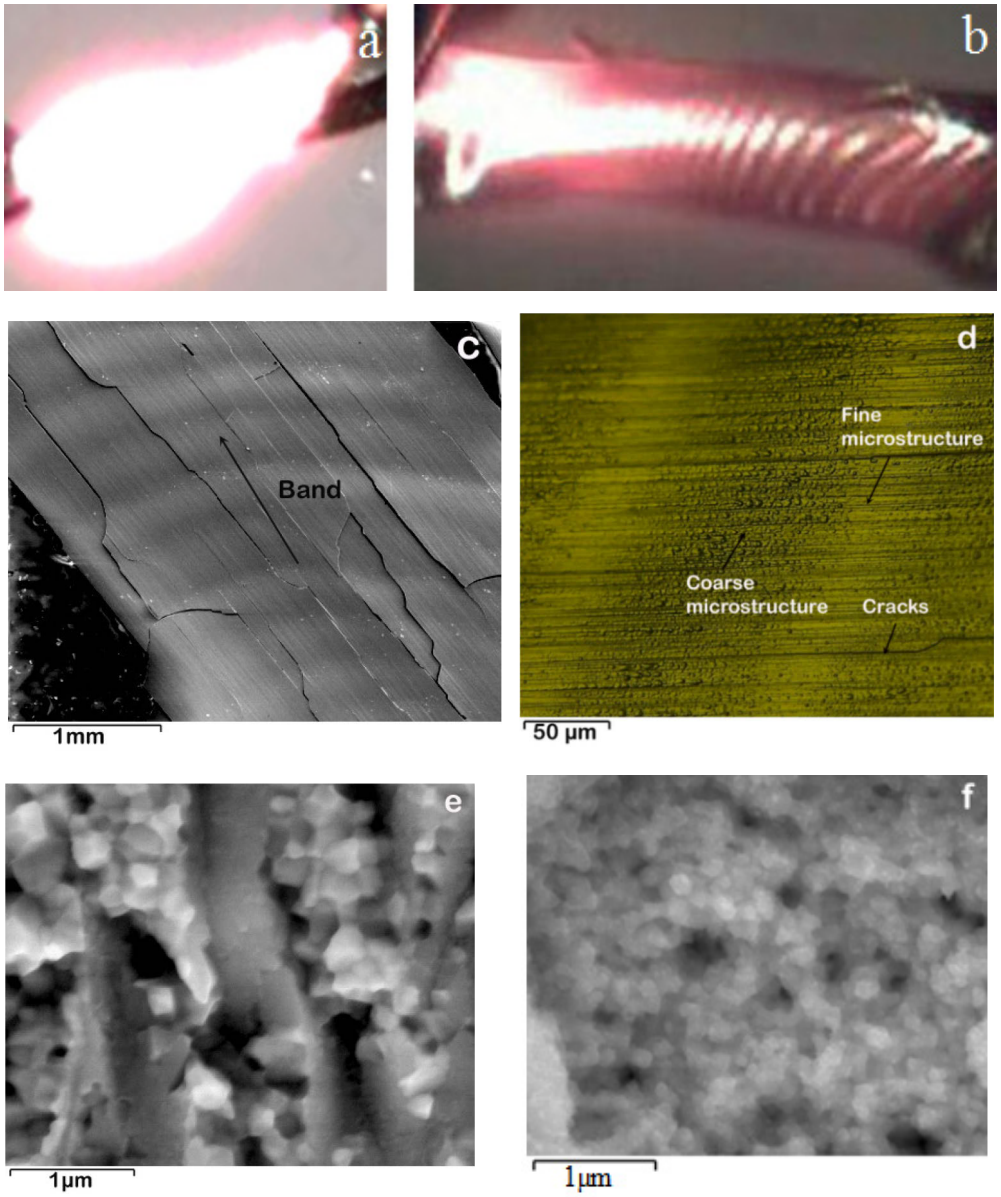

Figure 6.10: Steady state reaction in 1Ti/2Al film (a), unsteady reaction in 1Ti/3Al film (b). Unsteady propagation was found mostly at 15-21 V ignition. SEM Image of macroscopic band formation (c), Optical microscopic image of ripple band with coarse and fine microstructures at top view (d) for unsteady propagation in 1Ti/3Al RMF. SEM cross-section of 1Ti/3Al film for unsteady reaction (e) and steady reaction in 1Ti/2Al film (f).

Fig. 6.10 (d) shows that the coarse microstructures are exist in the band and fine microstructures nearby the band. Cross-sectional SEM image presented in Fig. 6.10 (e) shows the coarsening of reaction products in case of unsteady propagation compared to that of the steady state propagation presented in Fig. 6.10 (f).

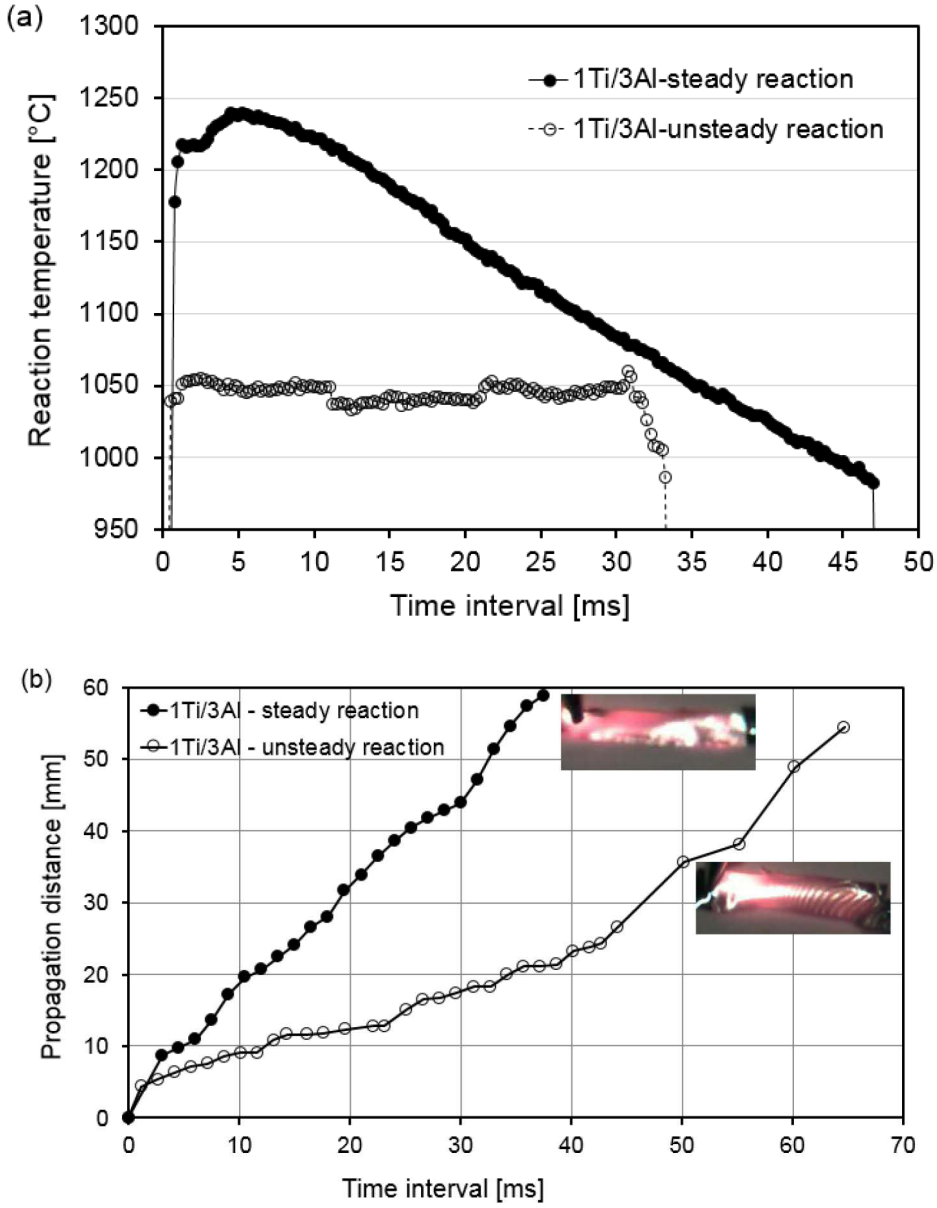

Figure 6.11: Temperature - time profiles for the steady and unsteady state reaction in 1Ti/3Al (d = 37 nm) RMFs measured by two color pyrometer (HQ22) (a), propagation distance - time plot for both propagation modes (b). Measurement was performed in air without pre-heating of freestanding films.

This microstructure coarsening at cross-section and top surface of the reacted films for an unsteady propagation can be explained by the temperature profile, which has been presented in Fig. 6.11 (a). Here, temperature fluctuates in the range of 1033 °C to 1055 °C for a certain period during an unsteady propagation, which is nearly constant. This cascade temperature profile extends for a certain period of time before cooling, which results in coarse and fine microstructures. Fig. 6.10 (f) shows the formation of finely and

homogeneously distributed reaction products in case of a steady state propagation. However, the formation of similar types of reaction products was noticed for both propagation modes. As presented in Fig. 6.11 (a), the maximum temperature of 1240 °C was found for a steady state reaction. Here, temperature increases sharply and then cools down, whereas T-t profile shows temperature fluctuation for an unsteady reaction.

Fig. 6.11 (b) shows how the propagation changes with time during steady and unsteady state reaction. The steady propagation exhibits the steeper slope, whereas an unsteady reaction shows a low slope with a ramp manner. Therefore, unsteady reaction propagation reduces the reaction velocity. Recent studies also report the unsteady propagation in other planner multilayer films [65, 131-133]. The comparative analysis of unsteady propagation in this developed Ti/3Al RMF and other multilayers from available literature has been listed in table 6.3.

This table lists several multilayer films with the characteristics of unsteady propagation. In this case, the ambient temperature, film composition and morphology are expected to influence the unsteady propagation. Recent studies also reported the transition of propagation modes for a given multilayer film, where the influences of preheating and film thickness are expected to shift steady propagation into unsteady in Co/Al and Ti/Al reactive films [11, 39].

In this work, both propagation modes were found in the Ti/3Al RMFs. Here, we can hypothesize that film composition (especially higher bilayer thickness and Al content) and high ignition potentials effect on such an unsteady propagation mode. Here, melting of low temperature Al constituent and the change of mass flow kinetics are expected to fluctuate the temperature. The temperature profile presented in Fig. 6.11 (a) shows the cascade feature, where the temperature of reaction front is not constant due to oscillating manner. Therefore, it expected that reactants mix together and then reaction products form and become coarse-grained.

Table 6.3: Reactive multilayer films with unsteady reaction propagation. Here, ignition conditions (T_o= initial temperature, ignition type and environment), film morphology (d = bilayer, l = total thickness) and reaction properties (υ_{un} = velocity, T_{un} = max. reaction temperature for unsteady propagation) were compared.

Film type **d [nm], l [µm]**	**Ignition conditions,** **T_o [°C]**	**Velocity, υ_{un} [m/s]** **Temperature, T_{un} [°C]**	**[Ref.]**
1Ti/3Al d = 37 nm l = 7 µm	9 - 21 V, in air T_o = 25 °C	υ_{un} = 0.75-1.62 m/s T_{un} = 1044±15 °C	[This work]
Co/Al d = 66-250 nm l = 7.5 µm	Capacitive discharge T_o = 21°C	υ_{un} = 0.5-2 m/s	Adams et al. 2008 [11]
Ti/Al d = 5-110 nm l = 15-20 µm	30 V, Point and global heating, $T_o \leq 400$ K air, vacuum	υ_{un} = 10-20 cm/s T_{un} = 1040±50 K	Rogachev et al. 2004 [39]
Zr/Al/NiCu -	30 V, T_o = -20 °C to 94 °C, in air, on Cu block	-	Trenkle et al. 2005 [131]
Sc/Ag, Sc/Cu d = 41.2 nm l = 2.5 µm	9 V in air	υ_{un} = 0.1-1 m/s	McDonald et al. 2010 [132]
Ni/Al d = 50 nm l = 150-1250 nm	9 V N_2 atmosphere	-	Aurongzeb et al. 2008 [133]

However, temperature profile of an unsteady reaction shows intense heat loss compared to that of steady propagation. This can be due to the convective heat loss besides conductive heat loss. On the other hand, the radiative heat loss also dominances during cooling process. The radiative heat losses for steady and unsteady propagation can be described by the Stephan-Boltzmann law showing equation 25 and 26:

$$Q_{st} = \varepsilon.\sigma.\mathrm{A}_f\left(T_{st}^4 - T_o^4\right) \quad (25)$$

$$Q_{un} = \varepsilon.\sigma.\mathrm{A}_f\left(T_{un}^4 - T_o^4\right) \quad (26)$$

Here, ε is the emissivity, σ is the Stephan-Boltzmann constant and A_f indicates the foil exposed area. T_0, T_{st}, T_{un} indicate the room temperature and maximum reaction temperature for steady and unsteady reaction propagation, respectively. Room temperature is negligible over the high temperature. Therefore, the radiative heat loss ratio is estimated as Q_{un}/Q_{st} = 0.58. In case of unsteady propagation, the thermal structure is also found low.

6.5 Characterization of reacted Ti/Al films

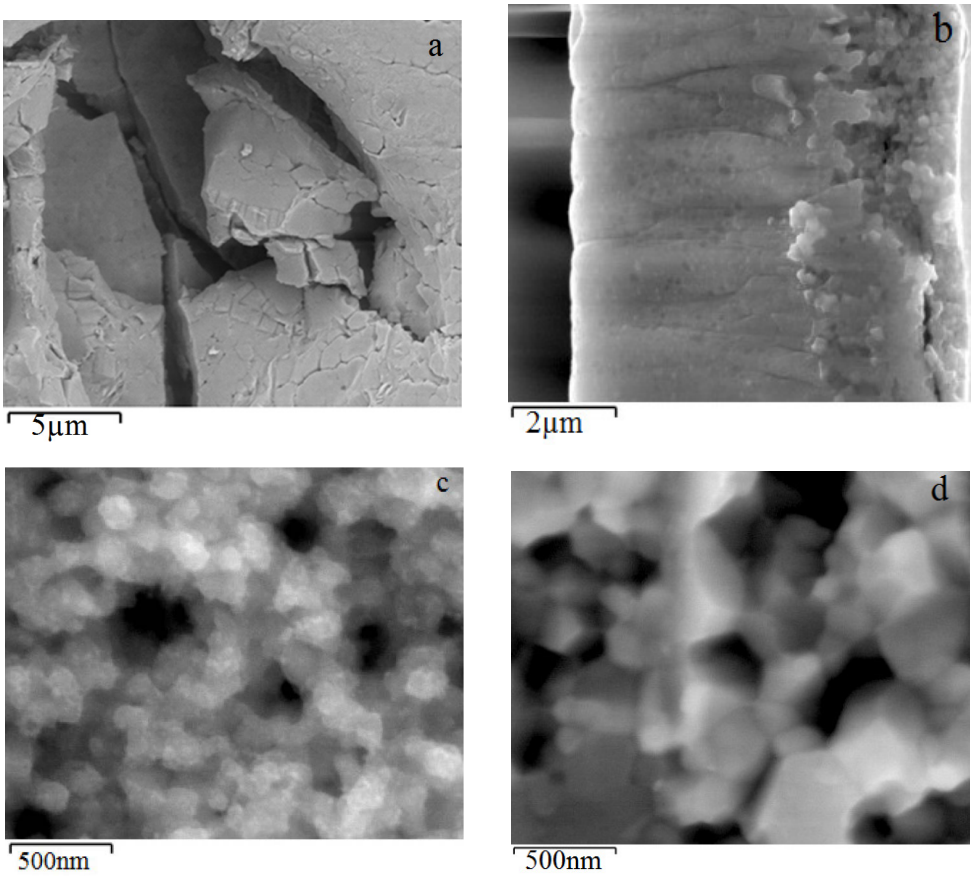

Figure 6.12: Detailed SEM image of the fracture surface of reacted 1Ti/2Al film at the point of activation, top view (a). Cross-sectional SEM images of reacted 1Ti/3Al foils with 90° orientation (b). Reacted 1Ti/2Al (c) and 1Ti/3Al foil (d).

The microstructural features of reacted Ti/Al films are shown in Fig. 6.12 (a-d). Here, Fig. 6.12 (a) shows the reacted Ti/2Al film at a plan view. Reacted

Ti/3Al film presented in Fig. 6.12 (b), shows the fused columnar grains in the cross-section. Here, micro-cracks and pores are exist to some extent. But Ti and Al reactant layers are not detectable anymore after a self-propagating reaction as they produce reaction products, which are visible in Fig. 6.12 (c-d). Here, the microstructural features were changed by fast diffusion in nanoscale. Therefore, two types of diffusion can be considered for the reactive multilayer films with columnar morphology. First diffusion type is the atomic mixing in multilayers. The second one is the diffusion at the columnar grain boundary.

The schematic illustration of both diffusion types is presented in Fig. 6.13. It shows the atom diffusion in the periodic layers and the diffusion at the grain boundary. During self-propagating reactions, the atomic mixing in multilayers is regulated by the diffusion distance. According to the recent studies, this diffusion distance depends on the periodic thickness, molar ratio and the diffusivity of the elemental [45, 65]. The grain boundary diffusion of the columnar microstructure is also very fast due to higher volume fraction of vacancies. Therefore, both diffusion types of nanoscale inter-reactant diffusion in multilayers and columnar grain boundary diffusion increase the reaction propagation rate.

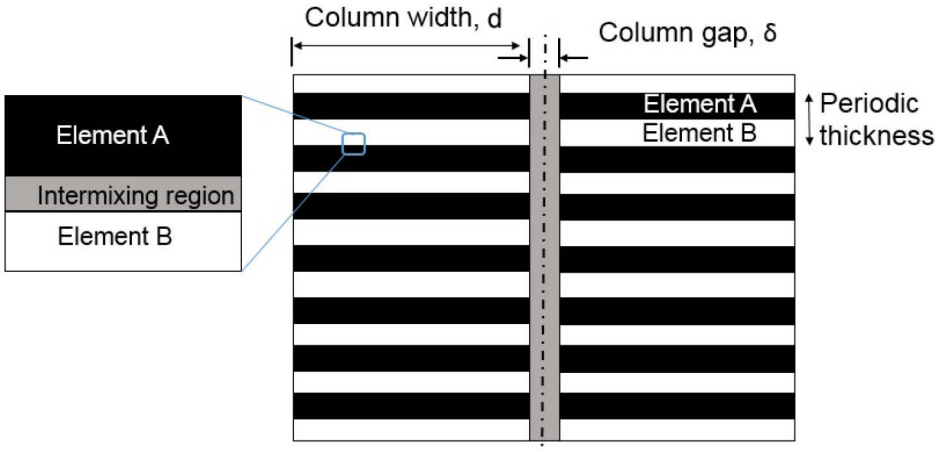

Figure 6.13: Schematic illustration of two types of diffusion during a self-propagating reaction in the columnar multilayer films having reactants diffusion in periodic layers and grain boundary diffusion. Here, A and B elements stand for reactants.

In this work, the mathematical combustion layer model as demonstrated in Refs. [124, 134-135] can be implemented to estimate the atomic diffusion

coefficient in Ti/Al RMFs. This layer model is the theoretical basis of reaction wave propagation of multilayer films.

According to this model, the width of the heated zone near the reaction zone is equal to the ratio of the thermal diffusivity to the reaction propagation speed. Therefore, the time (t_1) of this heated zone is defined by equation 27.

$$t_1 \approx \frac{\lambda}{\upsilon^2} \tag{27}$$

Here, λ is the thermal diffusivity of the reaction medium and υ is the reaction front velocity. The reactant mixing occurs in the narrow zone near the maximum temperature during a self-propagating reaction. The maximum reaction rate is assumed to proceed within the time (t_2), which can be expressed as:

$$t_2 \approx \frac{d^2}{16D} \tag{28}$$

Where, d is the periodic layer thickness and D is the diffusion coefficient. According to the combustion model, the relation between diffusion coefficient and the maximum reaction speed is expressed as follows:

$$\upsilon_{\max} \approx \frac{4\sqrt{\lambda D}}{d} \tag{29}$$

For all Ti/Al foils, the maximum reaction velocities and layer thickness were listed in the table 6.1. Substituting these parameters in equation 29, diffusion coefficient can be estimated. If we consider the largest diffusivity of 1×10^{-4} m^2s^{-1} as mentioned in Ref. [124], the calculated diffusion coefficient (D) of 1Ti/1Al, 1Ti/2Al and 1Ti/3Al foils are found in the range of ~ 1.56×10^{-12} m^2s^{-1}, ~1.05×10^{-12} m^2s^{-1} and ~2.19×10^{-12} m^2s^{-1}, respectively. The diffusion coefficients of Ti/nAl RMFs illustrate a good agreement with the diffusion coefficient of Al in beta-Ti (10^{-13} m^2s^{-1} - 10^{-11} m^2s^{-1}) [136].

Similarly, grain boundary diffusion can be also estimated according to the works as mentioned [137-138]. For simplicity if we consider the width of rectangular columnar grain of d_w and width of grain boundary or columnar

gap of d_g, then lattice diffusion and grain boundary diffusion fluxes (J_l, J_g) can be expressed as follows;

$$J_l = -D_l \frac{dC}{dx} \tag{30}$$

$$J_g = -D_g \frac{dC}{dx} \tag{31}$$

The effective diffusion flux (J_{eff}) can be stated in case of $d_w >> d_g$;

$$J_{eff} = \frac{dJ_l + \delta J_g}{d+\delta} \approx \frac{dJ_l + \delta J_g}{d} = -\left(D_l + \frac{\delta}{d} D_g \right) \frac{dC}{dx} = -D_{eff} \frac{dC}{dx} \tag{32}$$

Here, D_l, D_g indicate the atomic and grain boundary diffusion coefficient. If we assume fraction of the grain boundary area (f), then the effective diffusion coefficient (D_{eff}) can be expressed as:

$$D_{eff} = (1-f) D_l + f D_g \tag{33}$$

Grain boundary diffusion follows also an Arrhenius type temperature dependence. The activation energy for the grain boundary diffusion is smaller. These two diffusion modes in nanoscale columnar Ti/Al multilayer films can even show faster diffusion during the self-propagating reaction, which influences positively on the reaction propagation. Please note that, large columnar gap can influence negatively and reduce reaction heat flow. Therefore, the critical column gap should be defined in the future studies.

In this work, the formation of protrusion microstructure was observed mainly for unsteady reacted 1Ti/3Al films. SEM images of the protrusion structure are presented in Fig. 6.14 (a, c). The AFM topographical image has been also shown in Fig. 6.14 (b). It shows that the sizes of protrusion microstructures vary within 2-15 µm. They lift up from the surface to the height of approx. 250-400 nm. The phenomenon for protrusion structure formation is not clear yet. However, it is expected that Al-evaporation by changing vapour pressure at high reaction temperature and microstructural features can influence on it.

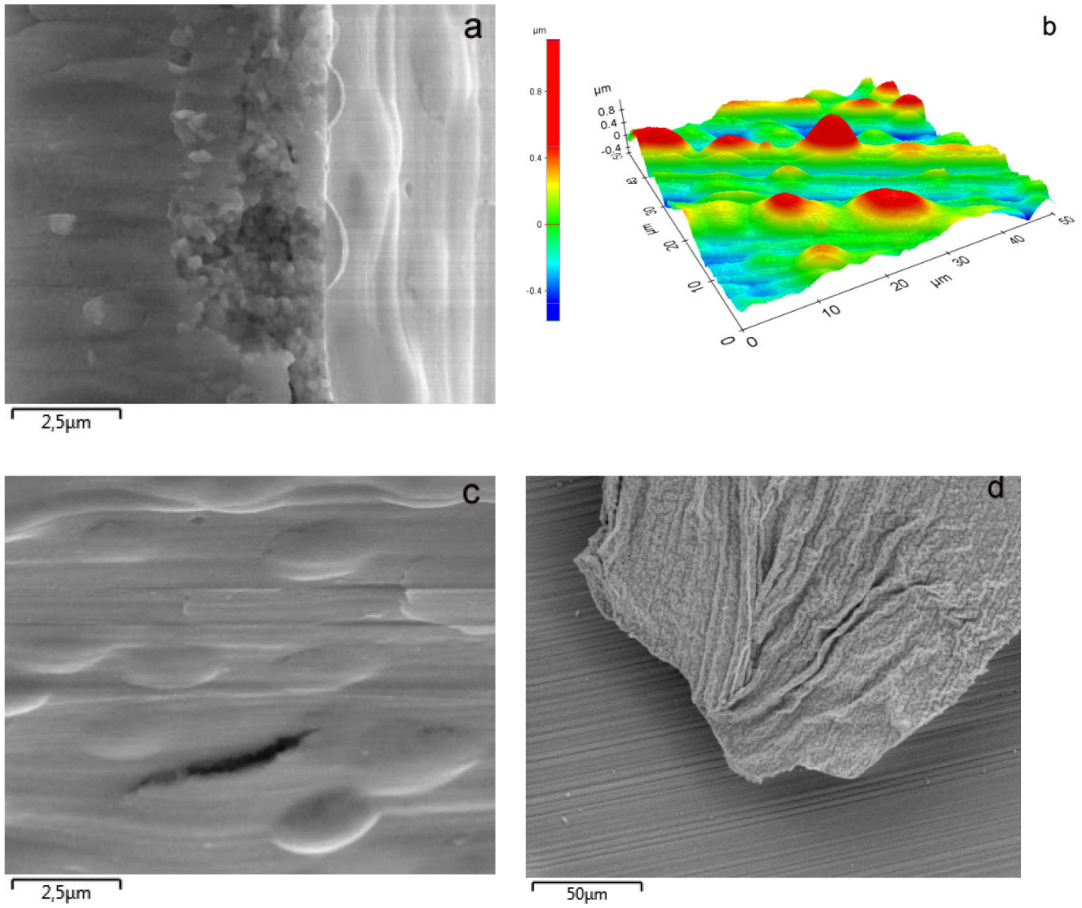

Figure 6.14: Cross-sectional SEM image (a) and AFM topographic image (b) of protrusion microstructure in the unsteady reacted 1Ti/3Al film. Micro cracks and protrusion structure in reacted Ti/3Al reactive film (c). Deformation of reacted 1Ti/1Al film (d).

In addition, possible defects formation during a self-propagating reaction was also characterized. The formation of micro crack is also shown in Fig. 6.14 (c). The residual stress or thermal stress due to fast cooling from high reaction temperature can be responsible for micro crack formation. The reacted 1Ti/1Al film with an excessive deformation has been shown in Fig. 6.14 (d). In this case, a curled feature forms and a high amount of heat loss is expected by doing excessive deformation, which can quench further reaction. The overall summary of our developed Ti/Al RMFs comparing with available literatures is listed in table 6.4.

Table 6.4: Comparative analysis of Ti/Al RMFs. This table includes the fabrication method, film morphology (bilayer, d; film thickness, l) and reaction front velocity (υ).

Foil type	**Fabrication method, *d* [nm], *l* [µm]**	**Ignition type, conditions**	***υ* [cm/s]**	**Reaction mode**	**[Ref.]**
1Ti/1Al 1Ti/2Al 1Ti/3Al	Magnetron sputtering *d* =20-37 nm *l* =3 - 7 µm	3 - 21 V no preheating	68 - 257	Steady Steady Unsteady	[This work]
Ti/Al Ti/3Al	Plasma sputtering *d* =5-70 nm *l* =18-20 µm	hot W wire and sparks; preheating	15 - 45	Steady Pulsating	Gachon et al. 2005 [118]
Ti/Al Ti/3Al	Magnetron sputtering *d*=5 -110 nm *l*=15-20 µm	W wire and 30 V electric pulse, Preheating	10 – 45 max. 150	Steady pulsating	Rogachev et al. 2004 [39]
Ti/Al Ti/3Al	Magnetron sputtering *d*=100 - 110 nm *l*=16±2 µm	W wire, heat pulse; no preheating for Ti/3Al	5 - 26 150	-	Grigoryan et al. 2001 [139]
Ti/Al	Cold rolling *d* = several µm *l* = 280 µm	flame heating; preheating	-	No self-propagating reaction	Qiu et al. 2009 [140]

This table describes the fabrication methods, film morphology, ignition conditions and reaction propagation. For example, Ti/Al films fabricated by PVD method are showing spontaneous self-propagating reaction than cold rolled. In addition, the steady reaction mode regulates the reaction properties by assuring the higher temperature and reaction velocity. Therefore, to expand their usability in joining or other applications, the detailed description of the multilayers fabrication, testing and corresponding reaction properties will help to design the Ti/Al films as a controllable heat source.

7 Zr/Al reactive multilayer film

7.1 Synthesis and characterization of Zr/Al RMFs

Secondly, Zr/Al RMFs were investigated as a middle energy classed reactive material system. Previously, Thermo-Calc results of Zr-Al system presented in Fig. 5.2, exhibit that intermetallics formation for (0.5-0.67) Al-mole fraction can release a high reaction heat. Therefore, equimolar 1Zr/1Al composition was chosen and deposited with different bilayer thicknesses in the range of 20 nm and 55 nm. The microstructural features of the as-deposited films are presented in Fig 7.1 (a-b). SEM cross-sectional image presented in Fig. 7.1 (a), exhibits fine columnar microstructure. In the columnar structure, the alternating layer sequence of Zr and Al reactants are observed in TEM image as demonstrated in Fig. 7.1 (b). Here, Zr (grey) and Al (light) bilayers are arranged in a controlled thickness. Between reactant layers, the premixing layer (*w*) with a thickness of 1-3 nm was estimated.

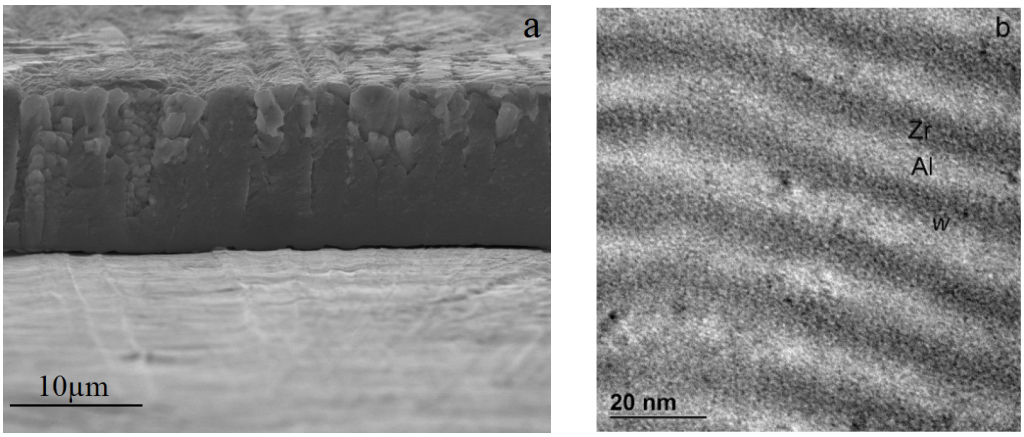

Figure 7.1: Cross-sectional SEM image of as-deposited freestanding 1Zr/1Al film (a). This film has bilayer of approx. 37 nm and total thickness of (11± 0.5) µm. TEM image of 1Zr/1Al RMF with controlled and homogeneous multilayer arrangement (b). Here, w indicates the premixing layer between Zr and Al reactant layers.

The quantitative image analysis of all 1Zr/1Al RMFs shows the average bilayer thicknesses of 20 nm, 25 nm, 30 nm, 37 nm, 45 nm and 55 nm. Here, total thickness varies in the range of (8±0.3) µm and (17±1) µm. The elemental analysis conducted by EDX equipped with SEM, shows the presence of 56 at. % Al and 44 at. % Zr in as deposited films. If we correlate the overall film, morphology with the structure zone model [113-114], this

columnar texture can fit mainly to the zone T. The overall film morphology plays also an important role to introduce additional grain boundary diffusion and to control the heat flow. However, with increasing film thickness, texture may slightly shift to the zone-2 to some extent. The details of homogeneous film growth will be discussed in the section 10.1.

7.2 Reaction products identification by XRD

The phase formation in reacted 1Zr/1Al RMFs films was investigated. Fig. 2 exhibits XRD diffractograms for increasing bilayer thicknesses after a fast self-propagating reaction in air. All reflexes were analyzed according to ref. [141]. The results indicate the formation of intermetallic compounds of tetragonal Al_3Zr (COD # 2100751, 2100751) and orthorhombic AlZr (COD # 4062731). It also shows the presence of ZrO_2 (COD # 9009919, # 2101234 and # 2300296), Al_2O_3 (COD # 1200005) and a small amount of hexagonal Zr (COD # 9008523) in the reacted film. With an increasing bilayer thickness, the similar intermetallics have been found. Many authors indicate also the formation of coherent metastable phase Al_3Zr with a simple cubic structure (L_{12}) in Al rich Zr-Al alloy, which is responsible for the effectiveness of Zr to control recrystallization [142]. In this work, stable tetragonal Al_3Zr was noticed.

The important features of oxide formation were observed in 1Zr/1Al films ignited in air during a self-propagating reaction. These characteristics are expected to influence on such reaction kinetics to form Al-rich major intermetallic compounds of Al_3Zr and then AlZr. Here, hcp-Zr transforms to bcc-Zr occurs at the temperature of 863 °C. The maximum solubilities of Al in hcp-Zr and bcc-Zr are about 11.5 at.% and 26 at.% [107]. On the other hand, hcp and bcc-Zr can dissolve different concentrations of oxygen. The oxygen solubility in bcc-Zr is as high as 10.5 at. % oxygen at high temperatures, while the maximum solubility in hcp-Zr reaches values as high as 28.6–35 at. % oxygen [97, 143]. The oxygen solubility increases up to 35 at. % with increasing temperatures in hcp-Zr. The oxygen occupancy in hcp Zr was also demonstrated in the work of Puchala et al. [144]. With increasing bilayers, the similar reaction products and increasing amount of oxides have been found. The details of oxidation will be discussed in the section 7.3.4.

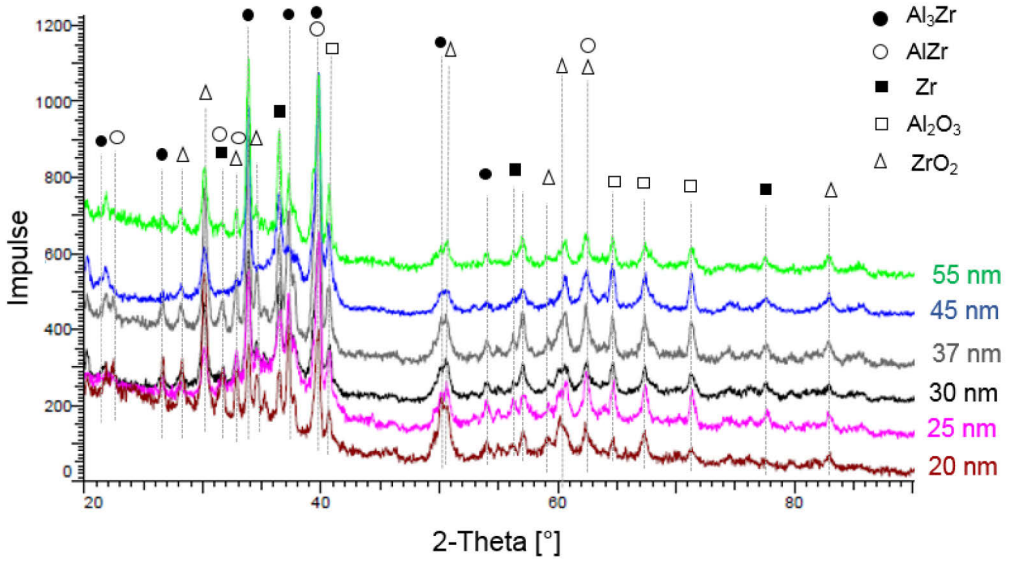

Figure 7.2: XRD patterns of reacted 1Zr/1Al RMFs for different bilayer thicknesses after a self-propagating exothermic reaction in air. Traces are offset for clarity. Reflexes are marked according to Ref. [141].

7.3 Exothermic reaction properties

7.3.1 Evaluation of phase change temperature and heat flows

The DSC plots of 1Zr/1Al RMFs are shown in Fig. 7.3. DSC traces for different bilayer thicknesses were performed at heating rate of 5-30 K/min within temperature range of 100 °C to 550 °C. A high power signal was obtained for 30 K/min. The second heating run has been performed, which confirms the complete phase transformation in first run. In Fig. 7.3, DSC curves of 1Zr/1Al RMFs at the heating rate of 30 K/min are shown by Y-offset. For different bilyer thicknesses, the major peak was detected at the temperature of (345±20) °C. Shallow peaks also may exist in the temperature range of 470 °C-520 °C. For 20 nm bilayer, the major exothermic peak broadens. On the other hand, the increased volume fraction of premixed zone decreases the reaction heat for smaller bilayers. For other samples, the peak height increases and becomes pronounce with bilayers. This is because of the formation of higher amount of reaction product. It also shows the peak shift to higher temperature for incresed bilayer thickness and also may appear other small peaks. By integrating the net heat flow with respect to time based on base line, the transformation heat can be obtained. Here, heat flows vary in the range of 224 J/g and 282 J/g for increasing bilayers. Please note that, at

this heating rate or given mass (5 mg) or film thickness, the power signal is not high. Therfore, the transformation heat can not be quantified as reaction heat and it requires further development. However, this result can be treated as qualitative heat analysis for different bilayers. In addition, this result shows the similar approach to the recent studies, where bilayer dependent heat flow has strong influence on the shape, number and position of the exothermic peaks in Al-Ni multilayers as mentioned in Refs. [6, 34, 45].

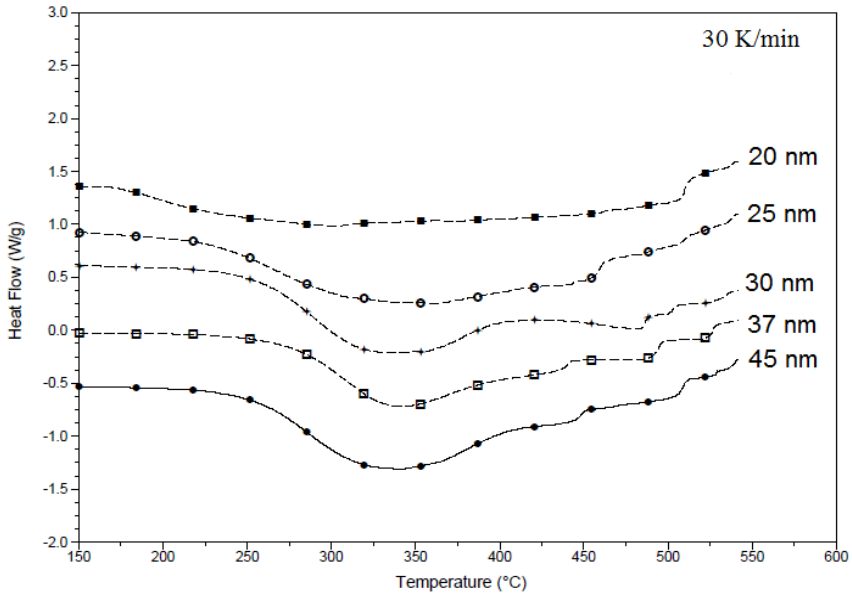

Figure 7.3: DSC plots of Zr/Al RMFs for different bilayer thicknesses.

In practice, a premixed layer is commonly formed in multilayers during the deposition process. By considering the formation of similar intermetallic also in multilayers, the reaction heat can be analyzed by using equation 11. For simplicity, the reaction heat for the major intermetallic compound of $ZrAl_3$ (ΔH = -40.7 kJ/mol) was quantified for premixed layer thickness of 1-3 nm. The dependency of reaction heat on premixed layer has been plotted in Fig 7.4. It shows that with increasing premixed zone, the reaction heat decreases for a given bilayer. For lower bilayer thickness, premixed layer reduces the reaction heat pronouncedly.

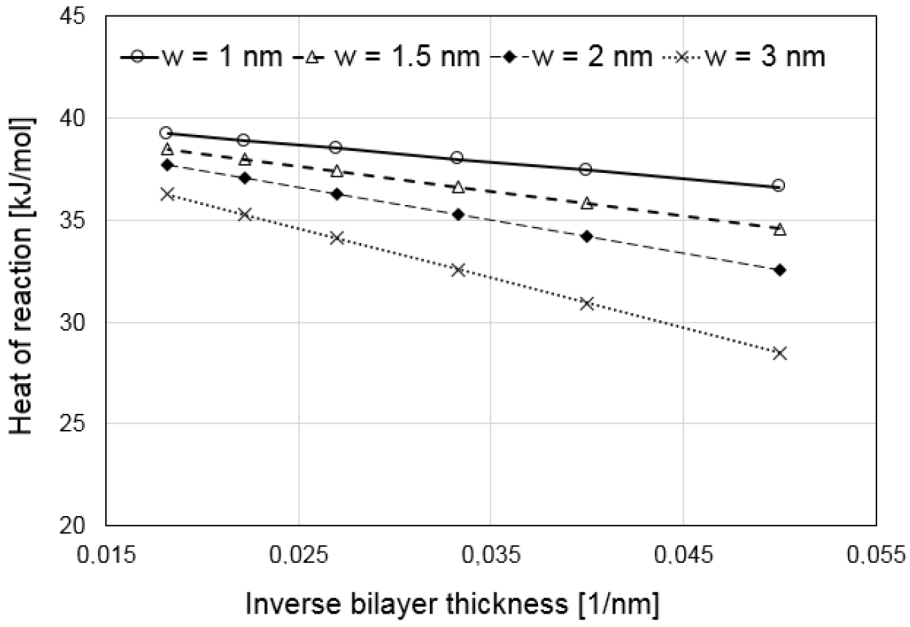

Figure 7.4: Reaction heat as function of premixed layer for bilayer thicknesses in 1Zr/1Al RMFs.

7.3.2 Reaction front velocity of Zr/Al RMFs

The reaction front propagation of freestanding 1Zr/1Al RMF was characterized in the plan view after 9 V ignition. Then the reaction front velocity was measured from successive propagation images with time variation. The successive photographs captured by a high speed camera of 1Zr/1Al foil have been shown in Fig. 7.5. It shows that a reaction front propagates through the foils with a bright glow within millisecond. For this foil type, the reaction velocity has been measured (0.49 ± 0.2) m/s. Zr/Al foils take less waiting time to start the reaction compared to the Ti/Al RMFs.

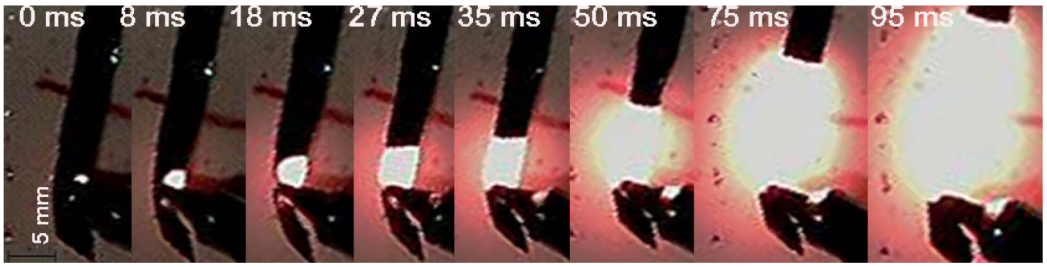

Figure 7.5: High speed photographic images of a reaction front propagation in 1Zr/1Al RMF (d = 20 nm, l = 8 µm) at 9 V electrical ignition in air.

The reaction front velocity as a function of bilayer thickness has been shown in Fig.7.6. Multiple tests were performed to determine the average reaction

front velocity at 9 V in air. The reaction front velocity of at least ten samples for every bilayer thickness has been measured.

Fig. 7.6 illustrates the dependency of reaction velocity on bilayer thickness. A high reaction speed of (1.22±0.4) m/s has been found for 30 nm bilayer thickness. At increased bilayer thickness, the reaction front velocity decreases. The possible reason is that the higher bilayers increase the diffusion distance, which slows down the diffusion rate and reaction velocity. A similar attribution of bilayer dependent reaction speed of other multilayers has been mentioned in Refs. [6, 45, 125]. The recent study indicates also the unsteady propagation in 1Zr/1Al reactive films with bilayer thickness of 90 nm [37]. However, only steady state reaction has been noticed in all Zr/Al RMFs (d = 20 - 55 nm) in this work.

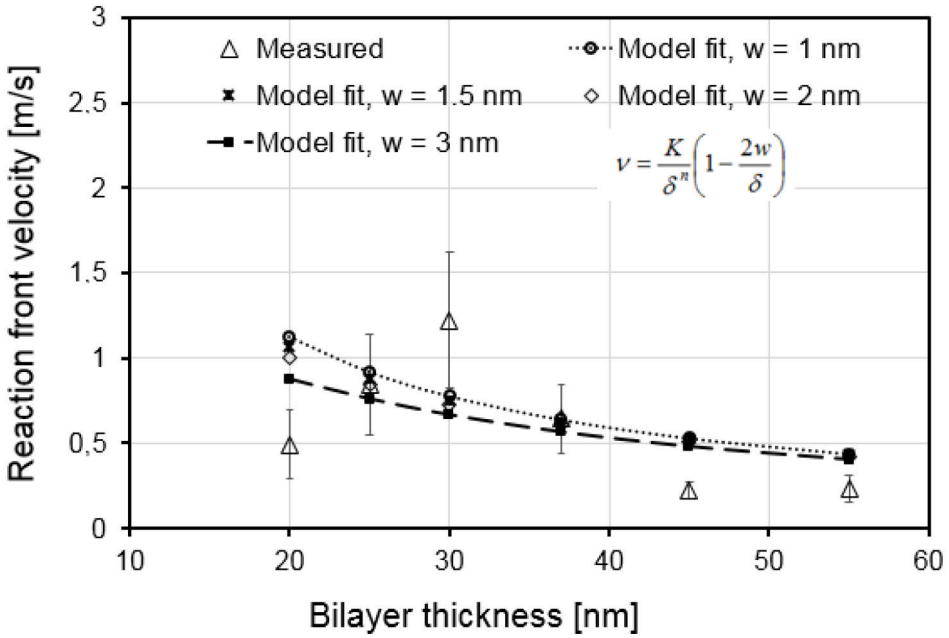

Figure 7.6: Reaction front velocity vs. bilayer thickness plot in 1Zr/1Al reactive film. The measured reaction velocity was then compared with a model fit as developed by Barbee et al. 1996 [43] for premixed layer thickness of w = 1-3 nm.

The measured reaction front velocity of 1Zr/1Al RMFs in this work was then compared with the empirical model fit as mentioned in Ref. [43]. By considering fitting parameter, n = 1 and energy release rate constant, K = 25 nm.ms^{-1} as suggested in Ref. [37, 43] for one dimensional diffusion, a numerical model has been fitted by using equation 10. The reaction front velocity for this model fit for premixed layer thickness of 1-3 nm, has been

shown also in Fig. 7.6. This model fits well the reaction velocity for bilayer thickness of 25-40 nm. It underestimates the velocity for higher bilayer thickness. Possibly, reaction kinetics influence on this reaction velocity. However, this model fit also shows the pronounced reduction of reaction velocity for very shorter bilayer than thicker bilayer. Here, one should consider the deviation of one dimensional atomic diffusion in bilayers and also account the allotropic phase change, constituent melting or oxidation during the reaction.

7.3.3 Reaction temperature in Zr/Al RMFs

The T-t profiles of 1Zr/1Al RMFs have been shown in Fig. 7.7. Initially, the temperature increases to the maximum temperature and then drops. Due to chemical mixing of distinct reactants, it reaches to the maximum temperature, which is lower than the melting temperature of Zr (T_m = 1855 °C) and much higher than the Al (T_m = 660 °C). Therefore, the state of reaction products is expected to be solid and liquid. In the temperature increment cycle, the allotropic hcp to bcc phase transformation of Zr can influence on the final reaction temperature and heat. The temperature decreases after reaching to the maximum temperature. Interestingly, a plateau at 1275 °C during cooling cycle was found for shorter bilayer thickness of 20 nm and 25 nm. Here, we expect the secondary isothermal reaction to form the stable reaction products from metastable phases. With increasing bilayer thicknesses, the cooling characteristics change and become slow to cool down. Here, the sluggish reaction is expected to slow down the cooling. Possibly the reaction kinetics, chemical compositions, premixing and oxidation effects influence on this temperature profile.

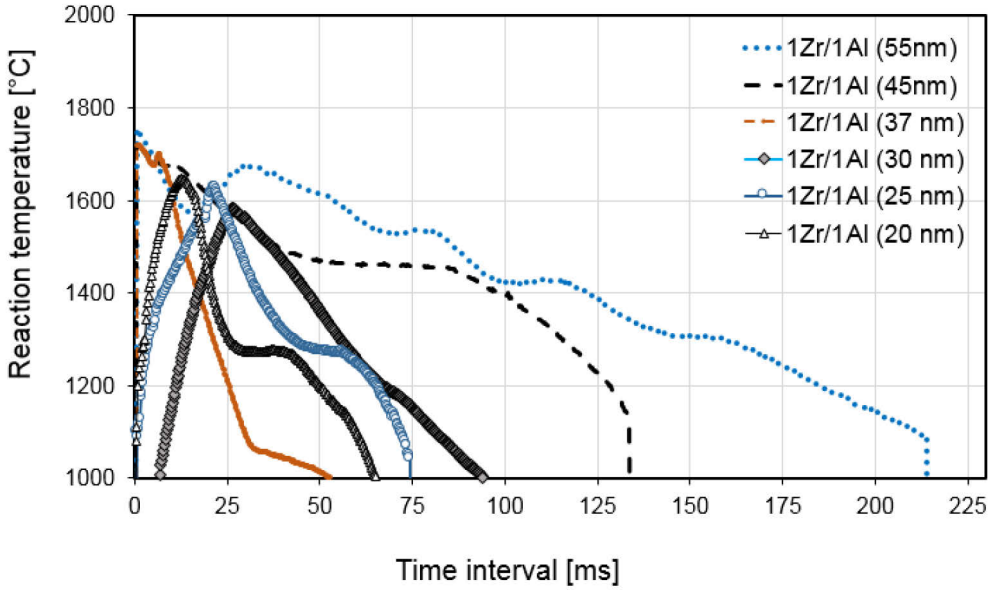

Figure 7.7: T-t profiles of 1Zr/1Al reactive films for various bilayer thickness. Temperature measurement was performed in air using two-color pyrometer (Metis HQ22) in a high speed mode.

Moreover, the reaction temperature profile can be influenced by reaction kinetics; atmosphere and heat loss by reactant melting, propagation mode mentioned for other multilayer foils [29, 34, 124]. The overall temperature plot shows similar profile estimated for the Ni/Zr multilayers [145]. Fig. 7.8 illustrates the dependency of maximum reaction temperature on bilayer thicknesses. The measured average temperature is the result of seven measurements with error bars. Here, the measured reaction temperatures vary in the range between 1581-1707 °C for different bilayers. With increasing bilayer thicknesses, the reaction temperatures increase. This is because of the pronounced effect of premixed layer for smaller bilayer thickness to reduce thermal flow. In addition, the increment trend of reaction temperature is not steep for larger bilayers. This is because of the formation of similar types of reaction products. However, these results are consistent with the results in Refs. [37, 127].

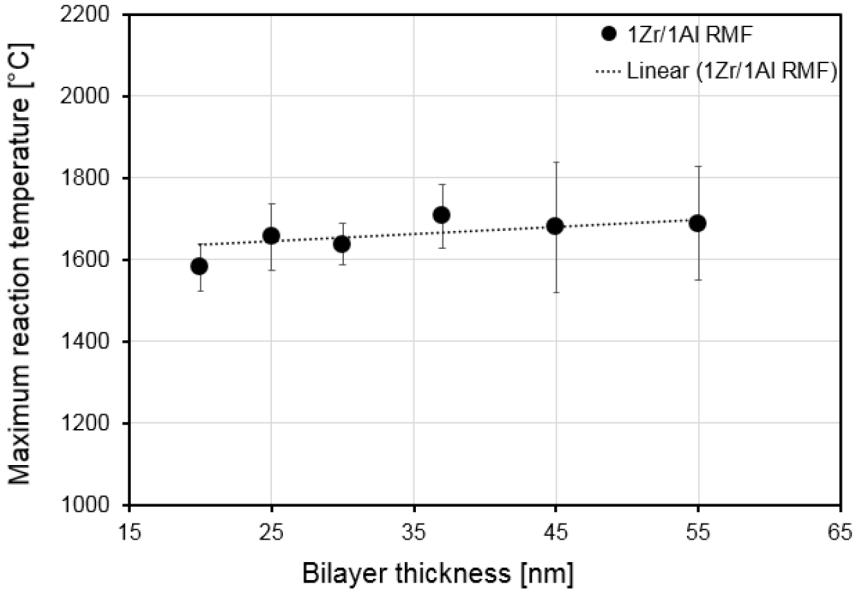

Figure 7.8: Maximum reaction front velocity vs. bilayer plots in 1Zr/1Al RMFs. Freestanding foils were activated by 9 V electrical arc in air and temperature was measured by two-color pyrometer (Metis HQ22) in high speed mode.

7.3.4 Oxidation effects during reaction in Zr/Al RMFs

Fig. 7.9 shows the temperature-time profiles with an oxidation effect in Zr/Al RMFs for different bilayers. A typical T-t plot includes the temperature increment to the maximum temperature and then the cooling. However, this characteristic changes due to presence of the temperature plateau in T-t profile, which characterizes a cooling delay due to an additional oxidation reaction during a self-propagating reaction in films ignited in air.

For different bilayer thicknesses, a rapid rise of temperature to the maximum temperature has been observed in Fig. 7.9. In Zr/Al RMF (d = 20 nm), the cooling occurs just after reaching the temperature of T_{max}. However, Zr/Al RMFs with higher bilayers exhibit the temperature plateau for an extended duration, which corresponds the significant oxidation during a self-propagating reaction in air. A similar approach was reported in Ref. [126].

The result shows that the cooling delay time (t_a) in 1Zr/1Al film (d = 20 nm) is nearly zero. With increasing bilayer thicknesses, the cooling delay increases. For bilayer thicknesses of 30 nm, 37 nm and 55 nm, the cooling delay times extend as follows; t_b = ~ 30 ms within 1536-1546 °C, t_c = ~ 41 ms within 1620-1650 °C and t_d = ~195 ms within 1475 – 1588 °C,

respectively. The overall oxidation characteristics for different bilayers are also listed in table 7.1.

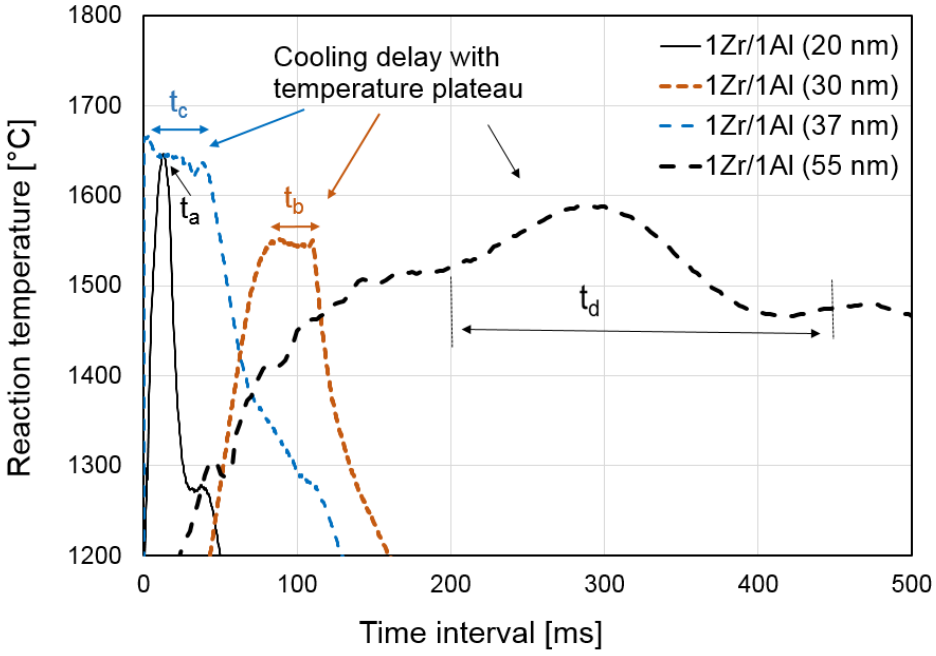

Figure 7.9: Reaction T-t profiles of 1Zr/1Al RMFs with oxidation characteristic. These films were ignited in air. Here, the cooling delay time (20 nm) ta is nearly zero and (55 nm) td > (37 nm) tc > (30 nm) tb.

Table 7.1: Oxidation characteristics in 1Zr/1Al RMFs for different bilayer thicknesses during a self-propagating reaction in air.

Bilayer thickness [nm]	Temperature plateau [°C]	Significant oxidation
20	No	No
25	No	No
30	1536-1546	Yes
37	1508-1552	Yes
45	1473-1509	Yes
55	1475-1588	Yes

It shows pronounced oxidation effects mainly for higher bilayer thickness, where no temperature plateau was identified for bilayers below 25 nm. Here, the significant oxidation was characterized by presence of the temperature plateau, which was found slightly lower than the maximum reaction temperature. Therefore, it is expected that secondary oxidation reaction occurs after the formation of intermetallics and temperature plateau corresponds the dissociation of intermetallic compounds to form oxides. A similar approach was reported in Refs. [126-127], where ZrAl intermetallic dissociates to form ZrO_2 and $ZrAl_2$ and also oxidation reaction follows a combined diffusion limited and surface reaction growth model in 1Zr/1Al composition ignited in air. In this work, besides formation of intermetallic compounds of Al-rich Al_3Zr and AlZr as major products, oxides of Zr and Al were noticed as minor products in films ignited in air. However, no oxide of intermetallic compound (e.g. $Zr_xAl_yO_z$) was found.

On the other hand, the oxidation mechanism for the formation of Al_2O_3 can differ compared to that of ZrO_2. With a temperature rise during an exothermic reaction, the Al may evaporate due to the change of vapor pressure and can form oxides. It may also presence mixed oxides on the film surface. In addition, oxygen can diffuse through the columnar grain boundary. On the other hand, oxides of Zr-O preferably form than Al-O according to the Ellingham diagram at high temperature above 500 K [125]. Recent study also reports that the oxidation affinity reduces in Al-rich Zr/3Al films due to insufficient Zr content even ignited those films in air [126].

For comparison, 1Zr/1Al RMFs ignited in argon 4.6 were characterized. XRD analysis presented in Fig. 7.10, shows the presence of a small amount of only ZrO_2. However, no Al_2O_3 was observed in films ignited in argon. It is expected that purity grade of Ar 4.6 and as-deposited oxides in films can influence on the formation of ZrO_2. However, it shows a very small amount of ZrO_2 formation compared to that formed in films ignited in air. Fig. 7.10 also shows that peak intensities increase with bilayers.

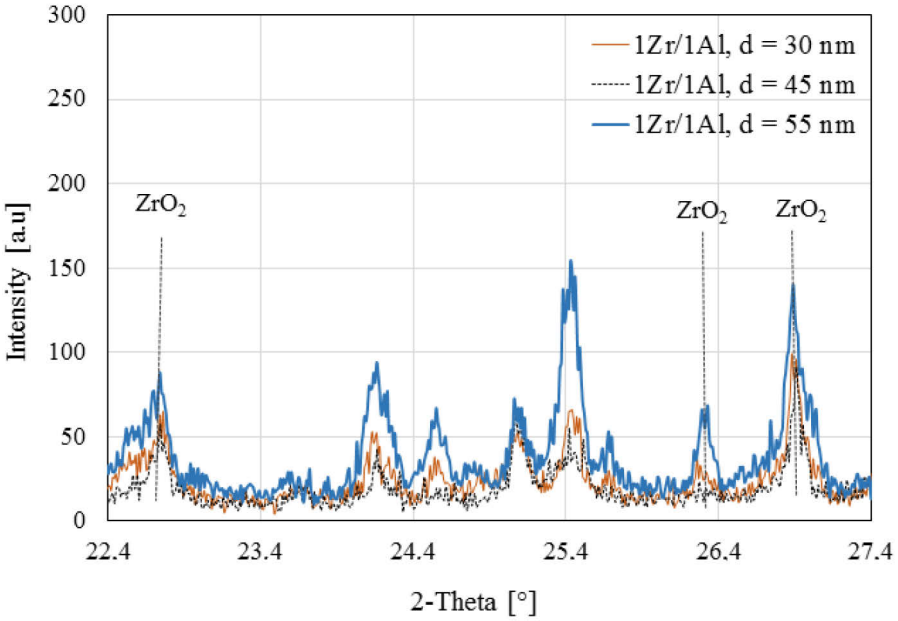

Figure 7.10: XRD patterns of reacted 1Zr/1Al films for different bilayer thicknesses ignited in argon. Measurement was performed by using X-ray diffractometer (STOE-STADI MP). Here, only ZrO_2 reflexes are marked for simplicity.

During a self-propagating reaction, the ignition environment plays an significant role in phase formation. The question that now arises is whether the types of intermetallics formation change in reacted films ignited in different enviorments. Fig. 7.11 shows the XRD patterns of 1Zr/1Al RMFs for different bilayers ignited in Ar 4.6. Here, results show the formation of intermetallic phases of Al_2Zr (JCPDS # 48-1384), Zr_2Al_3 (JCPDS # 16-0075) as major constituents and ZrO_2 (JCPDS #79-1771) as minor component (approx. 1%). The amount of intermetallics of Al_2Zr (66-41 %), Zr_2Al_3 (33-58 %) as major constituents was detected in reacted films with bilayers. Compared to this result, the XRD analysis of Zr/Al RMFs ignited in air (Fig. 7.2, page 86) shows the formation of different products, whereas Al-rich intermetallic of Al_3Zr was noticed as major constituent. The formation of ZrO_2 after consumption of Zr from bilayers, is expected to form Al-rich constituent. A similar approach was also reported in Refs. [127, 132]. In contrast, Zr/Al films ignited in argon show the major constituents of Zr_2Al_3, which is expected according to the initial 1Zr/1Al film design. However, this work identifies different products in Zr/Al RMFs ignited in air and argon, which will be beneficial to expand their uses.

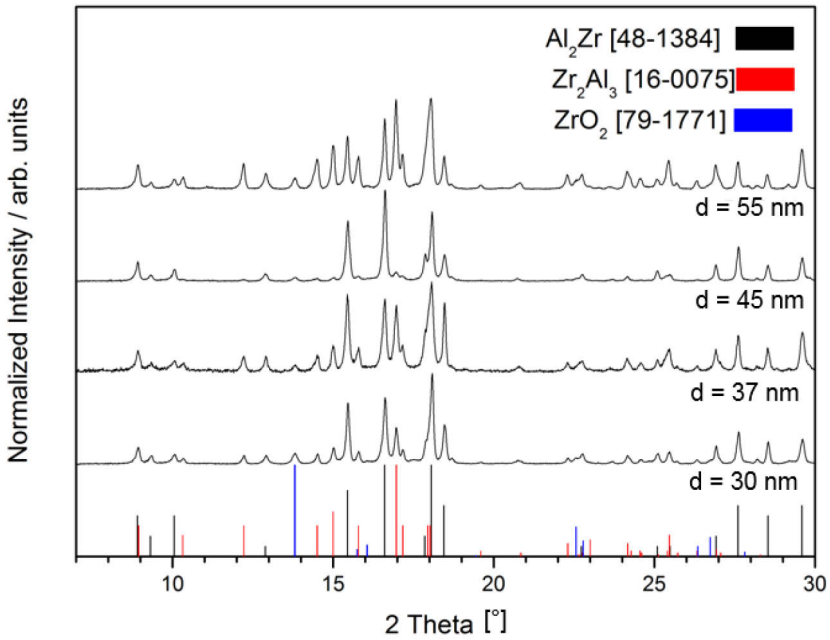

Figure 7.11: XRD patterns of reacted 1Zr/1Al films ignited in argon 4.6. Measurement was performed by using X-ray diffractometer (STOE-STADI MP). Here, reflexes are marked after Refs. [146].

Microstructural analysis was also performed of reacted Zr/Al RMFs ignited in air and argon. Fig. 7.12 (a) shows SEM image of a reacted 1Zr/1Al film (*d* = 30 nm) ignited in argon. Here, no Al_2O_3 has observed, but still a very small amount ZrO_2 is present. Therefore, the columnar grains are visible to some extent after an exothermic reaction in argon. In contrast, Zr/Al films ignited in air are covered with oxides, which is clearly visible in Fig. 7.12 (b-d). Here, both oxides of ZrO_2 and Al_2O_3 mainly form on the reacted films. They can presence as particles or as a layer or combined of both. However, microstructural analysis shows the thicker oxide layer for increased bilayer thickness. The quantitative image analysis shows that oxide layers vary in the range from (0.9±0.2) µm to (2.2±0.2) µm for increased bilayers. The oxidation during a self-propagating reaction influences on the reaction properties by increasing reaction heat as mentioned in Refs. [126-127]. Additional exothermic heats (standard enthalpy of formation) of -279 kJ/mol and -275 kJ/mol were to be included for the formation of ZrO_2 and Al_2O_3, respectively according to Ref. [148]. However, the secondary oxidation reaction in 1Zr/1Al RMF with temperature plateau at high temperature can supply heat for an extended period and can open up new applications. In that

case, this RMF type will be preferable in such joining or other applications, which require localized heat for relatively longer period.

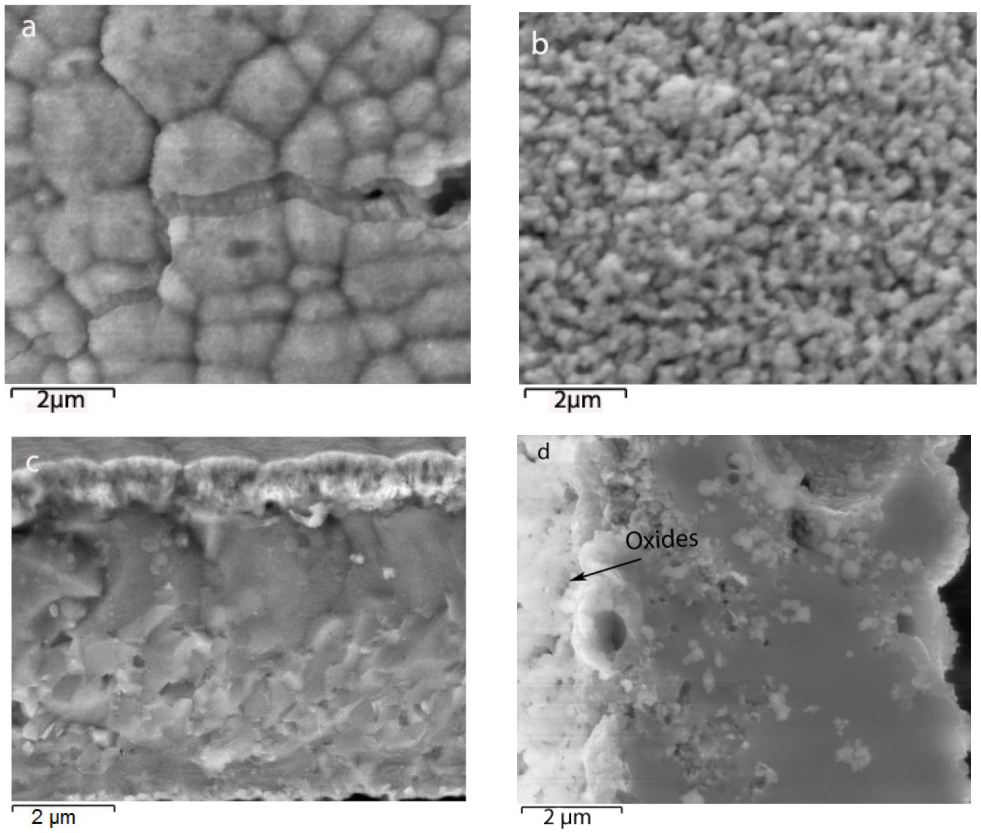

Figure 7.12: SEM image of top surface of a reacted 1Zr/1Al film (d = 30 nm) in argon (a) and air (b). Cross-sectional SEM images of 1Zr/1Al films (c) and (d) after a self-propagating reaction in air. Sample d has 90° tilt alignment.

7.4 Microstructural analysis of reacted Zr/Al films

The microstructural features of the reacted Zr/Al RMFs were investigated by using electron microscopes. Fig. 7.13 (a) shows reacted 1Zr/1Al RMFs, where columnar microstructures fused together after an exothermic reaction. The reacted foil has the tendency to fold together and become curly, which is clearly visible in Fig. 7.13 (a, b). It also shows the formation of different types of defects during self-propagating reaction. For example, the formation of micropore has been shown in Fig. 7.13 (a, b). The sublimation of Al by changing vapour pressure at high temperature during reaction can influence on it. Similarly, film characterization shows also the formation of micro-crack, which has been presented in Fig. 7.13 (c). The residual or the thermal stresses can influence on it.

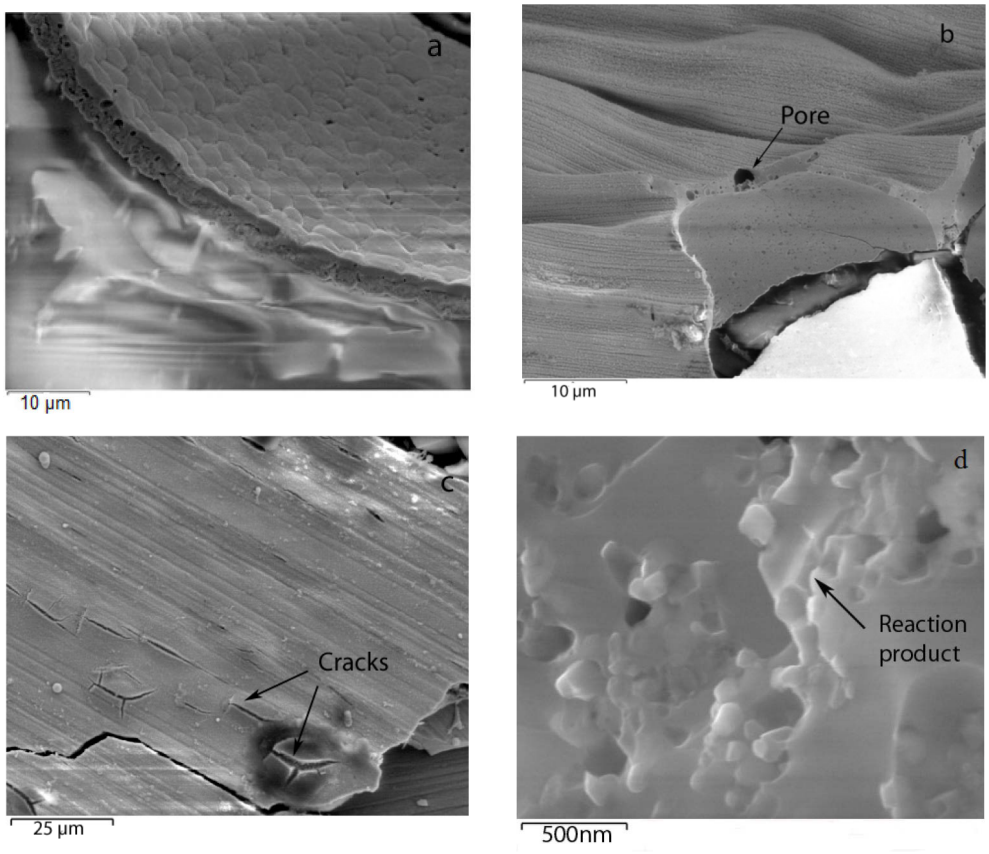

Figure 7.13: SEM images of reacted 1Zr/1Al RMFs (d = 20 nm) (a), at the point of activation (b), Reacted foils viewed from the top (c). Cross-sectional SEM image of reacted 1Zr/1Al RMF (d = 37 nm, l = 9 µm) (d).

The reacted cross-section of Zr/Al film presented in Fig. 7.13 (d) indicates the formation of intermetallic compounds after reaction, where no distinct multilayers are detectable. However, the microstructural analysis of this film type shows no ripple band formation as that formed in Ti/3Al film. In this work, 1Zr/1Al RMFs show only steady state reaction propagation. The overall summary of developed Zr/Al RMFs and corresponding reaction properties are summarized in table 7.2.

Table 7.2: Film morphology, resistivity and reaction properties of 1Zr/1Al RMFs.

Bilayer thickness (*d*) [nm]	Electrical resistivity [mili.ohm.cm]	Max. reaction temperature [°C] at 9 V	Reaction velocity [m/s] at 9V
20	0.52±0.22	1581±57	0.49±0.2
25	0.61±0.22	1657±81	0.84±0.3
30	0.63±0.21	1637±52	1.22±0.4
37	1.47±0.31	1707±77	0.64±0.2
45	1.23±0.11	1679±158	0.22±0.1
55	1.43±0.18	1689±137	0.23±0.1

Moreover, results of this work were compared with available literatures and listed in table 7.3. This table includes the fabrication method, film morphology, ignition type and reaction conditions with reaction propagation. In this work, the effects of bilayer thickness on reaction properties in 1Zr/1Al RMFs have been investigated. All films show steady reaction propagation. For 30 nm bilayer thickness, a high reaction velocity of (1.22±0.4) m/s and maximum reaction temperature of (1637±52) °C were noticed. On the other hand, the oxidation effect becomes pronounced in RMFs with higher bilayers. Therefore, 1Zr/1Al RMF with bilayer of 30 nm was considered for large area fabrication, which will be highlighted in the section 10. The large volume of reactive films with appropriate reaction properties will expand their usability in joining or other applications.

Table 7.3: Comparative analysis of Zr/Al reactive films with available literatures. This table includes the fabrication method, film morphology (bilayer, d; film thickness, l) and reaction front velocity (υ) and maximum reaction temperature (T_{max}).

Foil type	**Fabrication method** **Bilayer (*d*),** **total thickness (*l*)**	**Ignition type; condition**	**Velocity, *υ* [m/s]** **Temperature, T_{max}** **Reaction characteristic**	**[Ref]**
1Zr/1Al	MSIP *d* = 20-55 nm *l* = 8-16 µm	9V electric park; no preheating, air	*υ* = 0.5±0.2-1.22±0.4 m/s T_{max} =1581±57-1707±77 °C Steady state propagation, oxidation in air	[This work]
1Zr/nAl (n = 2, 3)	Magnetron sputtering *d* = 5-55 nm *l* = 16-27 µm; 25-50 µm	-	υ_{max} = 7.7 m/s υ_{min} = ~2 m/s T_{max} =1425-1675 K Steady state	[37]

8 Ternary reactive films of Ti, Si and Al reactants

8.1 Investigation of Si/Ti/Al/Si and Ti/Si/Ti/nAl RMFs

Recently developed layer by layer deposited multilayer films mostly consist of binary reactants. However, the exothermic reaction analysis in ternary multilayer having active ternary reactants was not been reported yet to our knowledge. In this work, the RMFs design having titanium, silicon and aluminum reactants were demonstrated. For the first time, ternary films with two different multilayer arrangements of Si/Ti/Al/Si and Ti/Si/Ti/Al and different Al-molar ratios of Ti/Si/Ti/nAl (n = 1 - 3) were deposited and characterized. The schematic illustrations of ternary multilayer arrangements with distinct reacting interfaces in Si/Ti/Al/Ti (a), Ti/Si/Ti/Al (b) Ti/Si/Ti/3Al (c) RMFs have been shown in Fig. 8.1. Here, we attempt to understand the role of reactant arrangements and Al-molar ratios for the formation of reaction products, heat release and reaction propagation. For two multilayer designs of Si/Ti/Al/Si and Ti/Si/Ti/Al films, identical bilayer thickness and total thickness were chosen.

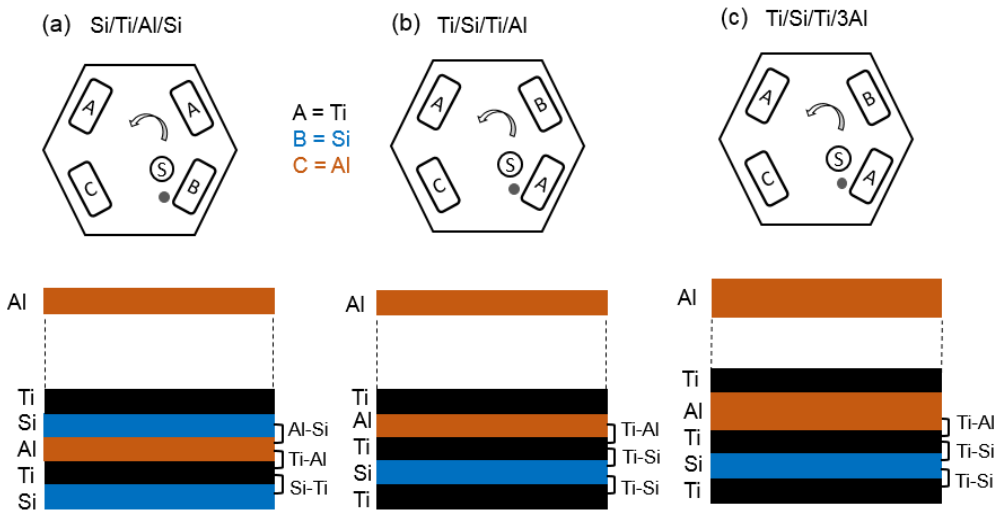

Figure 8.1: Schematic illustration of target arrangements in a MSIP method with four targets. Initial reactant layer was marked by dot. Here, A, B and C correspond Ti, Si and Al targets and S is the substrate. Film design in Si/Ti/Al/Si (a), Ti/Si/Ti/Al (b) and Ti/Si/Ti/3Al (c) compositions with corresponding local reacting interfaces.

Although they have similar reactant types and morphology, the difference is only the multilayer arrangements and distinct atomic mixing interfaces of Ti-Si, Al-Si and Ti-Al. In addition, ternary films of Ti/Si/Ti/nAl (n = 1, 2, 3) having Ti/Si/Ti/1Al, Ti/Si/Ti/2Al and Ti/Si/Ti/3Al compositions were investigated. All films were deposited on copper substrate by using MSIP method having the alternating layer sequences of Cu/Ti/Si/Ti/Al/Ti/Si/…/Al, which show the dual bilayers of Ti/Si and Ti/Al. The self-propagating reaction was analysed of freestanding ternary RMFs and the effects of multilayer arrangements and different Al-molar ratios on reaction velocity, temperature and heat release were comprehensively studied.

8.2 Characterization of unreacted ternary RMFs

The microstructural feature of as-deposited freestanding ternary films was characterized. The overall cross-section of unreacted 1Si/1Ti/1Al/1Si film is presented in Fig. 8.2 (a). Here, it shows the columnar microstructural morphology, where the column width differs between 163 nm and 210 nm. Fig. 8.2 (b) shows the as-deposited 1Ti/1Si//1Ti/1Al/ RMF with the column width of (580±25) nm. The cross-sectional TEM and SEM images of Ti/Si/Ti/Al RMFs have been presented in Fig. 8.2 (c, d). Here, the elemental layers of Ti, Si and Al are arranged in an alternating way in the columnar microstructure with a controlled thickness. Please note that due to very close atomic contrast of Si and Al, it is hard to make them distinguishable. However, EDX analysis confirms the presence of Ti, Si and Al in as-deposited films. For two multilayer arrangements of Si/Ti/Al/Si and Ti/Si/Ti/Al RMFs, dual bilayer thicknesses are about (29±5) nm. For increased Al-molar ratios in 1Ti/Si/1Ti/nAl (n = 1, 2, 3) RMFs, Ti/Al bilayer increases till (47±5) nm and Ti/Si bilayer remains constant. All ternary films have approx. 188 - 214 bilayers and total thickness of ~ 6 μm.

However, the formation of premixing layer in ternary RMFs is non-negligible. There can form solid solution, intermetallic or amorphous phases in the premixing zone. It is preferable to form premixing layer in Ti-Si bilayer compared to that in Ti-Al bilayer. A similar approach was reported by Ramos et al. [149-150], where no intermetallic or amorphous phase was found in Ti-Al film compared to the films with higher reaction heat. However, this premixing zone reduces the reaction heat and diffusion rate.

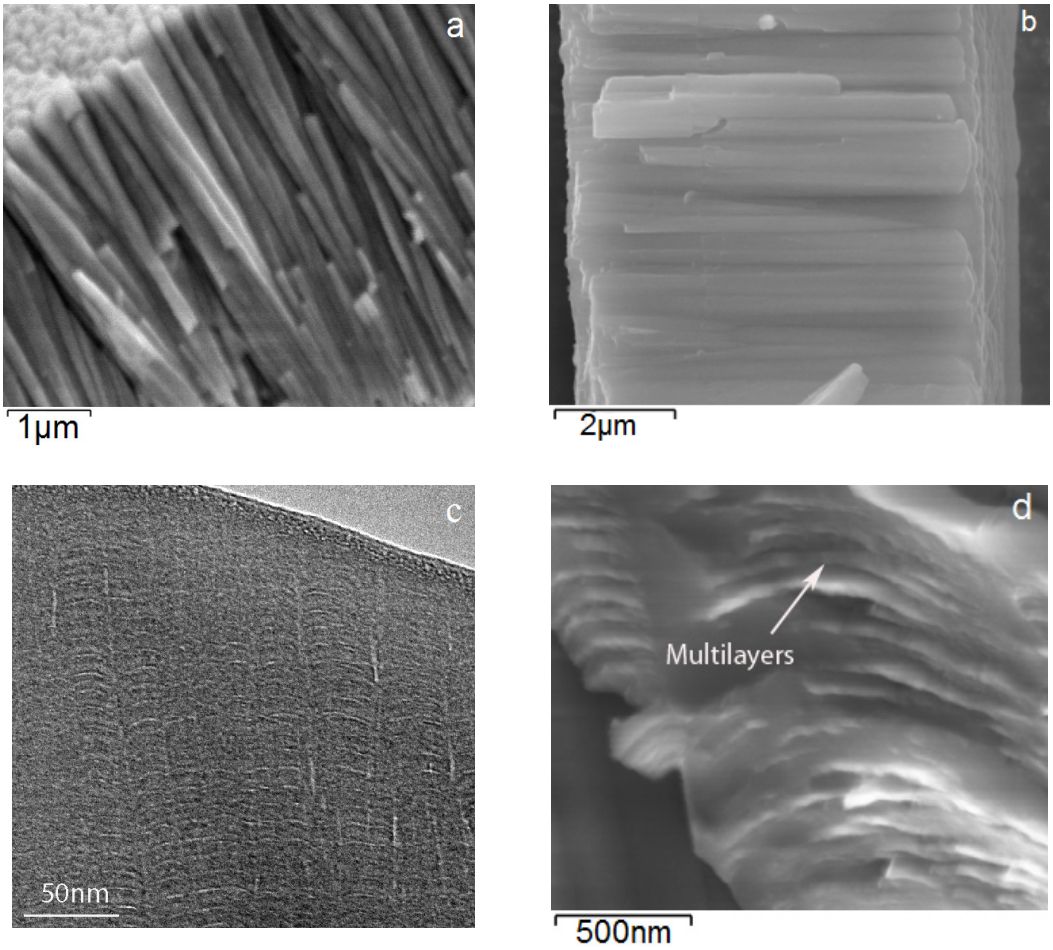

Figure 8.2: SEM image of as-deposited ternary 1Si/1Ti/1Al/1Si RMF (a). SEM cross-section of 1Ti/1Si/1Ti/1Al RMF. Here, samples a, b have identical bilayer and total thickness of d = (29±5) nm, l = ~ 6 µm. TEM image (c) and SEM cross-section of multilayers arrangement (d) in 1Ti/1Si/1Ti/1Al ternary film.

8.3 Reaction products identification by XRD

The phase formation in the reacted ternary film was investigated by X-ray-diffraction analysis (XRD D5000 Theta-Theta Brucker). Here, reaction product has been investigated after fast self-propagating reaction in air considering the unarrested reaction front and no intense heat losses, which corresponds the real condition of practical applications. Fig. 8.3 (a, b) exhibits the XRD patterns (y-offset) of the reaction products in all reacted ternary films. Here, reflexes are marked according to Ref. [151].

In Fig. 8.3 (a), the major intermetallic compound of orthorhombic Si_2Ti (COD # 1009012, 1010453) was found in reacted Ti/Si/Ti/Al film. The formation of Al_2Ti (also can presence as Al_2O_5Ti, COD #2206495) was noticed. A minor amount of bcc-Ti and $SiTi_3$ can be found in this film type. On the other hand, in reacted Si/Ti/Al/Si films have the reaction products of Si_2Ti, Al_2Ti. In addition, Al_2O_5Si (COD #1008755), orthorhombic Si (COD #9011656), cubic Al (COD #4313210) were found in this film. In case of Al-Si interface, Si has less solubility in Al and the maximum solubility is about 12 wt. % at the eutectic temperature [152]. Therefore, Al and Si constituents were also noticed in reacted Si/Ti/Al/Si film because of their less solubility to each other. Here, the XRD patterns also include oxide peaks. As, the capping layers or products can oxidize due to higher oxygen diffusivities at high reaction temperature. This work shows also a similar approach of oxidation during self-propagating reaction in air, which was demonstrated as a secondary combustion reaction in Refs. [7, 153].

Fig. 8.3 (b) shows the XRD patterns of reacted Ti/Si/Ti/nAl RMFs. Here, the major reaction product of Si_2Ti (orthorhombic) was found with a small amount of $SiTi_3$ (hexagonal) and Al_2Ti (orthorhombic) intermetallic. A very small amount of bcc - Ti in this reacted film was noticed. With increasing Al-molar ratios in films, the increment amount of $SiTi_3$ phase was noticed and bcc-Ti was reduced. Here, the patterns may include peaks of intermetallic or constituents incorporating with a few amount of impurities (for example, C, O_2) from deposition process or reaction in air. Therefore, the overlapping of peaks is also understandable. Here, multiple reaction products of binary systems are noticed in reacted ternary films. No ternary compound of Ti, Si and Al was noticed due to layer by layer planar multilayer design. Please note that, in case of ternary reactive particle systems, the formation of ternary compound needs to be considered. This XRD result shows that Al-molar ratios and multilayer arrangements influence on the formation of reaction products in ternary RMFs. Here, distinct atomic mixing rates in the Ti-Si, Ti-Al and Si-Al interfaces control the reaction propagation.

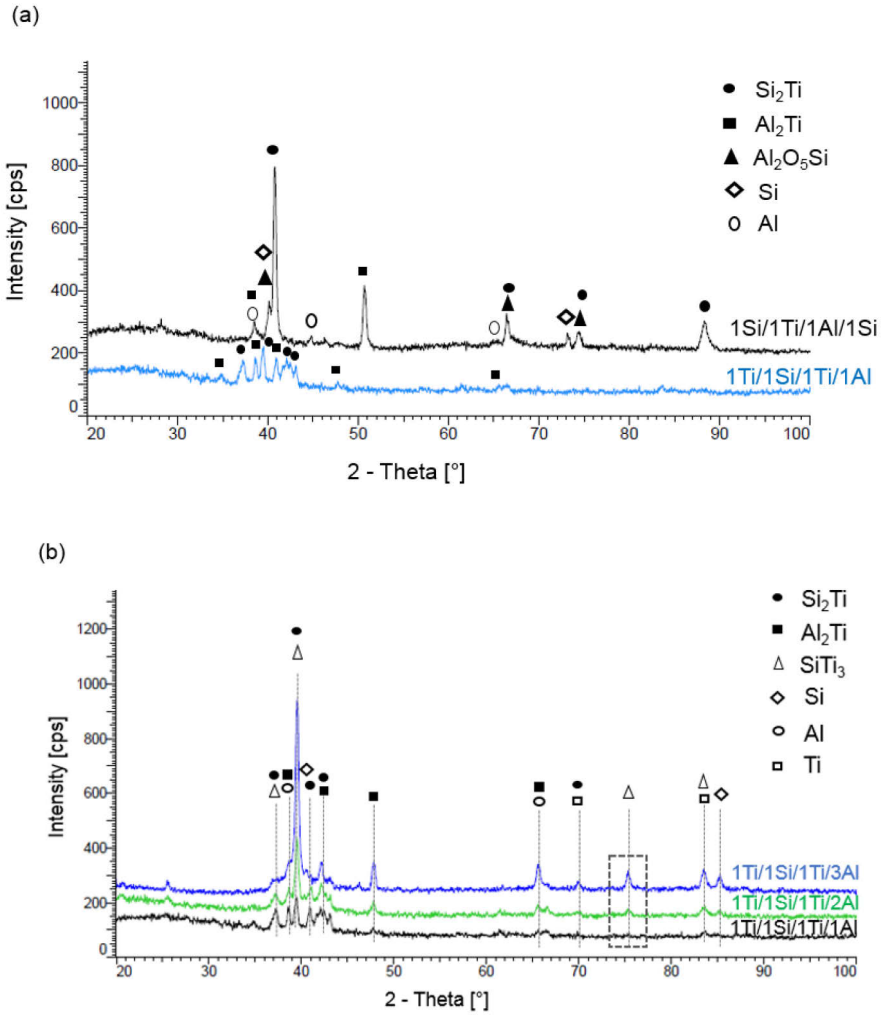

Figure 8.3: XRD patterns of the reacted Ti/Si/Ti/Al and Si/Ti/Al/Si RMFs (a) and ternary films with different Al-molar ratios (b) after a fast self-propagating reaction. The freestanding films were ignited by 9 V electrical arc in air.

Now the question arises which reactant interfaces are forming preferably the intermetallic in the ternary film. This can be described by the free energies of the interfaces and grain boundaries, which will determine the relative stability of each layer and the system. According to the work of Lewis et al. [154], reactants with higher melting temperature are scaled with higher grain boundary energies. Therefore, the formation of intermetallic compounds in Ti-Si system is more preferable compared to that in Ti-Al system. In contrast, Si-Al interface contributes negatively by the endothermic reaction heat.

8.4 Exothermic reaction properties of ternary RMFs

8.4.1 Phase change temperature and transformation heat

The DSC plots of ternary RMFs have been shown in Fig. 8.4 (a, b) with a heating rate of 30 K/min. DSC traces of two multilayer arrangements and different Al-molar ratios were compared. Fig. 8.4 (a) shows DSC traces of 1st and 2nd heating run of 1Si/1Ti/1Al/1Si foils. Here, 2nd heating shows the complete transformation. The major exothermic peak was detected at the temperature range of (300±15) °C. Other exothermic peaks exist also in the temperature range of 130 °C-190 °C. An endothermic peak can be noticed at the temperature of (220±20) °C. This is because of the less solubility of Si and Al elements to each other and thus segregation.

Fig. 8.4 (b) shows the DSC analysis of 1Ti/1Si/1Ti/nAl (n = 1, 2, 3) reactive films with by Y-offset. The exothermic transformation (*R1*) in all ternary films occurs at temperature of (284±20) °C. An endothermic peak (*R2*) has been found at (353±10) °C in 1Ti/1Si/1Ti/3Al RMF. In 1Ti/1Si/1Ti/1Al and 1Ti/1Si/1Ti/2Al RMFs, this endothermic peak shifts at temperature of (422±10) °C. It is expected that the dissociation of premixed compounds especially in Ti-Si interface can correspond this peak. However, a high intermixing at Ti-Si interface was also reported in the work of Chaix-Pluchery et al. [155]. The exothermic peak (*R3*) becomes intense for 1Ti/1Si/1Ti/3Al film compared to other compositions. DSC analysis shows that the shape and position of peaks in ternary films are influenced by multilayer arrangements and the compositions. However, total transformation heat in this work can be used preferably for qualitative comparision of reaction kinetics during a slow heating of different ternary RMFs.

However, the overall reaction heat of ternary films can be quantified depending on the reaction products, bilayer thickness and premixed layer. For Ti/Si/Ti/Al RMFs, the overall reaction heat can be expressed by equation 34, derived from equation 14 as mentioned in Ref. [34].

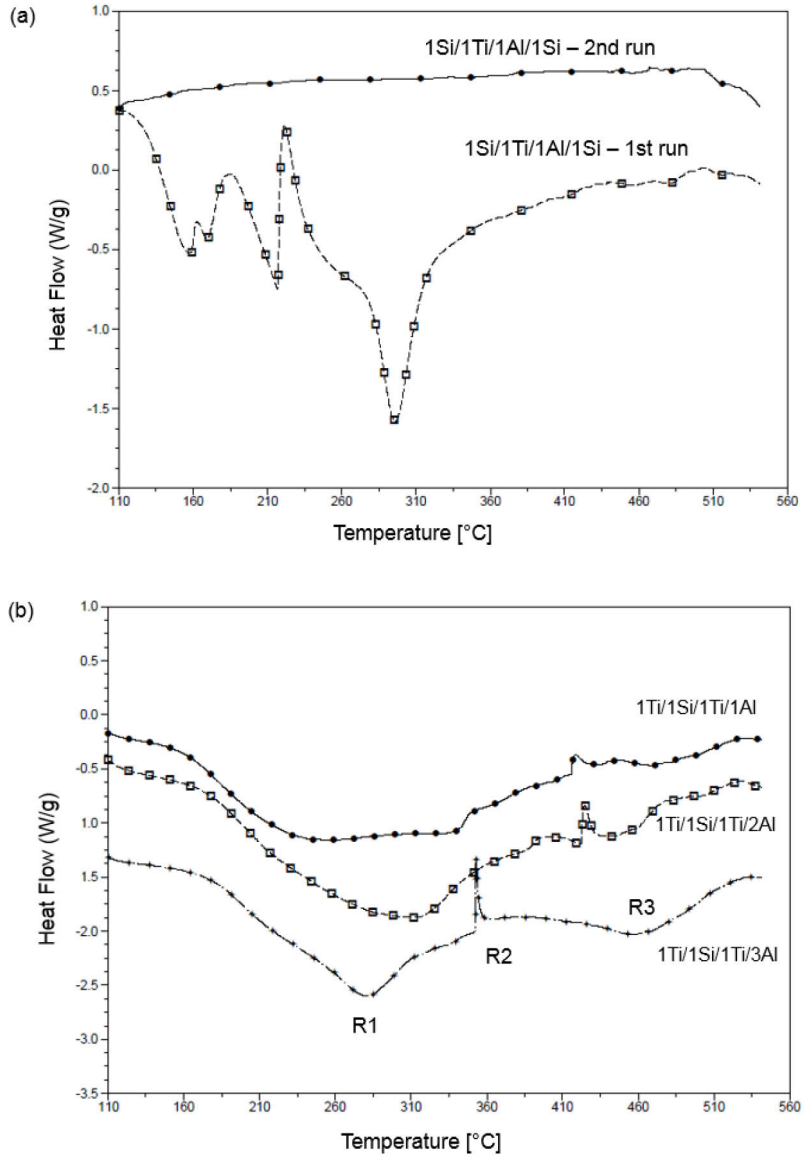

Figure 8.4: DSC plots of 1Si/1Ti/1Al/1Si RMF with 1st and 2nd heating run (a) and Ti/Si/Ti/nAl (n = 1, 2, 3) RMFs (b) at 30 K/min heating rate.

For simplicity, it is assumed that final intermetallic compounds also form in the premixed zone with a thickness of 1 nm in Ti-Si and Ti-Al interfaces (e. g. $\omega_{Ti\text{-}Si} = \omega_{Ti\text{-}Si} = 1$ nm). In ternary Ti/Si/Ti/Al film with Ti-Si and Ti-Al dual periodicity, there presence 2/3 Ti-Si and 1/3 Ti-Al interfaces. Therefore, we can expect 67 % reaction products of Ti-Si system and rest of Ti-Al system.

$$\Delta H_{rxn} = \frac{2}{3}\Delta H_{Ti-Si}\left(1 - \frac{\omega_{Ti-Si}}{\lambda_{Ti-Si}/2}\right) + \frac{1}{3}\Delta H_{Ti-Al}\left(1 - \frac{\omega_{Ti-Al}}{\lambda_{Ti-Al}/2}\right) \qquad (34)$$

The dual periods of Ti-Si and Ti-Al layers have thickness of (29±5) nm. After an exothermic reaction, the reaction products of $TiSi_2$ (ΔH= - 58.52 kJ/mol) and $TiAl_2$ (ΔH= - 40.48 kJ/mol), then the overall reaction heat will be (49.9 ±0.5) kJ/mol. Please note that without 1 nm pre-mixed layer, the estimated heat is about 52 kJ/mol. Moreover, besides the effect of premixing on reaction heat, this research also shows that the major reaction product controls the heat release, in case of multiple products formation.

8.4.2 Reaction front velocity

Fig. 8.5 shows the high speed photographic images of a reaction front propagation in a ternary 1Ti/1Si/1Ti/1Al RMF. The direction of a reaction propagation has been also stated. Here, a steady reaction front with a bright glow propagates fully within approximately 7 milliseconds. No preheating was required to start the reaction.

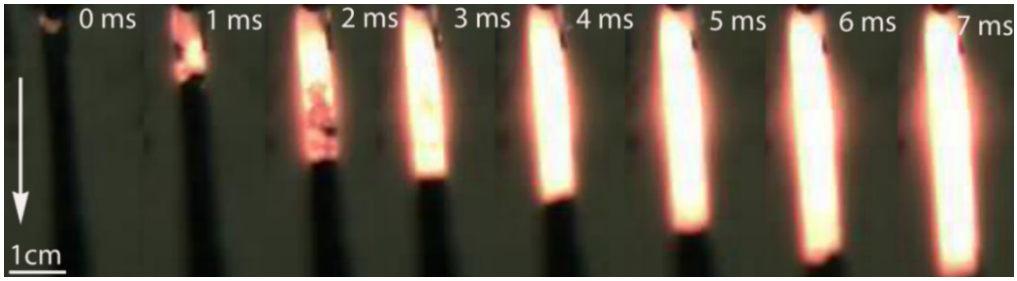

Figure 8.5: High speed photographic images showing a reaction front propagation in a Ti/Si/Ti/Al (d = 29 nm, l = 6 µm) RMF. The propagation direction has been marked. The freestanding film was ignited by 9 V electrical arc. Images were shot at 10000 fps.

The reaction front velocity was measured by taking successive images in a plan view captured with the high-speed camera. At least 8-10 tests were performed for every composition. Reaction velocity was measured by sizing the travelling distance of a reaction front in a time variation between the individual frames.

Fig. 8.6 shows the reaction front velocity plots of all ternary RMFs. Here, 1Ti/1Si/1Ti/1Al composition exhibits the higher reaction velocity in the range of (9.2±2) m/s compared to other ternary films. For increasing Al-molar ratios, reaction front velocity drops to (7.7±2) m/s and (6.2±2) m/s

respectively. This is because of the increased diffusion distance slows down the atomic mixing rate. In addition, the formation of multiple reaction products also introduces the distinct reactant mixing rate.

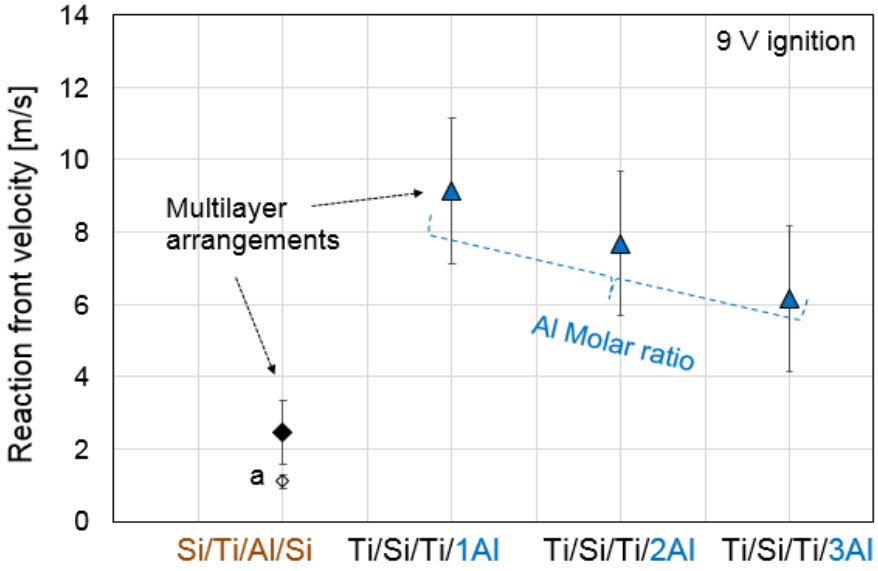

Figure 8.6: Reaction front velocity of all ternary RMFs at 9 V in air. Here, (a) indicates the unsteady reaction propagation of Si/Ti/Al/Si/../Al film. All Ti/Si/Ti/nAl films show steady state reaction propagation.

On the other hand, the steady state propagation in Si/Ti/Al/Si RMF exhibits a low reaction velocity of (2.5±0.8) m/s compared to the Ti/Si/Ti/Al film, although both films have similar bilayer, total thickness and columnar microstructural texture. The possible reason is that the distinct atomic mixing interfaces and thus heterogeneous diffusion rates control the reaction propagation. In 1Si/1Ti/1Al/1Si RMF, the diffusion takes place preferably in Ti-Si interface and Al-Si interface is expected to influence negatively. Whereas, in Ti/Si/Ti/Al film, Ti-Si and Ti-Al interfaces contribute positively. Therefore, the attribution of the dependency of reaction velocity on film morphology (bilayer thickness, molar ratios) in binary film as mentioned in Refs. [15, 45, 122], is not only directly applicable for ternary multilayer. In this work, it is demonstrated that multilayer arrangements with distinct atomic mixing interfaces also influence on the exothermic reaction. However, Si/Ti/Al/Si ternary composition shows also the unsteady reaction propagation, which reduces the reaction velocity to (1.1±0.2) m/s.

The effect of ignition potentials on reaction front velocity in ternary films was investigated. Fig. 8.7 (a-d) shows the reaction velocity at 9 V, 15 V and 21 V ignition potentials in air. Fig. 8.7 (a) shows that the reaction velocities of Si/Ti/Al/Si films increase with ignition potentials. This reaction velocity is about (3.7±0.5) m/s, which is lower than that of other compositions. On the other hand, this film type exhibits an unsteady propagation. In this plot, both steady and unsteady reaction velocities were considered.

In Fig. 8.7 (b), the reaction velocity of 1Ti/1Si/1Ti/1Al RMF is higher than the other compositions. With increasing ignition potentials, the reaction velocity remains nearly constant, which is in the range of 9-9.2 m/s. The reaction front velocity of Ti/Si/Ti/2Al, presented in Fig. 8.7 (c) is also nearly constant, which is about 7-7.8 m/s.

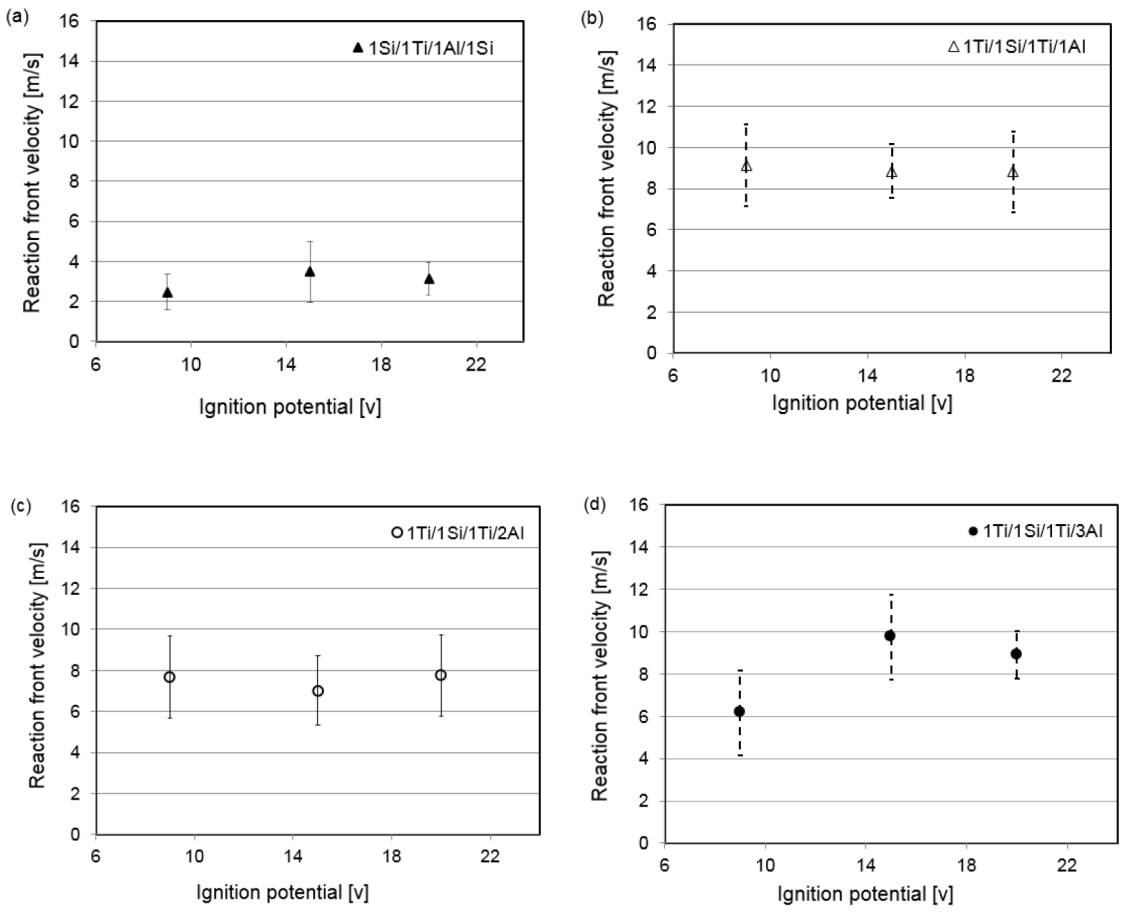

Figure 8.7: Dependency of reaction front velocity on ignition potentials in Si/Ti/Al/Si (a), Ti/Si/Ti/Al (b), Ti/Si/Ti/2Al (c) and Ti/Si/Ti/3Al (d) ternary RMFs.

For Ti/Si/Ti/3Al reactive films, the reaction velocity of (6±2) m/s has been noticed at 9 V ignition. Whereas, the reaction velocity increases till (9±1) m/s at an ignition potential of 15 V and then drops. The study of the dependency of reaction front velocity on ignition potential is important in order to minimize the energy input as well as economic costs. This work shows the optimum ignition potentials of 9-15 V in ternary RMFs.

8.4.3 Reaction temperature in ternary RMFs

Fig. 8.8 shows the typical T-t profiles of all ternary films during an exothermic reaction in air. This profile includes the preheating and reaction temperature in the temperature increment cycle. It shows the higher preheating rate in 1Ti/1Si/1Ti/1Al reactive films due to presence of higher slope. This film also shows lower resistivity, which is listed in table 8.1. For this film type, the maximum reaction temperature of 1775 °C is observed, which is higher than the melting temperature of Si (T_m = 1414 °C), Ti (T_m = 1650 °C) and Al (T_m = 660 °C). Therefore, the state of reaction products at maximum temperature is expected to be liquid or solid-liquid. Here, the allotropic phase transformation can influence on the reaction temperature and heat.

On the other hand, the cooling section shows a small temperature plateau at (1410±20) °C. At this temperature, the formation of Si_2Ti is expected. For 1Ti/1Si/1Ti/2Al RMF, the maximum reaction temperature is also higher than the reactant's melting temperature. Here, a temperature plateau at (1700±10) °C has been found. Here, the metastable (solid and liquid) phases transform to stable phases. For 1Ti/1Si/1Ti/3Al RMF, the maximum temperature is even. With increased Al- molar ratios, the increment amount of $SiTi_3$ phase reduces the reaction heat and thus reaction temperature. The T-t profiles of 1Si/1Ti/1Al/1Si presented in Fig. 8.8, include both steady and unsteady reaction propagation. For the steady state reaction in 1Si/1Ti/1Al/1Si ternary RMF, the reaction temperature is lower than 1Ti/1Si/1Ti/1Al reactive films although both have similar bilayer thickness. For this unsteady reaction of this film type, the reaction temperature is found even low in the range of (1250±30) °C.

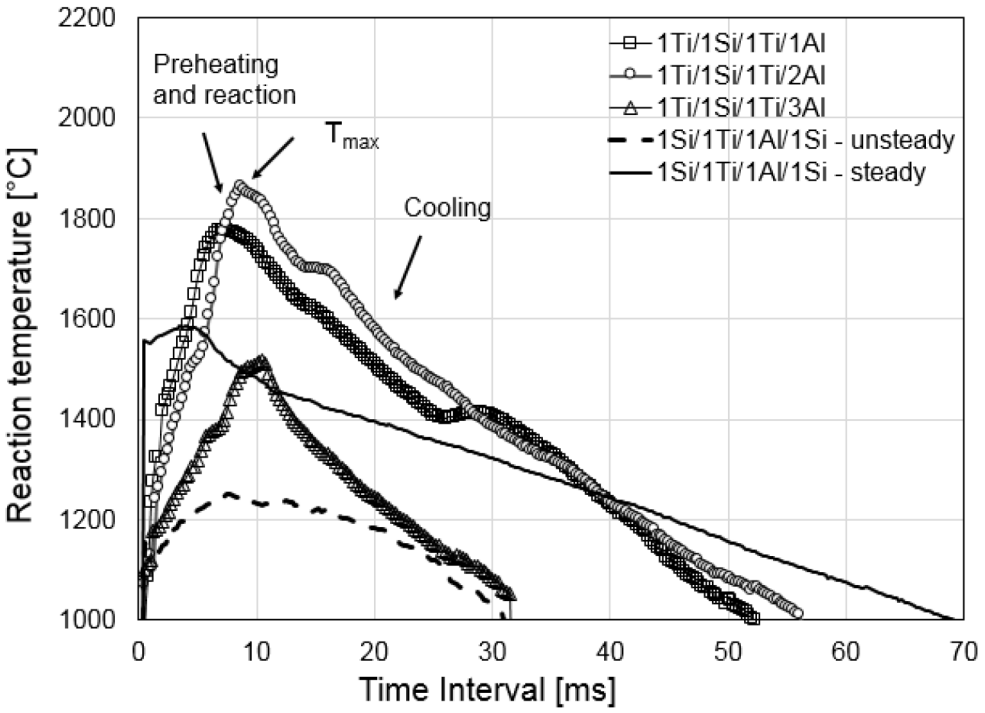

Figure 8.8: Reaction temperature-time profiles of all ternary RMFs in air measured by high speed two-color pyrometer (Metis HQ22).

Temperature profile of an unsteady reaction in Si/Ti/Al/Si RMF shows nearly static temperature after reaching to the maximum temperature for certain periods and then the cooling occurs. Here, the segregation or melting of the reaction constituents or the oxidation can enhance on such an unsteady propagation. In addition, oxidation color band was observed at the surface of reacted 1Si/1Ti/Al/Si films in case of unsteady propagation. Interestingly, recent study on unsteady reaction propagation also indicates the occurrence of an oxidation reaction in air, which can contribute to proceed an oscillatory reaction fronts [132]. Here, the capping layers or reaction products both can be oxidized due to higher oxygen diffusivities at high reaction temperature during an exothermic reaction. A similar approach of unsteady reaction propagation was reported in recent studies for other multilayer foils as mentioned in Refs. [11, 65, 131-133]. Moreover, Ti/Si/Ti/nAl RMFs show no significant oxidation characteristics with temperature plateau or unsteady propagation.

However, the states of reaction products at maximum temperature are mainly liquid or solid-liquid. Therefore, final reaction products could not form at maximum temperature, which may transform later to form stable products

during cooling. However, different shapes of T-t profile show characteristics reaction kinetics, besides maximum reaction temperature.

Fig. 8.9 illustrates the maximum reaction temperature of four different ternary RMFs. The measured maximum temperature is the result of ten measurements with error bars. The estimated error bars can associate with the oxidation and structural effects. Here the maximum reaction temperatures vary in the range of (1768±42) °C and (1297±95) °C for ternary Ti/Si/Ti/Al and Si/Ti/Al/Si multilayers, respectively. The reaction temperature increases for Ti/Si/Ti/Al multilayers. This is because of the formation of an increased amount of Si_2Ti phase, which has higher reaction heat.

Please note that, average reaction temperature of Si/Ti/Al/Si foils includes both steady and unsteady propagation. Similarly, the reaction temperatures of 1Ti/1Si/1Ti/2Al and 1Ti/1Si/1Ti/3A RMFs are found in the range of (1812±71) °C and (1462±99) °C, respectively. The overall reaction propagation and temperature with film morphology have been listed in table 8.1.

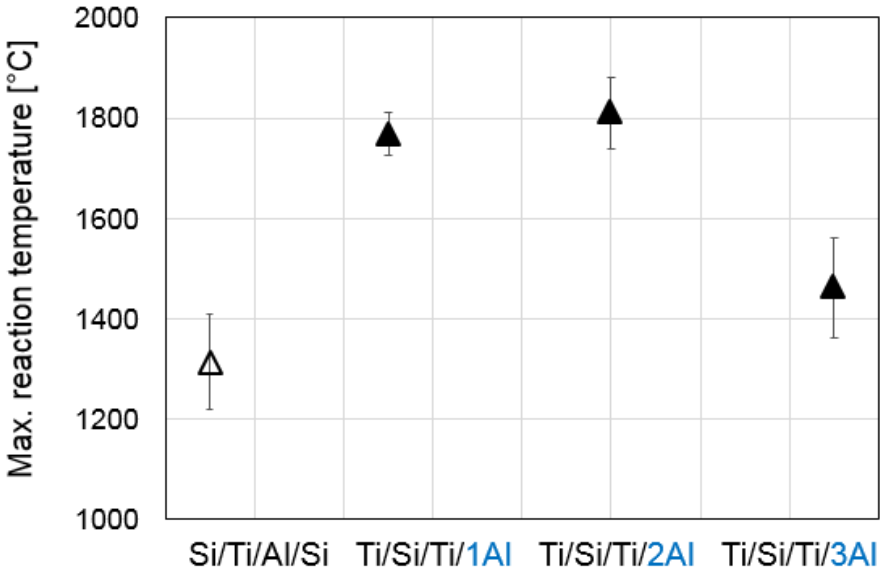

Figure 8.9: Maximum reaction temperature of all ternary RMFs measured by two-color pyrometer (Metis HQ22) in a high speed mode. Films were ignited by using 9 V electric spark in air.

8.5 Microstructural analysis of reacted ternary films

The reacted fracture surfaces of ternary RMFs are presented in Fig. 8.10 (a-d). Fig. 8.10 (a) shows the reacted Ti/Si/Ti/Al film, which has the tendency to deform and become curly. During a self-propagating reaction, generally micropores and cracks may form due to residual or the thermal stresses. Reacted fracture cross-sections of 1Ti/1Si/1Ti/1Al and 1Si/1Ti/1Al/1Si reactive films are shown in Fig. 8.10 (b, c). It shows that columnar microstructures fused together after a self-propagating reaction. For an unsteady propagation in 1Si/1Ti/1Al/1Ti films, only color band was observed due to different oxide layer thicknesses. However, no characteristic of ripple band formation like 1Ti/3Al films with fine and coarse microstructure was observed. Fig. 8.10 (d) shows the reacted Ti/Si/Ti/2Al films with the formation of multiple reaction products.

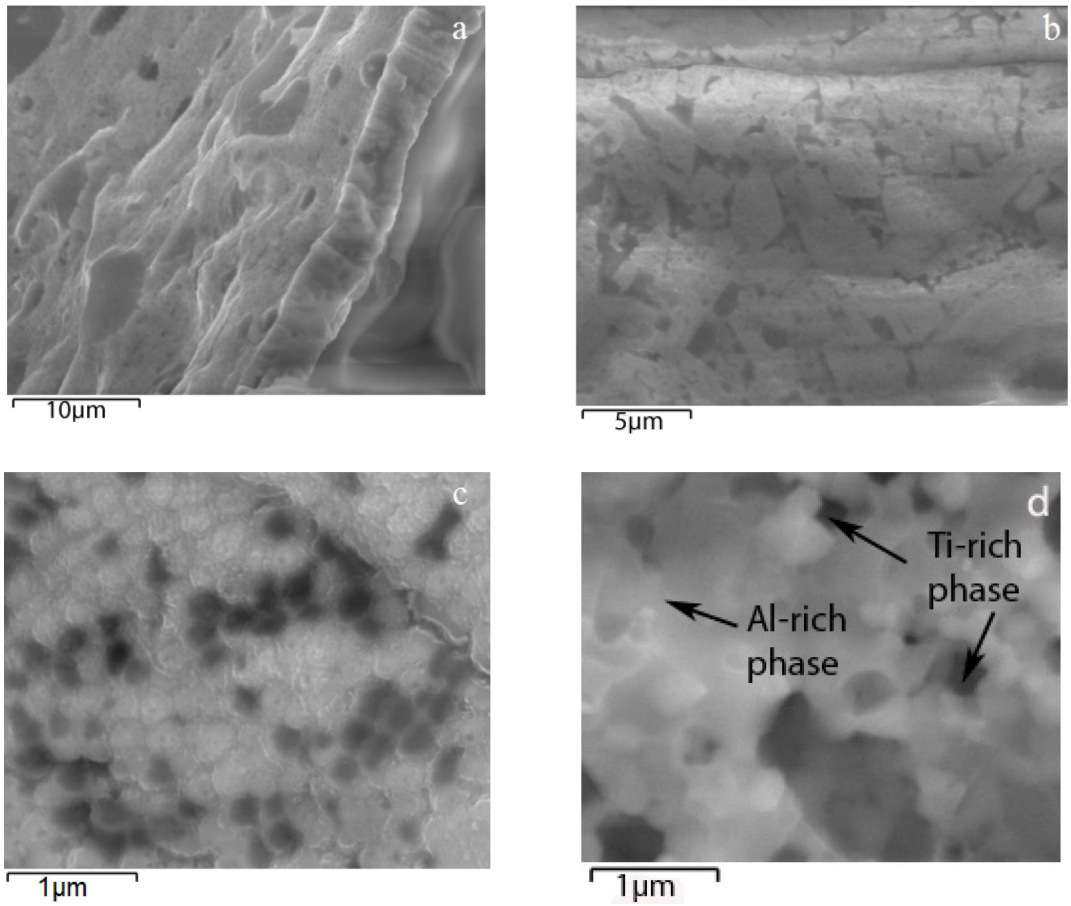

Figure 8.10: Cross-sectional SEM images of reacted 1Ti/1Si/1Ti/1Al RMFs (a) and at top view (b). Reacted top surface of 1Si/1Ti/1Al/1Si RMF (c), reacted cross-section of 1Ti/1Si/1Ti/2Al RMFs with formation of reaction products (d).

The overall summary of film morphology and reaction properties of ternary RMFs is listed in the table 8.1. Ternary multilayer films of Ti-Si-Al systems considering effects of multilayer arrangements and molar ratios of low melting constituents were developed. This table includes the foil chemistry, electrical resistivity, reaction temperature and propagation. The effects of multilayer arrangements and molar ratios on reaction properties have been also compared. In comparison with other compositions, a steady reaction mode with a higher reaction velocity of (9.2±2) m/s and temperature of (1768±42) °C were found in 1Ti/1Si/1Ti/1Al film. Therefore, this composition was taken for fabricating with large surface area, which will be discussed in the section 10.

Table 8.1: Film morphology, resistivity, reaction front velocity and maximum reaction temperature of ternary RMFs of Ti, Si and Al reactants. This table lists the reaction properties at 9 V ignition. Here, both steady and unsteady propagation were considered for the reaction temperature of ternary 1Si/1Ti/1Al/1Si RMF.

RMF composition	**Morphology** ***d*** **= bilayer [nm]** ***l*** **= thickness [µm]**	**Resistivity [Ω. m]**	**Max. reaction temperature,** T_{max} **[°C]**	**Reaction front velocity** u **[m/s]**
1Si/1Ti/1Al/1Si	$d_{Si\text{-}Ti}$ and $d_{Al\text{-}Si}$ = 28±3 nm l = 5.8±0.3 µm	(5.2±0.3)×10^{-10}	1297±95 °C	u_{st} = 2.5±0.8 u_{un} = 1.1±0.2
1Ti/1Si/1Ti/1Al	$d_{Ti\text{-}Si}$ and $d_{Ti\text{-}Al}$ = 29±4 nm l = 5.7±0.8 µm	(1.4±0.4)×10^{-10}	1768±42 °C	u_{st} = 9.2±2
1Ti/1Si/1Ti/2Al	$d_{Ti\text{-}Si}$ = 28±4 nm $d_{Ti\text{-}Al}$ = 36±6 nm l = 5.2±0.1 µm	(2.6±1.3)×10^{-10}	1812±71 °C	u_{st} = 7.7±2
1Ti/1Si/1Ti/3Al	$d_{Ti\text{-}Si}$ = 28±4 nm $d_{Ti\text{-}Al}$ = 47±5 nm l = 5.9±0.2 µm	(2.4±0.5)×10^{-10}	1462±99 °C	u_{st} = 6.2±2

9 Comparative analysis on reaction properties in developed RMFs

In this work, three types of reactive films of Ti-Al, Zr-Al and Ti-Si-Al systems were developed. A brief description of developed RMFs with their morphology and consequent reaction properties have been highlighted. Here, this work shows how the reaction propagation rate, reaction temperature, reaction heat are to be tailored via reactive film design. For example, Ti/Al and Zr/Al planar multilayers were designed with different compositions and bilayer thickness. For ternary Ti-Si-Al system, reactants arrangement and Al-molar ratios were controlled. After that the overall reaction properties of three RMFs were compared with the commercial Ni/Al nanofoil. Table 9.1 lists Thermo-Calc calculated standard enthalpy of formation of different phases in Zr-Al, Ti-Al, Ti-Si-Al and Ni-Al reactive systems.

Table 9.1: Standard enthalpy of formation (reaction heat) of different phases in Zr-Al, Ti-Al, Ti-Si and Ni-Al reactive systems calculated by Thermo-Calc 3.1.

RMF	Mole fraction	Possible phases	Reaction heat (-ΔH), kJ/mol
Zr-Al	0.44 - 0.75 (Al)	Al_4Zr_5, AlZr, Al_3Zr_2, Al_2Zr, Al_3Zr	40-47
Ti-Si-Al			
Ti-Si	0.25 - 0.67 (Si)	$SiTi_3$, Si_3Ti_5, Si_4Ti_5, SiTi, Si_2Ti	50-79
Ti-Al	0.30 - 0.74 (Al)	$AlTi_3$, AlTi, Al_2Ti, $Al_{11}Ti_5$, Al_3Ti	30-41
Ni-Al	0.36 - 0.75 (Al)	NiAl, $AlNi_3$, Al_3Ni_2, Al_3Ni_1, Al_3Ni_5	42-62

The overall thermodynamic simulation was also explained in the previous section 5.1. The phases in Ti-Si system exhibit the higher enthalpy of formation than Zr-Al and Ti-Al system. Compared to the Ni-Al system, Ti-Si system also shows higher reaction heat for the phase formation. However, the types of intermetallic compound formation after self-propagating reaction controls the heat release. In case of multiple reaction products, the major

intermetallic compound will control the reaction heat, which was demonstrated for ternary film in the section 8.4.1. Therefore, the developed ternary Ti/Si/Ti/Al film is considered to be in the middle energy class reactive system. On the other hand, reaction velocity indicates how fast the reaction products form. The reaction temperature and heat depend on the types of reaction products. The overall reaction properties of all developed RMFs and commercial nanofoil are also listed in table 9.2.

Table 9.2: Comparative analysis of reaction properties in RMFs of Zr-Al, Ti-Al, Ti-Si-Al systems in this work and commercial nanofoil from available literatures.

Material combination	**Bilayer, *d* [nm]**	**Variable**	**Reaction front velocity, *υ* [m/s]**	**Reaction temperature, T_{max} [°C]**
1Ti/nAl (n = 1-3) [This work]	20 - 40	Molar ratios	0.68±0.5 - 2.57±0.6	1215 - 1298
1Zr/1Al [This work]	20 - 55	Bilayer	0.23±0.1 - 1.22±0.4	1581 - 1707
Si/Ti/Al/Si, Ti/Si/Ti/nAl (n = 1-3) [This work]	28 - 50	Layer sequence, Al-molar ratios	2.50±1.0 - 9.10±2.0	1345 - 1872
Ni/Al [34, 70]	20 - 150	Bilayer	2±0.5 - 13±0.5	1400 - 1600

In this work, three types of developed RMFs show expanded reaction properties, which will open up new possibilities to use these films in joining and other applications. Compared to Ti/Al and Zr/Al RMFs, a higher reaction velocity of (9.1±2) m/s and maximum reaction temperature of 1872 °C have been found for ternary Ti/Si/Ti/Al RMFs. On the other hand, the established Ni/Al nanofoil exhibits the reaction velocity of 2-13 m/s and temperature of 1400°C-1600°C [34, 70]. Compared to nanofoil, the developed ternary Ti/Si/Ti/Al RMFs in this work show a comparable reaction velocity and

relatively higher reaction temperature. Our attempt to use this ternary film in joining will be discussed in the chapter 10.

However, the question is generally still open in regard to the characteristics of an ideal reactive film. The work of Weihs et al. [6] suggests that distinct reactant layers without heat losses, the inverse dependence of reaction velocity on the thickness of the layers and exponentially dependent on the final temperature of the reaction can be appropriate for an ideal reactive system.

However, after analyzing the reaction properties of three types of RMFs in this work, the characteristics of an ideal film were also highlighted by focusing on the joining application. The schematic representations of T-t profiles of an ideal and non-ideal reactive film have been shown in Fig. 9.1 (a-b). An ideal reactive film can include the characteristics of fast atomic mixing rate and release heat without heat loss. That means the unsteady reaction propagation with decreasing reaction velocity and temperature cannot be considered. Obviously, reaction properties dependent on reactant combinations. High energetic reactants pairs with very fast reaction velocity and high reaction heat could be uncontrollable to handle. In that case, reactive films will be failed to melt the solder or brazes to bond components. In addition, reactant pairs with very low reaction heat and decreased reaction velocity will not be adequate in the reactive joining. Therefore, the reactive films from middle energy classed systems as mentioned in Fig 3.3 could be suitable for joining applications.

In contrast, RMFs with unsteady reaction propagation can be treated as non-ideal for joining as this reaction kinetic corresponds a high heat loss. Although, recent studies reported positive effects of oxidation on reaction heat [126], this oxidation could be also non-ideal, which is also presented in Fig 9.1 (b). This characteristic introduces a sluggish reaction and oxide constituent is expected to influence to reduce the bond strength of the components. In addition, an ideal RMF with a definite chemical composition should provide appropriate reaction heat, high reaction temperature and steady reaction propagation without intense heat loss. In this study, developed binary and ternary reactive films show a wide range of quantified reaction velocities, temperature and heat, which will be beneficial to provide application flexibility.

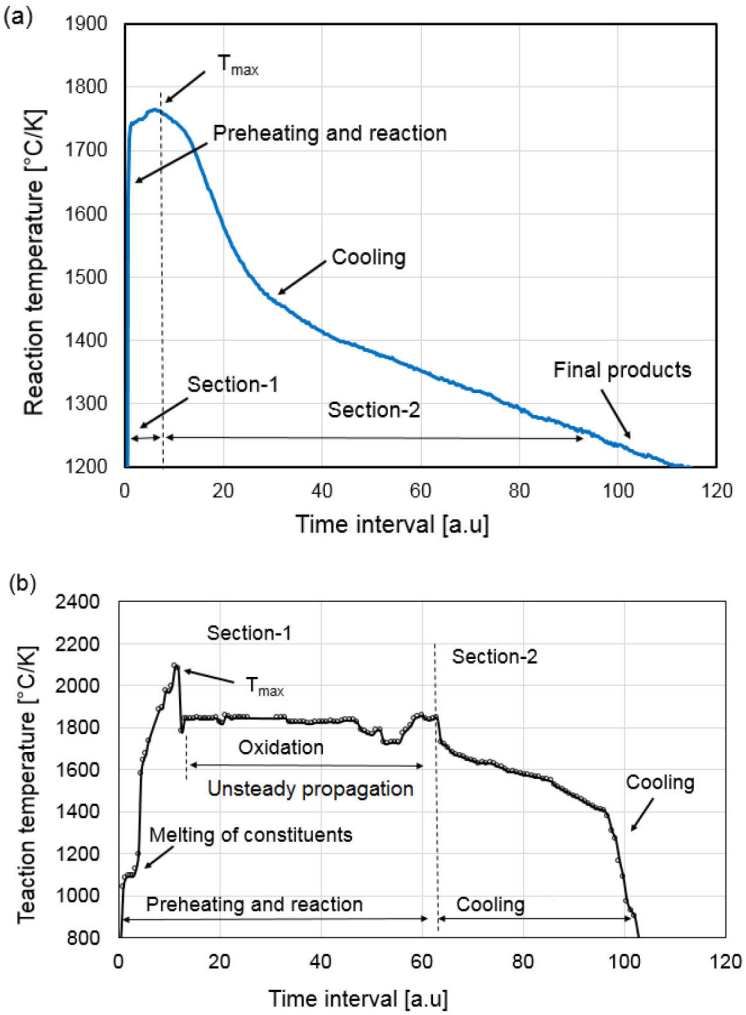

Figure 9.1: Schematic representation of reaction temperature - time profile of an ideal (a) and non-ideal reactive multilayer system (b).

10 Certain considerations for synthesis and uses

10.1 Process development for large sized freestanding film synthesis

Another focus of this research is to fabricate reactive films with large surface area. Therefore, the development of thick and large reactive films pays special attention in order to expand their applications. However, it is very difficult to produce chemically stable thick multilayers with uniform microstructural features. Therefore, certain considerations should be accounted. For example, the avoidance of mixing of distinct atom fluxes, overheating and deposition of highly pure multilayers with homogeneous microstructure and uniform film growth through the cross-section should be considered. The chemically distinct reactant layers were deposited on copper from alternating arranged four target sources. The schematic illustration of the deposition process has been shown in Fig. 10.1.

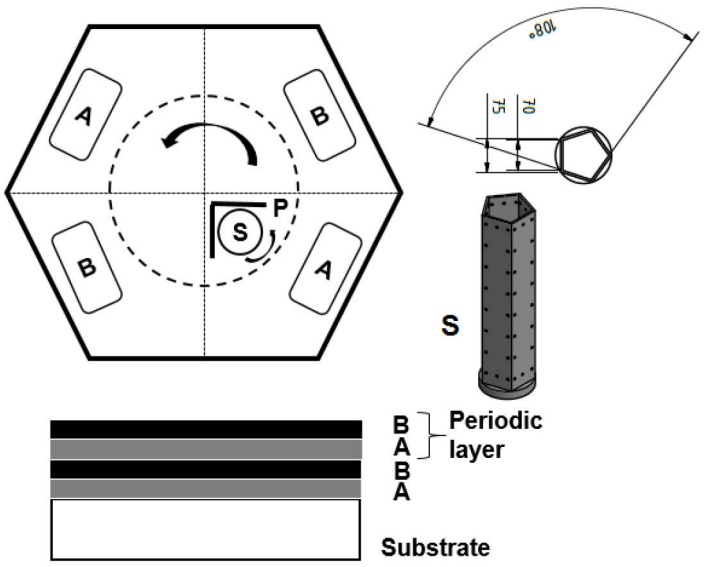

Figure 10.1: Schematic representation of the MSIP-PVD coating facility for A/B multilayer film synthesis. Here, A and B indicate the alternating targets. S is the substrate holder and P is the shielding plate. Hexagonal sample holder construction for large area film synthesis.

Here, copper substrate was clamped in a sample holder (S). A shielding plate (P) was inserted in order to avoid the mixing of atom fluxes from dissimilar targets. Targets were previously pre-sputtered. In addition, substrate was etched by introducing ionized argon. Moreover, the highly pure argon with a

flow rate of 185-230 mln was used as process gas for the film deposition. The overall deposition was described at section 4.2 and process parameters were listed in the table 4.1. The film was deposited on the cooled copper substrate at room temperature. Compared to conventional MSIP process, no heating step was used to fabricate the reactive films. The overall fabrication process includes the steps of (1) evacuation, (2) etching, (3) coating and (4) cooling. On the other hand, two different coating processes were used to control the microstructural morphology in order to fabricate thick films.

First process (process-1) includes the continuous coating. Second process (process-2) includes the coating with interval etching throughout the deposition. In this case, after every 1.5 hr of multilayer deposition, argon ion etching was performed for 1-2 minutes. The effects of both coating processes on microstructural homogeneity are shown in Fig. 10.2 (a, b). The 15-μm thick 1Zr/1Al film prepared by process-1 has shown in Fig. 10.2 (a). The film possesses non-uniform microstructures through the cross-section. For continuous deposition, overheating is expected to influence on such a film growth. The 45-μm thick 1Zr/1Al reactive film prepared by process-2 is shown in Fig. 10.2 (b).

The 52 μm thick 1Ti/1Si/1Ti/1Al ternary RMF deposited by process-2 has been shown in Fig. 10.2 (c). In process-2, additional interval etching during coating phases was included, which not only serves the homogenous film growth but also assured to reduce the overheating. Here, it is expected that the interval etching would help to grow the film with a layer deposition mechanism rather than the island growth mechanism. In this work, process-1 provides uniform microstructure and film growth for the film thickness less than (7±3) μm. Process-2 can provide structural homogeneity for increased film thickness. In both processes, the maximum chilled temperature during the deposition was in the range of (100±20) °C. This shows a good agreement regarding the chilled temperature of substrate as mentioned in Ref. [8]. Besides controlling the alternating reactant layers, the film morphology of sputtered deposited RMFs proposed an important aspect to understand the microstructure dependent reaction properties in terms of additional grain boundary diffusion and heat flows.

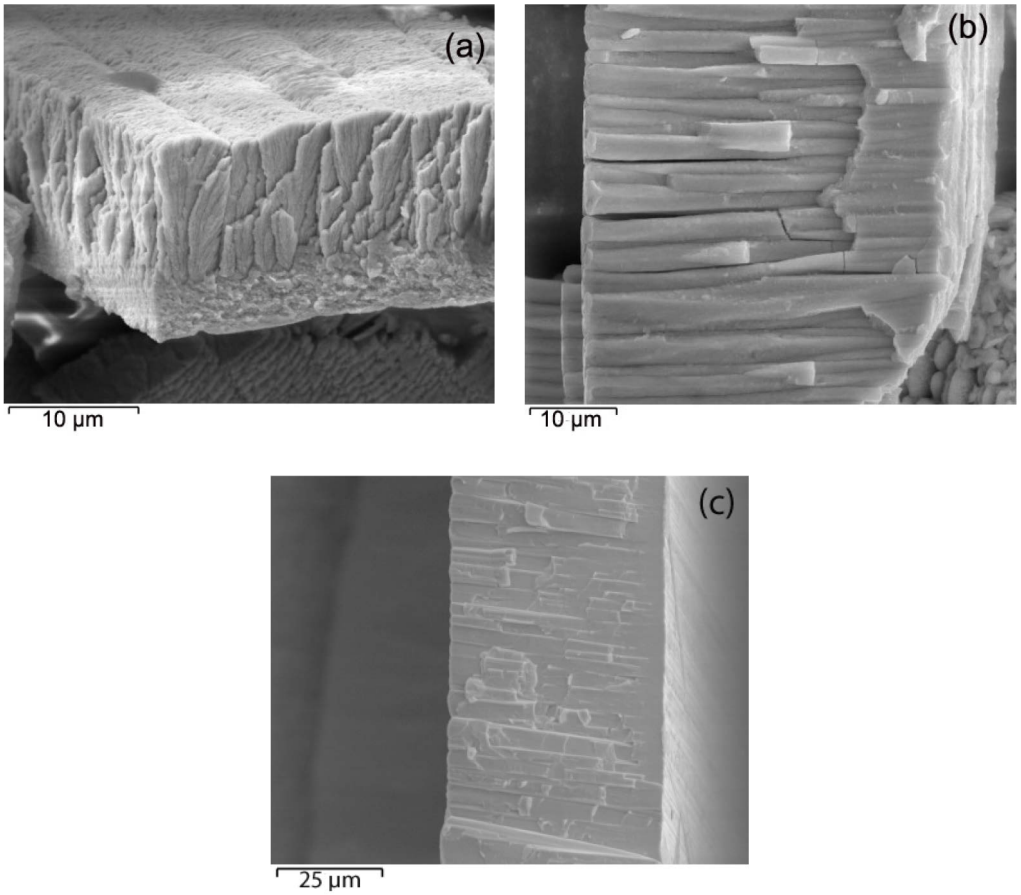

Figure 10.2: Cross-sectional SEM images of as-deposited freestanding 15 µm thick Zr/Al (d = 30 nm) RMF fabricated by process-1 (a), 45 µm thick Zr/Al reactive films (d = 30 nm) deposited by process-2 (b). This sample has 90° tilt alignment. 52 µm thick Ti/Si/Ti/Al reactive films (d = 29 nm) deposited by using process-2 (c). In this sample, an additional 70 V bias voltage was used during the coating process.

In this work, freestanding films were fabricated by chemical etching of Cu, which was also demonstrated in the previous section 4.3. Freestanding RMFs with large surface area are shown in Fig. 10.3 (a-c). Fig. 10.3 (a) shows the fabrication of freestanding Ti/3Al reactive film (d = 37 nm, l = 10 µm) with a surface area of 3 cm × 1 cm. Fig. 10.3 (b) represents 45 µm thick Zr/Al RMF with a dimension of 11 cm × (2-4) cm. Freestanding Ti/Si/Ti/Al reactive film with a dimension of 8 cm × 4 cm × 52 µm has been presented in Fig. 10.3 (c). With increasing film thickness, RMFs become straight, whereas thin film shows the bending possibility. The estimated dimension of freestanding films in this work is expected to be beneficial to expand their uses in joining and industrial applications.

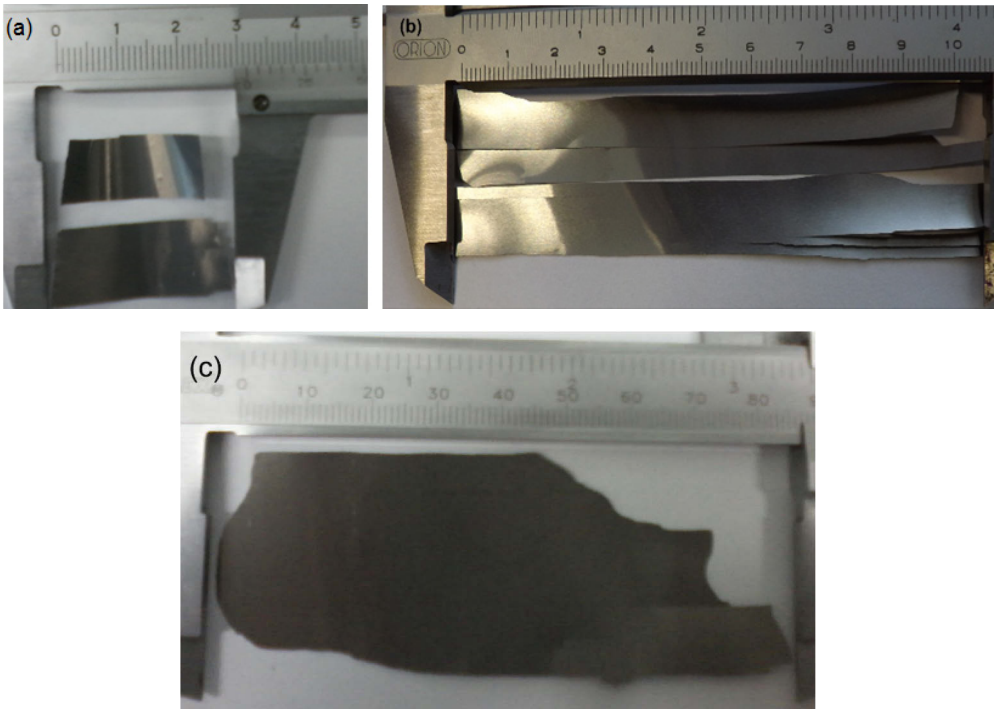

Figure 10.3: Freestanding MSIP-PVD coated Ti/3Al RMF (d = 37 nm) with a dimension of 3 cm × 1 cm × 10 µm (a). Zr/Al RMF (d = 30 nm) with a dimension of 11 cm × 2 cm × 45 µm (b) and Ti/Si/Ti/Al RMF(d = 29 nm) having a dimension of 8 cm × 4 cm × 52 µm (c).

10.2 Stability and handling

The alternating distinct multilayers are expected to be chemically stable. Nevertheless, distinct layers react together even at low temperature due to higher diffusivity at nanoscale during deposition process. The reactant combinations of high energetic system can form premixed layer preferentially compared to that of lower energetic system. This premixed layer is actually another distinct layer, which forms between two reactant layers, which could be a solid solution, intermetallic or amorphous phases. RMFs are made of mainly alternating nanoscale layers. Therefore, this film may become self-annealing even at low temperature during storage, which results in the growth of premixed layer. It reduces the reaction heat and propagation rate. In addition, this film can be oxidized in air even at room temperature. Therefore, RMFs process a certain service life that mainly depends on the reactant combinations and microstructural morphology. For the commercial Ni/Al nanofoil, the general self-life has proposed to be one year as demonstrated in Ref. [70]. The self-life of high energetic films will be reduced faster.

However, the thermodynamic driving force of chemical energy, elastic strain energy and interfacial free energies control the instabilities in multilayers through either reactants mixing or atomic rearrangement as mentioned in Ref. [154]. On the other hand, reactive multilayers are very brittle. Therefore, precautions are required to handle these films carefully. The film surface should be free from absorbent materials, dirt deposits, moisture, oil or grease. It would be beneficial to deposit an additional melting layer or oxidation resistance coating on top of these films depending on their uses.

10.3 Expanded applications of developed reactive films

Several applications were proposed to use the developed reactive films in this work. Among them two important uses have received most attention. These are the medical and joining applications. Initially, the concept was generated to use freestanding RMFs in the form of particles (rod, elongated, round, or encapsulated, etc.) having a size of micrometer scale in medical applications. Due to processing a noble property of supplying very fast and quantified heat, the idea was generated to kill the abnormal cancer cells, tumor or other relevant diseases by using these reactive systems. In this case, reactive systems from low and medium energy classed will be very beneficial. Specially, it requires a lots of efforts in regard to methodology, storage and process in further developments. However, a simple fabrication method of freestanding reactive films having flexible sizes (μm to cm) and shapes in this work (presented in Fig. 4.4 a), offers also an abundance of possibilities in medical sciences.

10.3.1 Developed ternary RMFs for reactive joining

Reactive films supply direct and concentrated heat within milliseconds to the joint area to bond the components. The recent study shows mostly the uses of commercial Ni/Al nanofoil in various structural joining applications [49, 156]. In this work, developed Ti/Si/Ti/Al RMF shows a comparable reaction velocity and even higher reaction temperature compared to that of commercial nanofoil (see table 9.2 chapter 9). Therefore, this work attempts to use the developed ternary film to join stainless steel components. Here, Sn melting layer with a thickness of (15±5 μm) was electrodeposited on the steel

components and then joined with ternary 1Ti/1Si/1Ti/1Al (l = 52 µm) RMF by applying joining pressure of 32 MPa.

At the same time, a reactive joining was performed by stacking 80 µm thick commercial Ni/Al nanofoil (from Indium Corporation) between the stainless steels coated with the melting layers. Here, two types of melting layers: only Sn (15±2 µm) layer and Ni (6 µm) coated Sn (10±2 µm) layer were taken. Reactive films slightly larger than the size of bonded area were sandwiched between the joint components. Then a uniaxial compressive load was applied in order to build uniform contact to the joint assembly. For Ni/Al nanofoil, the joining pressure of approx. 100 MPa was considered as mentioned in Ref. [48]. For both joints, an electrical ignition of 15 V was used.

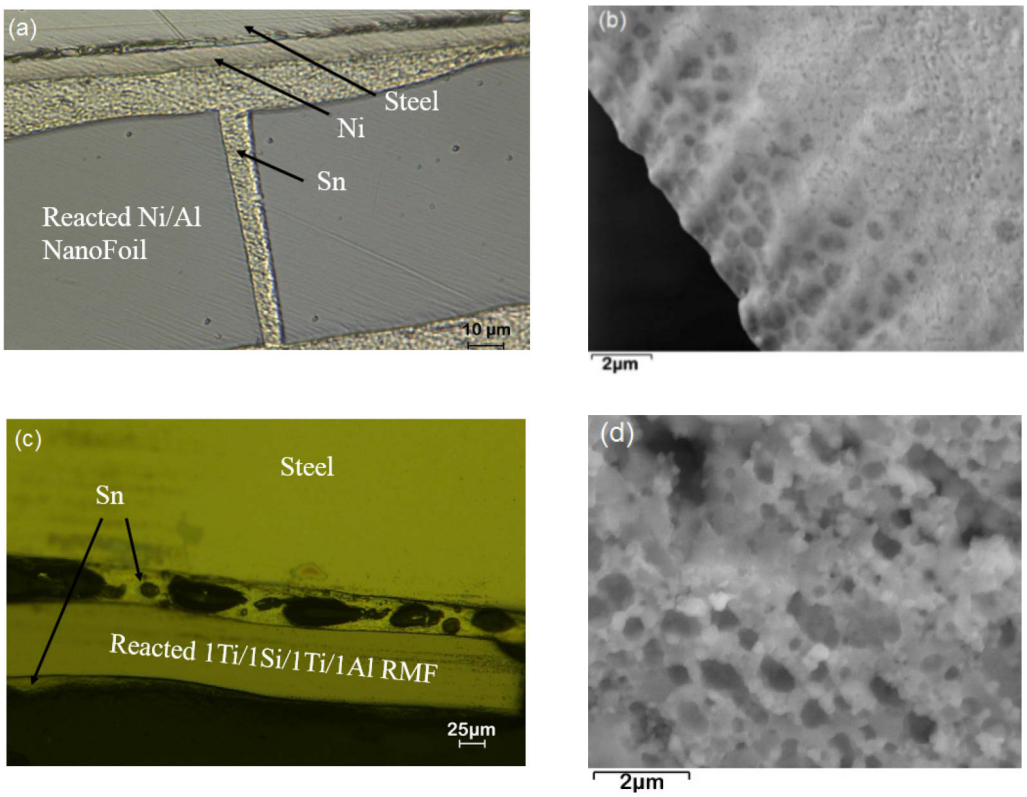

Figure 10.4: Cross-sectional optical micrograph of a reactive joint of stainless steel using commercial Ni/Al (d = 50 nm) nanofoil (a) and SEM image of reacted Ni/Al nanofoil (b). Cross-section of a reactive joining using developed 1Ti/1Si/1Ti/1Al (d = 29) RMF (c) and SEM image of reacted ternary film (d).

The microstructural analysis of both joints by nanofoil and ternary RMF has been presented in Fig. 10.4. Sn melts and flows to the crack gap in the reacted nanofoil, which has been shown in Fig 10.4 (a). Here, macro cracks form in

reacted nanofoil due to fast cooling of intermetallic compounds from high temperature. Reacted nanofoil has been shown in Fig. 10.4 (b). Here, the formation of beta-NiAl (51.5 at. % Ni and 48.5 at. % Al) intermetallic compound was observed. The reactive joining by using Ti/Si/Ti/Al RMF has been presented in Fig 10.4 (c). The microstructural analysis shows that joint components are connected loosely. Sn layer melts and adheres to the components. Compared to joining with nanofoil, no macro-crack forms in this reacted ternary film. However, micro-cracks can form in the reacted film. Fig 10. 4 (d) shows the reacted ternary film. As major reaction products, intermetallic compounds of Si_2Ti and Al_2Ti were observed. Multiple reaction products of ternary film can introduce ductile nature, which could be beneficial in regard to joint quality. However, the investigations of property and quality of this joint are still open for future studies.

Here, further developments are required to estimate the appropriate film thickness, morphology and melting layers, to adjust the joining pressure and activation method in order to have a sound joint. However, this research confirms our first attempt to perform reactive joining by using developed 1Ti/1Si/1Ti/1Al RMF, which will open up a lot of opportunity in advanced joining technology.

11 Conclusions and outlook

This scientific study concerns with the development of magnetron sputtered deposited Ti/Al, Zr/Al and Ti/Si/Ti/Al reactive films with large surface area, understanding of their reaction properties and expansion of their uses. For the first time, this research focuses on the development of ternary film of Ti-Si-Al systems besides Al-based binary Ti/Al and Zr/Al RMFs. It also attempts to use developed Ti/Si/Ti/Al RMFs for reactive joining of stainless steels. The analysis of reaction properties along with propagation kinetics has been investigated, which shows a wide range of possibilities and flexibilities for utilizing their reaction heat, temperature and velocity. A simple and cost effective approach to fabricate large sized freestanding multilayer films with uniform film morphology will be beneficial to expand their uses. The main conclusions are summarized as follows:

Microstructure morphology:

Both binary and ternary RMFs in this work show the columnar microstructural morphology with coherent alternating reactant layers. The microstructures of Ti/Al and Ti/Si/Ti/nAl (n = 1, 2, 3) reactive films may fit in the transition zone T. However, the morphology of Zr/Al may fit in zone T or zone 2. This columnar morphology in RMFs introduces an additional grain boundary diffusion along with reactants mixing in multilayers. Both diffusion processes can introduce even faster reaction rate. However, as a high columnar gap can introduce negative effects by reducing reaction propagation and introducing heat loss. Therefore, the details of microstructural features and critical columnar gap could be investigated in the future work. After a fast self-propagating reaction, alternating layers react together and form the reaction products, which were investigated by XRD. Final reaction products depend on the bilayer thickness, molar ratios and multilayer design. In addition, reaction kinetics also effects on the formation of reaction products. Here, the secondary oxidation during self-propagating reaction influences to form the Al-rich intermetallics in Ti/Al and Zr/Al RMFs in air. Further investigations should be performed for these RMFs considering the exothermic reaction in other atmospheres also for different ignition methods.

Reaction front propagation:

In binary Ti/Al RMFs, a high reaction velocity of (2.6±0.6) m/s was estimated for 1Ti/1Al composition. Here, only 1Ti/3Al composition shows also the unsteady reaction, which reduces the reaction propagation. Zr/Al RMF (d = 30 nm), shows a maximum reaction velocity of (1.22±0.4) m/s. Here, ternary 1Ti/1Si/1Ti/1Al compositions show a high reaction velocity of (9.1±2) m/s compared to other ternary compositions and both binary films. The reaction front velocity depends on the reactant combination, chemical composition, bilayer thickness and multilayer arrangement. Moreover, this work shows that the reaction propagation can be controlled by distinct interacting interfaces in multilayer design having similar reactant types and bilayer thickness. Moreover, this work also shows that the reaction velocity depends on electrical ignition potentials for a given composition. Too low ignition potential shows slower propagation and too high potential can introduce unstable propagation. As an optimal activation potential, 9 V was identified for three types of reactive films. However, different activation methods can show different reaction properties, which could be conducted in the future study.

Reaction temperature:

In this work, Ti/Al and Zr/Al binary RMFs RMFs show the average reaction temperatures of 1215-1298 °C and 1581-1707 °C, respectively. For the ternary RMFs, the maximum reaction temperatures of 1345-1872 °C have been estimated. In comparison with nanofoil, ternary 1Ti/1Si/1Ti/1Al and binary 1Zr/1Al RMFs exhibit even higher reaction temperature. In three types of films, the state of products at maximum temperature is considered to be solid or solid-liquid. The melting of constituents or allotropic phase change of the reactants can also influence on maximum reaction temperature. In addition, reaction temperature profile exhibits important reaction kinetics of oxidation and propagation manner.

Reaction heat:

The Thermo-Calc simulation was conducted initially in order to calculate the standard reaction heat of three types of film systems. The result shows that reaction heat depends on the type and number of reaction products. In

addition, transformation heat flows and phase change temperatures of three RMFs were investigated by DSC analysis, which characterize the dependency of heat flow on the bilayer, molar ratios or layer arrangements. However, the transformation heat measured by DSC cannot be considered as total reaction heat due to low signal. Further developments are required concerning film morphology and experimental parameters. Here, ternary reactive films show higher reaction heat due to higher heat of formation. In case of formation of multiple reaction products, reaction heat can be adjusted by their volume fraction. However, in reality the maximum reaction heat and temperature of a definite RMF cannot be achieved due to heat loss by premixing, constituents melting, sluggish reaction and unsteady propagation. However, this work confirms that reaction kinetics influence on reaction properties. Further studies could be highlighted to quantify the heat loss for an unsteady propagation.

Secondary oxidation reaction:

During the self-propagating reaction, the oxidation reaction with a temperature plateau was found in the T-t profiles of Zr/Al and Ti/2Al RMFs. The significant oxidation has been noticed in 1Zr/1Al films mainly for higher bilayer thickness larger than 25 nm. Here, it is expected that intermetallic compounds form prior to the oxidation reaction and later oxides form as a secondary reaction. Generally, oxidation may occur of the reactants, metastable phases or final reaction products during a self-propagating reaction. The oxidation effect during self-propagating reaction assures the high temperature for a certain period, which can open a new application fields. However, the more details of oxidation characteristics should be studied further.

Steady and unsteady propagation:

In this work, the reaction kinetics of steady and unsteady propagation were also investigated. Here, 1Ti/1Al, 1Ti/2Al, 1Zr/1Al, 1Ti/1Si/1Ti/nAl compositions show the steady state propagation, whereas 1Ti/3Al and 1Si/1Ti/1Al/1Si multilayer films exhibit both steady and unsteady propagation. For unsteady reaction, a ripple band with fine and coarse microstructures form, which was identified in reacted 1Ti/3Al RMF. This

propagation mode reduces the reaction front velocity and maximum reaction temperature. The unsteady propagation in 1Ti/3Al films reduces the maximum reaction temperature to (200±15) °C compared to same film with steady propagation.

The ternary 1Si/1Ti/1Al/1Si RMFs also show the unsteady propagation, where only color band was observed. Here, the surface oxidation is expected to influence such an unsteady propagation. This ternary film type shows a maximum reaction velocity of (2.7±0.8) m/s and maximum temperature of (1400±23) °C for the steady propagation. Whereas, the unsteady propagation reduces the reaction front velocity to (1.1±0.2) m/s and temperature to (1228±42) °C. However, no unsteady propagation having was observed in binary Zr/Al RMF. However, many questions are still open in regard to steady-unsteady transition even for similar composition, heat loss, constituent melting and preheating effect, which could be further studied.

Numerical simulation:

In this work, CFD simulation was performed to characterize nanoscale reactant mixing and temperature flow in 1Ti/1Al film for the steady reaction. Here, it shows that thermal flow is faster than atomic mixing in 1Ti/1Al composition for 20 nm bilayer. However, further study can be conducted of this film for different film morphology and unsteady propagation. CFD simulation of other multilayer systems can be studied further.

Large area reactive film synthesis:

This work shows a simple method to produce large sized freestanding reactive films. As an efficient and cost effective substrate, Cu shows the benefits to make RMFs freestanding only by etching. The modification of deposition process having the coating with an interval argon ion etching confirms the uniform film growth throughout the cross-section. This work confirms the fabrication of freestanding 1Zr/1Al reactive film (d = 30 nm) with the size of 11 cm × 2 cm × 45 µm and freestanding 1Ti/1Al film with a size of 4 cm × 2 cm × 10 µm, respectively. Ternary 1Ti/1Si/1Ti/1Al reactive film with a dimension of 8 cm × 5 cm × 52 µm was synthesized. The special considerations should be accounted to characterize the self-life and to design,

handle and store of these films in regard to utilize maximum stored energy in the further study.

Reactive joining using ternary RMF:

This work shows the first attempt to use developed ternary 1Ti/1Si/1Ti/1Al film in reactive joining of steels. The joint cross-section was compared to that of commercial nanofoil. The microstructural analysis shows that like nanofoil, it does not exhibit macro sized crack gap. However, micro cracks may presence on it and Sn melts and adheres to the components. The details investigation of joint quality and properties should be studied further. However, this first attempt of reactive joining using ternary RMF shows a wide range of possibilities in joining technology. Further developments are required by introducing appropriate film morphology and thickness, melting layers (solder or brazes types and thickness), adjusting joining parameters (pressure, preheating, ignition type, atmosphere) to have a sound joint. The understanding of different thermal properties of joint components could be further developed. In addition, the uses of these developed RMFs could be also expanded in the diffusion bonding.

In conclusion, developed Ti/Al, Zr/Al and Ti/Si/Ti/nAl RMFs in this work show a wide range of reaction heat, velocity and temperature along with reaction kinetics, which can introduce application flexibility. This work confirms that reaction properties cannot only be controlled by adjustment of chemical reactants, bilayers or molar ratios but also multilayer designs. For the first time, this work shows that reaction propagation and kinetics could also be controlled by introducing distinct atomic mixing interfaces in ternary reactant system. It also introduces a simple and cost effective synthesis method to fabricate large sized freestanding RMFs with uniform microstructure. This research represents the flexibility to design reactive multilayer films in order to utilize their quantified stored chemical energy, which will show an abundance possibilities in scientific fields, joining, industrial and medical applications.

References

[1] A. S. Rogachev, A. S. Mukasyan, Combustion of heterogeneous nanostructural systems (Review), *Combust. Explos. Shock Waves*, 46.3 (2010) 243-266.

[2] A. S. Rogachev, S. G. Vadchenko, A. S. Mukasyan, Self-sustained waves of exothermic dissolution in reactive multilayer nanofoils, *Appl. Phys. Lett.* 101 (2012) 063119.

[3] J. Wang, E. Besnoin, A. Duckham, S. J. Spey, M. E. Reiss, O. M. Knio, T. P. Weihs, Room-temperature soldering with nanostructured foils, *Appl. Phys. Lett.* 83.19 (2003) 3987-3989.

[4] T.W. Barbee, Jr., R.L. Simpson, A.E. Gash, J.H. Satcher, Jr., Nano-laminate-based ignitors, US. Pat. 8,328,967 (11 December 2012).

[5] J. N. Johnson, I.B. Schild, Methods of making multilayered, hydrogen containing thermite structures, US. Pat. 7,829,157 (2010).

[6] T. P. Weihs, Fabrication and characterization of reactive multilayer films and foils. *Metallic Films for Electronic, Optical and Magnetic Applications, Swaston: Woodhead*, (2014) 160-243.

[7] D. P. Adams, Reactive multilayers fabricated by vapor deposition: A critical review, Thin Solid Films, 576 (2015) 98-128.

[8] Y. Xun, D. Lunking, E. Besnoin, D. van Heerden, T. P. Weihs, O. Knio, Methods of making reactive composite materials and resulting products, US Pat. 20110027547 A1, 2011.

[9] M. E. Reiss, C. M. Esber, D. Van Heerden, A. J. Gavens, M. E. Williams, P. Weihs, Self-propagating formation reactions in Nb/Si multilayers, *Mater. Sci. Eng. A* 261 (1999) 217–222.

[10] D. P. Adams, M. A. Rodriguez, J. P. McDonald, M. M. Bai, E. Jones Jr., L. Brewer and J. J. Moore, Reactive Ni/Ti nanolaminates, *J. Appl. Phys.* 106 (2009) 093505.

[11] D. P. Adams, V. C. Hodges, M. M. Bai, E. Jones, M. A. Rodriguez, T. Buchheit, J. J. Moore, Exothermic reactions in Co/Al nanolaminates, *J. Appl. Phys.*104 (2008) 043502.

[12] H. Goldschmidt, Verfahren zur Erzeugung hoher Temperaturen (Method for the production of high temperatures), *Z. Electrochem.* 6 (1899) 53.

[13] Yu.M. Maksimov, A.G. Merzhanov, A theory for the combustion of condensed materials, *Fiz. Goreniya Vzryva,* 1 (1966) 47.

[14] J. Floro, Propagation of explosive crystallization in thin Rh-Si multilayer films, *J. Vac. Sci. Technol A*, (1986) 631- 636.

[15] A.G.Merzhanov, I. P. Borovinskaya, Historical retrospective of SHS: an autoreview, *International Journal of Self-Propagating High-Temperature Synthesis*, 17(4) (2008) 242-265.

[16] Ya. B. Zel'dovich,. D. A. Frank-Kamenetskii, Theory of the Thermal Propagation of Flame, *Zh. Fiz. Khim.,* vol. 12, no. 1, (1938) 100-105.

[17] K. J. Blobaum, M.E. Reiss, J.M. Plitzko, T.P.Weihs, Deposition and characterization of a self-propagating CuOx/Al thermite reaction in a multilayer foil geometry, *J. Appl. Phys.* 94 (2003) 2915.

[18] T. S. Dyer, Z. A. Munir, V. Ruth, The combustion synthesis of multilayer NiAl systems, *Scripta Metallurgica et Materialia* 30 (1994)1281-1286.

[19] M. Herr: Fügen von Hochvolt-komponenten mittels reaktiver Nanometer Multischichten, Dissertation, TU Berlin, 2012.

[20] Indium Corporation, Nanofoil Product datasheet, 2016. http://www.indium.com (accessed 27.07.2016).

[21] I. Barin, O. Knacke, O Kubashewski, (eds) Thermal Properties of Inorganic Substances, Supplement, New York: Springer (1977).

[22] O. Knacke, O. Kubaschewski and K. Hesselmann, (eds) Thermochemical Properties of Inorganic Substances, 2nd edn, New York: Springer, (1991).

[23] F.R. de Boer, R. Boom, W.C.M. Mattens, A.R. Miedema, and A.K. Niessen, Cohesion in Metals. Transition Metal Alloys, Vol. 1 F: *Met. Phys.*, 18 (1988) 903.

[24] R. H. Willens, A. Kornblit, L. R. Testardi, and S. Nakahara, Melting of Pb as it approaches a two-dimensional solid, *Phys. Rev. B* 25, 290 (1982).

[25] J. H. Rose, John Ferrante, and John R. Smith, Universal Binding Energy Curves for Metals and Bimetallic Interfaces, *Phys. Rev. Lett.* 47 (1981) 675.

[26] W. H. Qi, Size effect on melting temperature of nanosolids, *Physica B,* 368 (2005) 46-50.

[27] A.L. Greer, Diffusion and reactions in thin films, *Appl. Surf. Sci.* 86 (1995) 329-337.

[28] A.L. Greer, Diffusion and phase nucleation in metallic multilayers, *J. Magn. Magn. Mater*, 126 (1993) 89-95.

[29] A. B. Mann, A. J. Gavens, M. E. Reiss, D.Van Heerden, G. Bao, T. Weihs, Modeling and characterizing the propagation velocity of exothermic reactions in multilayer foils, *J. Appl. Phys.*, 82 (1997) 1178-1188.

[30] A. Hardt, P. Phung, Propagation of gasless reactions in solids. 1. Analytical study of exothermic intermetallic reaction-rates, *Combust. Flame*, 21 (1973) 77-89.

[31] R. Armstrong, Models for gasless combustion in layered materials and random media, *Combust. Sci. Technol.*, 71(4–6) (1990)155-174.

[32] R. Armstrong, M. Koszykowski, Combustion theory for sandwiches of alloyable materials, in Munir, Z. and Holt, J. (eds), *Combustion and Plasma Synthesis of High-Temperature Materials*, New York: VCH, (1990) 88-99.

[33] T. W. Barbee, T. Weihs, Ignitable heterogeneous stratified structure for the propagating of an internal exothermic chemical reaction along an expanding wave front and method of making same. US Pat. 5538795, 1996.

[34] R. Knepper, M.R. Snyder, G. Fritz, K. Fisher, O.M. Knio, T.P. Weihs, Effect of varying bilayer spacing distribution on reaction heat and velocity in reactive Al/Ni multilayers, *J. Appl. Phys.* 105 (2009) 083504.

[35] D.P. Adams, V.C. Hodges, M.M. Bai, E. Jones Jr., M.A. Rodriguez, T. Buchheit, J.J. Moore, Exothermic reactions in Co/Al nanolaminates, *J. Appl. Phys.* 104 (2008) 043502.

[36] M.E. Reiss, C.M. Esber, D. Van Heerden, A.J. Gavens, M.E. Williams, T. P.Weihs, Selfpropagating formation reactions in Nb/Simultilayers, *Mater. Sci. Eng. A* 261 (1999) 217.

[37] S.C. Barron, S.T. Kelly, J. Kirchhoff, R. Knepper, K. Fisher, K.J.T. Livi, E.M. Dufresne, K. Fezzaa, T.W. Barbee, T.C. Hufnagel, T.P. Weihs, Self-propagating reactions in Al/Zr multilayers: anomalous dependence of reaction velocity on bilayer thickness, *J. Appl. Phys.,* 114 (2013) 223517.

[38] D.P. Adams, M.A. Rodriguez, J.P. McDonald, M.M. Bai, E. Jones Jr., L. Brewer, J.J. Moore, Reactive Ni/Ti nanolaminates, *J. Appl. Phys.,* 106 (2009) 093505.

[39] A.S. Rogachev, H.E. Grigoryan, E.V. Illarionova, I.G. Kanel, A.G. Merzhanov, A.N. Nosyrev, N.V. Sachkova, V.I. Khvesyuk, P.A. Tsygankov, Gasless combustion of Ti–Al bimetallic multilayer nanofoils, *Combust. Explos. Shock Waves,* 40 (2004) 166.

[40] D.P. Adams, M.A. Rodriguez, C.P. Tigges, P.G. Kotula, Self-propagating, high temperature combustion synthesis of rhombohedral AlPt thin films, *J. Mater. Res.,* 21 (2006) 3168.

[41] A. S. Tappan, J.P. McDonald, D.P. Adams, E.D. Jones Jr., Characterization of reactive Ti/2B multilayer films, *Pyrotechnics Sem. and Symp., (*2008) 143.

[42] J.P. McDonald, M.A. Rodriguez, E.D. Jones Jr., D.P. Adams, Rare-earth transition metal intermetallic compounds produced via self-propagating, high-temperature synthesis, *J. Mater. Res.,* 25 (2010) 718.

[43] T. W. Barbee, Jr., T. Weihs, Method for fabricating an ignitable heterogeneous stratified metal structure, *U.S. Patent No. 5,547,715*. 20 Aug. 1996.

[44] T. Weihs, M. Wall, Jr. T. Barbee, A low temperature technique for measuring enthalpies of formation, *J. Mater. Res.*, 11 (1996) 1403-1409.

[45] A. J. Gavens, D. Van Heerden, A.B. Mann, M.E. Reiss, T. P. Weihs, Effect of intermixing on self-propagating exothermic reactions in Al/Ni nanolaminate foils, *J. Appl. Phys.,* 87 (2000) 1255.

[46] R.V. Reeves, D.P. Adams, Reaction instabilities in Co/Al nanolaminates due to chemical kinetics varying over micron-scales, *J. Appl. Phys.,* 115 (2014) 044911.

[47] M. Vohra, J. Winokur, K. R. Overdeep, P. Marcello, P., Weihs, T. P., & Knio, O. M. (2014). Development of a reduced model of formation reactions in Zr-Al nanolaminates, *J. Appl. Phys.,* 116 (23), 233501.

[48] J. Wang, E. Besnoin, A. Duckham, S.J. Spey, M.E. Reiss, O.M. Knio, T.P.Weihs, Joining of stainless-steel specimens with nanostructured Al/Ni foils, *J. Appl. Phys.,* 95 (2004) 248.

[49] G. Lucadamo, K. Barmak, D. T. Carpenter, J. M. Rickmani, Microstructure evolution during solid state reactions of Nb/Al multilayers, *Acta mater.*, 49 (2001) 2813-2826.

[50] M. Kokonou, K.P. Giannakopoulos, I.E. Gunduz, K. Fadenberger, C. Rebholz, C.C. Doumanidis, Reactive bimetallic Al/Ni nanostructures for nanoscale heating applications fabricated using a porous alumina template, *Microelectron. Eng.*86 (2009), 836.

[51] L. Battezzati, P. Pappalepore, F. Purbiano, I. Gallino, Solid state reactions in Al/Ni alternate foils induced by cold rolling and annealing, *Acta. Mat.,* 47 (1999) 1901-1914.

[52] H. Sieber, J. S. Park, J. Weissmüller, H, Perepezko, Structural evolution and phase formation in cold-rolled aluminum–nickel multilayers, *Acta. Mat.,* 49 (2001) 1139-1151.

[53] X. Qiu: Reactive multilayer foils and their applications in joining, Doctoral thesis, (2007).

[54] W. Blum, The structure and properties of alternately deposited metals, *J. Electrochem. Soc.,* 40 (1921) 307-320.

[55] J. P. Celis, A. Haseeb, J.R. Roos, Electrodeposition of Cu/Ni compositionally modulated multilayers by the dual-plating bath technique, *Trans. Inst. Met. Finish.,* 70 (1992) 123-128.

[56] R. Knepper, G. Fritz, T. Weihs, Controlling the shape of Al/Ni multilayer foils using variations in stress, *J. Mater. Res.,* 23 (2008) 2009-2016.

[57] M. Guan, E.J. Podlaha: Electrodeposition of AuCo alloys and multilayers. *J. Appl. Electrochem*, 37 (2007) 549-555.

[58] J. D. Ferguson, K. J. Buechler, A.W. Weimer, S.M. George, SnO2 atomic layer deposition on ZrO_2 and Al nanoparticles: pathway to enhanced thermite materials, *Powder Technol*. 156 (2005) 154.

[59] S. M. George, J.D. Ferguson, A. W. Weimer, J.R. Wank, Insulating and Functionalizing Fine Metal-Containing Particles with Conformal Ultra-Thin Films, *European Patent* 1412175, 8 July, 2006.

[60] J. Kwon, J.-M. Ducéré, P. Alphonse, M. Bahrami, M. Petrantoni et al., Interfacial chemistry in Al/CuO nanomaterial and its role in exothermic reaction, *ACS Appl. Mater. Interfaces,* 5 (2013) 605.

[61] L. A. Clevenger, C. V. Thompson, K.N. Tu, Explosive silicidation in nickel/amorphous silicon multilayer thin films, *J. Appl. Phys.,* 67 (1990) 2894.

[62] Y. N. Picard, D. P. Adams, J. A. Palmer, S.M. Yalisove, Pulsed laser ignition of reactive multilayer films, *Appl. Phys. Lett.,* 88 (144102) (2006).

[63] Y. N. Picard, J. P. McDonald, T.A. Friedmann, S.M. Yalisove, D.P. Adams, Nanosecond laser induced ignition thresholds and reaction velocities of energetic bimetallic nanolaminates, *Appl. Phys. Lett.,* 103 (2008) 104103.

[64] Indium Corporation - Nanofoil® User Guide, (http://www.indium.com/technical-documents), 2016.

[65] G. M. Fritz, S. J. Spey Jr., M.D. Grapes, T. P. Weihs, Thresholds for igniting exothermic reactions in Al/Ni multilayers using pulses of electrical, mechanical, and thermal energy, *J. Appl. Phys.,* 113 (2013) 014901.

[66] C. E. Wickersham Jr., J. E. Poole, Explosive crystallization in zirconium/silicon multilayers, *J. Vac. Sci. Technol.,* 6 (1988) 1699.

[67] A. E. Gash, T.W. Barbee Jr., O. Cervantes, Stab sensitivity of energetic nanolaminates, *Proc. 33rd International Pyrotech. Sem*, ISBN: 0975527428 (2006) 59.

[68] B. A. Mason, L. J. Groven, and S. F. Son, The role of microstructure refinement on the impact ignition and combustion behavior of mechanically activated Ni/Al reactive composites, *J. Appl. Phys.*, 114.11 (2013): 113501.

[69] E. Ma, C.V. Thompson, L.A. Clevenger, K. N. Tu, Self-propagating explosive reactions in Al/Ni multilayer thin films, *Appl. Phys. Lett.,* 57 (1990) 1262.

[70] Nanofoil Wave Propagation, NanoBond, http://www.indium.com/blog/wave-propagation-of-nanofoil.php (accessed 07.01.2017)

[71] A. Duckham, S. J. Spey, J. Wang, M. E. Reiss, T. P. Weihs, E. Besnoin, O. M. Knio, Reactive nanostructured foil used as a heat source for joining titanium, *J. Appl. Phys.,* 96 (2004) 2336-2342.

[72] X. Qiu, J. Wang, Bonding silicon wafers with reactive multilayer foils, *Sensors and Actuators A - Physical,* A141 (2008) 476-481.

[73] L. I. Duarte, A. S. Ramos, M. F. Vieira, F. Viana, M. T. Vieira, M. Kocak, Solid-state diffusion bonding of gamma-TiAl alloys using Ti/Al thin films as interlayers. *Intermetallics,* 14 (2006) 1151-1156.

[74] S. Simões, F. Viana, M. Koçak, A.S. Ramos, M.T. Vieira, and M.F. Vieira, Diffusion bonding of TiAl using reactive Ni/Al nanolayers and Ti and Ni foils, *Mater. Chem. Phys.* 128 (2011) 202-207.

[75] J. Cao X. G. Song, L. Z. Wu, J. L. Qi, J. C. Feng, Characterization of Al/Ni multilayers and their application in diffusion bonding of TiAl to TiC cermet, *Thin Solid Films*, 520 (2012) 3528-3531.

[76] K. Raic‘, R. Rudolf, I. Anz’el, A. Todorovic‘, Multilayered nanofoils for low-temperature metal - ceramic joining, *Metalurgija, vol.* 14 (2008)143-154.

[77] K. Raic‘, R. Rudolf, B. Kosec, I. Anz’el, V. Lazic’, A. Todorovic‘, Nanofoils for soldering and jewellery manufacturing, *MTAEC9*, 43 (1) 3 (2009).

[78] T. A. Baginski, S. L. Taliaferro, W. D. Fahey, Novel electro explosive device incorporating a reactive laminated metallic bridge, *J. Propul. Power.,* 17 (2001) 184-189.

[79] X. Qiu, R. Tang, R. Liu, H. Huang, S. Guo, H. Yu, A micro initiator realized by reactive Ni/Al nanolaminates, *J. Mater. Sci. Mater. Electro*n, 23 (2012) 2140-2144.

[80] H. Pezous, C. Rossi, M Sanchez et al., Fabrication, assembly and tests of a MEMS-based safe, arm and fire device, *J. Phys. Chem. Solids*, 71(2010) 75-79.

[81] K. Zhang, C. Rossi, M. Petrantoni, N. Mauran, A nano initiator realized by integrating Al/CuO-based nanoenergetic materials with a Au/Pt/Cr microheater, *J. Microelectromech. Syst*., Vol. 17 (2008) 832-836.

[82] T. Weihs, BioAgent Defeat Using Gaseous Biocidals, Weihs research group, http://weihsgroup.jhu.edu/DTRA.html (accessed 07.01.2017).

[83] C. Jay, M. Ding, F. Krieger, J. Swank, G. Chen, C. McMullan, Nanofoil heating elements for thermal batteries, *Proceedings of the Army Science Conferenc*e, 2008.

[84] A. S. Ramos, M. T. Vieira, J. Morgiel, J., Grzonka, S. Simões, M. F. Vieira, Production of intermetallic compounds from Ti/Al and Ni/Al multilayer thin films-A comparative study. *J Alloys Compd.*, 484 (2009) 335-340.

[85] M. A. Guitar, H. Aboulfadl, C. Pauly, P. Leibenguth, S. Migot, F. Mücklich, Production of single-phase intermetallic films from Ru-Al multilayers. *Surf. Coat. Technol*., 244 (2014) 210-216.

[86] F. Spaepen, C. V. Thompson, Calorimetric studies of reactions in thin films and multilayers, *Appl. Surf. Sci.*, 38 (1989) 1-12.

[87] M. Salloum, O. Knio, Simulation of reactive nanolaminates using reduced models: III. Ingredients for a general multidimensional formulation, *Combust. Flame*, 157 (2010) 1154-1166.

[88] B. Müller, U. Renz, Development of a fast fiber-optic two-color pyrometer for the temperature measurement of surfaces with varying emissivities, *Review of scientific instruments*: RSI 72 (8), (2001) 3366-3374.

[89] H. L. Lukas, S. G. Fries, B. Sundman, Computational Thermodynamics-The Calphad method, Cambridge University Press, *Cambridge, U. K.,* 2007.

[90] U. R. Kattner, Thermodynamic modeling of multicomponent phase equilibria, *Jom,* Vol. 49 (1997), 14-19.

[91] M. Nassik, F. Z. Chrifi-Alaoui, K. Mahdouk, J. C. Gachon, Calorimetric study of the aluminium-titanium system. *J. Alloys Compd.,* 350(1) (2003) 151-154.

[92] O. Kubaschewski, W. A. Dench, The heats of formation in the systems titanium-aluminium and titanium-iron, *Acta Mater.,* 3(4) (1955) 339-346.

[93] O. Kubaschewski, G. Heymer, Heats of formation of transition-metal aluminides. *J. Chem. Soc. Faraday Tra.*, 56 (1960) 473-478.

[94] H. Okamoto, Al-Ti (Aluminum-Titanium), *J. Phase Equilibria.,* 14 (1993), 120-121.

[95] International Centre for Diffraction Data: JCPDS-ICDD: powder diffraction files. Bd Sets 1-50,70-88. PDF-2. 2000.

[96] G. Ghosh, M. Asta, First-principles calculation of structural energetics of Al-TM (TM= Ti, Zr, Hf) intermetallics. *Acta Mater.*, 53(11) (2005) 3225-3252.

[97] J. Murray, A. Peruzzi, J. P. Abriata, The Al-Zr (aluminum-zirconium) system, *J. Phase Equilibria.*, 13 (3) (1992) 277-291.

[98] R. J. Kematick, H. F. Franzen, Thermodynamic study of the zirconium-aluminum system. *J. Solid State Chem.*, 54(2) (1984) 226-234.

[99] M. Potzschke and K. Schubert, On the construction of some T4-B3 homologous and quasihomologous system. II. The Ti-Al, Zr-Al, Hf-Al, Mo-Al, and some ternary systems. *Z. Metallkd.,* 53 (8) (1962) 548-561.

[100] C. G. Wilson and D. Sams, The crystal structure of Zr2Al, *Acta Crystallogr.*, 14 (1961) 71-72.

[101] C. G. Wilson, D. Sams and T. J. Renouf, The crystal structure of Zr5Al3, *Acta Crystallogr.*, 12 (1959) 947-948.

[102] C. G. Wilson and F.J. Spooner, The crystal structure of Zr5Al2, *Acta Crystallogr.*,13 (1960) 358-359.

[103] F.J. Spooner and C. G. Wilson, The crystal structure of ZrAl, *Acta Crystallogr.*,15 (1962) 621-622.

[104] G. Brauer, The crystal structure of intermetallic alloys of aluminium with titanium, zirconium, thorium, niobium and tantalum, *Naturwissenschaften*, 26 (1938) 710.

[105] M. E. Schlesinger, Thermodynamics of solid transition-metal silicides, *Chem. Rev*., 90(4) (1990) 607-628.

[106] J. C. Hensel, J. M. Vandenberg, F. C. Unterwald, Electrical transport and in situ x-ray studies of the formation of TiSi2 thin films on Si, *Appl. Phys. Lett.,* 51, 1100 (1987).

[107] P. Villars, L. D. Calvert, Pearson's handbook of crystallographic data for intermetallic phases. Metals Park. Vol. 3. American Society for Metals, Metal Park, OH, 1989.

[108] G. K. Batchelor, An introduction to Fluid dynamics, Cambridge University Press, Cambridge, England, 1967.

[109] R. Grieseler, I. S. Au, T. Kups, P. Schaaf, Diffusion in thin bilayer films during rapid thermal annealing, *Phys. Status Solidi A* (2014) 1-10.

[110] Engineering Materials, Materials Home, Element Information of Titanium and Aluminum, http://www.efunda.com/materials/elements/element_list.cfm (accessed 15.04.2015).

[111] K. T. Raic`, R. Rudolf, P. Ternik, Z. Z`unic`, V. Lazic`, D. Stamenkovic`, T. Tanaskovic`, I. Anz'el, CFD analysis of exothermic reactions in Al-Au multi-layered foils, *Mater. Tehnol.,* 45(4) (2011) 335-338.

[112] A.G. Merzhanov, I.P. Borovinskaya, Self-propagating high-temperature synthesis of refractory inorganic compounds, *Dokl. Akad. Nauk SSSR*, 204 (1972) 366.

[113] J. A. Thornton, Influence of apparatus geometry and deposition conditions on the structure and topography of thick sputtered coatings, *J. Vac. Sci. Technol.*, 11(4) (1974) 666-670.

[114] P. B. Barna, M. Adamik, Fundamental structure forming phenomena of polycrystalline films and the structure zone models, *Thin Solid Films*, 317 (1998) 27-33.

[115] J. S. Kim, T. LaGrange, B. W. Reed, R. Knepper, T. P. Weihs, N. D. Browning, G. H. Campbell, Direct characterization of phase transformations and morphologies in moving reaction zones in Al/Ni nanolaminates using dynamic transmission electron microscopy, *Acta Mater.,* 59 (2011) 3571.

[116] D. Van Heerden, A. J. Gavens, S. Jayaraman, T.P. Weihs, Metastable phase formation and microstructural evolution during self-propagating reactions in Al/Ni and Al/Monel multilayers, Mater, *Res. Soc. Symp. Proc., 481* (1998) 533.

[117] Crystallography Open Database, http://www.crystallography.net/cod/search.html (accessed 07.06.2016).

[118] J. C. Gachon, A. S. Rogachev, H. E. Grigoryan, E. V. Illarionova, J. J. Kuntz, On the mechanism of heterogeneous reaction and phase formation in Ti/Al multilayer nanofilms, *Acta Mater.,* 53 (2005) 1225-1231.

[119] C. Michaelsen, K. Barmak, T. P. Weihs, Investigating the thermodynamics and kinetics of thin film reactions by differential scanning calorimetry, *J. Phys. D: Appl. Phys.* 30 (1997) 3167-3186.

[120] E. Illeková, J. C. Gachon, A. Rogachev, H. Grigoryan, J. C. Schuster, A. Nosyrev, P. Tsygankov, Kinetics of intermetallic phase formation in the Ti/Al multilayers, *Thermochim Acta,* 469 (2008) 77-85.

[121] A. S. Rogachev, J. C. Gachon, H. E. Grigoryan, E. Illeková, et. al, Diffraction of synchrotron radiation for in situ study of the heterogeneous reactions mechanisms in lamellar composites, obtained by mechanical activation and magnetron sputtering, *Nucl. Instrum. Methods Phys. Res. Sect*. A 575 (2007) 126-129.

[122] E. Besnoin, S. Cerutti, and O. M. Knio, Effect of reactant and product melting on self-propagating reactions in multilayer foils, *J. Appl. Phys.* 92 (2002) 5474.

[123] A. G. Merzhanov, B. I. Khaikin, Theory of combustion waves in homogeneous media, *Prog. Energy Combust*. *Sci.* 14 (1988) 1-98.

[124] A. S. Rogachev, Exothermic reaction waves in multilayer nanofilms, *Russian Chemical Reviews*, 77 (1) (2008) 21-37.

[125] Ellingham - Diagram, http://web.mit.edu/2.813/www/readings/Ellingham diagrams.pdf (accessed 09.08.2016).

[126] H. Joress, S. C. Barron, K. J. T. Livi, N. Aronhime, T. P. Weihs, Self-sustaining oxidation initiated by rapid formation reactions in multilayer foils, *Appl. Phys. Lett.,* 101 (2012) 111908.

[127] M. Vohra, T.P. Weihs, O. M. Knio, A simplified computational model of the oxidation of Zr/Al multilayers, *Combust. Flame*, 162 (2015) 249-257.

[128] C. Wagner, Reaktionstypen bei der oxydation von legierungen, *Z. Elektrochemie*, 63 (1959) 772.

[129] J. Y. David, High Temperature Oxidation and Corrosion of Metals, Second edition, ISBN: 978-0-08-100101-1.

[130] A. S. Khanna, Introduction to High Temperature Oxidation and Corrosion, 2012. ISBN-0-87170-762-4.

[131] J. C. Trenkle, J. Wang, T. P. Weihs, T. C. Hufnagel, Microstructural study of an oscillatory formation reaction in nanostructured reactive multilayer foils, *Appl. Phys. Lett*, 87 (2005) 153108.

[132] J. P. McDonald, M. A. Rodriguez, E. D. Jones, & D. P. Adams, Rare-earth transition-metal intermetallic compounds produced via self-propagating, high-temperature synthesis, *J. Mater. Res.* 25 (2010) 718-727.

[133] D. Aurongzeb, Pattern evolution due to energetic solid-state diffusion front in nanoscale thin film, *Appl. Phys. Lett.,* 92.14 (2008): 141914.

[134] A. S. Rogachev, F. Baras, Models of SHS: An overview, *International Journal of Self-Propagating High-Temperature Synthesis,* 16.3 (2007) 141-153.

[135] A. G. Mezhanov, The theory of stable homogeneous combustion of condensed substances, *combust. Flame*, 13 (1968) 143-156.

[136] Y. Mishin, Chr. Herzig, Diffusion in the Ti-Al systems, Acta Mater., 48 (2000) 589-623

[137] Y. Mishin, C. Herzig, Grain boundary diffusion: recent progress and future research. *Mater. Sci. Eng. A*, 260(1) (1999) 55-71.

[138] L. G. Harrison, Influence of dislocations on diffusion kinetics in solids with particular reference to the alkali halides, *Trans. Faraday Soc.*, 57:1191 (1961) 47.

[139] A. E. Grigoryan, N. G. Elistratov, D.Y. Kovalev, A. G. Merzhanov, A. N. Nosyrev, Auto wave propagation of exothermic reactions in Ti-Al thin multilayer films, *Doklady Physical Chemistry,* 381 (2001) 283-287.

[140] X. Qiu, R. Liu, S Guo, J. H. Graeter, L. Kecskes, J. Wang, Combustion synthesis reactions in cold-rolled Ni/Al and Ti/Al multilayers, *Metall. Mater. Trans., A* 40 (7) (2009) 1541-1546.

[141] Crystallography Open Database, http://www.crystallography.net/cod/search.html (accessed 17 Dec 2016).

[142] E. Nes, E. Precipitation of the metastable cubic Al3Zr-phase in subperitectic Al-Zr alloys, *Acta Metall., 20*(4) (1972) 499-506.

[143] C. Anghel, Modified oxygen and hydrogen transport in Zr-based oxides. Doctoral Thesis, Royal Institute of Technology KTH (2006).

[144] B. Puchala, A. Van der Ven, Thermodynamics of the Zr-O system from first-principles calculations, *Physical review B* 88 (2013) 094108.

[145] S. Barron, R. Knepper, N. Walker, T. Weihs, Characterization of self-propagating formation reactions in Ni/Zr multilayered foils using reaction heats, velocities, and temperature-time profiles, *J. Appl. Phys.*, 109, (2011) 013519.

[146] The International Centre for Diffraction Data - ICDD, http://www.icdd.com/search.htm, (accessed 15.02.2017).

[147] C. Guo, P. Hu, L. Yu, F. Yuan, Synthesis and characterization of ZrO2 hollow spheres, *Mater Lett.,* 63 (2009) 1013-1015.

[148] Physics and Technology of High-K Materials 8, ECS Transactions, Vol.33, No.3, The Electrochemical society, New Jersey, USA (2010).

[149] A. S. Ramos, A. J. Cavaleiro, M.T. Vieira, J. Morgiel, G. Safran, Thermal stability of nanoscale metallic multilayers, *Thin Solid Films,* 571 (P2) (2014) 268–274.

[150] A. S. Ramos, M. T. Vieira, Intermetallic compound formation in Pd/Al multilayer thin films, *Intermetallics*, 25 (2012) 70-74.

[151] Crystallography Open Database, http://www.crystallography.net/cod/search.html (accessed 07.07.2017).

[152] J. L. Murray, A. J. McAlister, The Al-Si (aluminum-silicon) system, *Bull. Alloy. Phase Diagr.* 5 (1984) 74-84, 89-90.

[153] A. S. Rogachev, S. G. Vadchenko, F. Baras, O. Politano, S. Rouvimov, N. V. Sachkova, A. S. Mukasyan, Combustion in reactive multilayer Ni/Al nanofoils: experiments and molecular dynamic simulation, *Combust. Flame*, 166 (2016) 158-169.

[154] A. C. Lewis, D. Josell, T. P. Weihs, Stability in thin film multilayers and microlaminates: the role of free energy, structure, and orientation at interfaces and grain boundaries, *Scr. Mater.*, 48(8) (2003) 1079-1085.

[155] O. Chaix-Pluchery, B. Chenevier, I. Matko, J. P. Sénateur, F. La Via, Investigations of transient phase formation in Ti/Si thin film reaction, *J. Appl. Phys.*, 96 (2004) 361-368.

List of figures

List of tables

List of abbreviations

RMS	*Reactive Multilayer System*
RMF	*Reactive Multilayer Film*
CALPHAD	*Calculation of Phase Diagrams*
Thermo-Calc	*Software package for thermodynamic calculations*
CFD	*Computational Fluid Dynamics*
FVM	*Finite Volume Methodology*
PVD	*Physical Vapor Deposition*
MSIP	*Magnetron Sputter Ion Plating*
ALD	*Atomic Layer Deposition*
mln	*Milliliter normal per minute*
Pa	*Pascal*
kW	*Kilo watt*
SEM	*Scanning Electron Microscope*
TEM	*Transmission Electron Microscope*
AFM	*Atomic Force Microscope*
EDX, EDS	*Energy Dispersive Spectrometer*
FIB	*Focused Ion Beam*
DSC	*Differential Scanning Calorimetry*
XRD	*X-ray powder diffraction*

List of symbols

T	*Temperature*
T_0	*Room temperature*
T_{max}	*Maximum reaction temperature*
T_{st}	*Max. reaction temperature for a steady propagation*
T_{un}	*Max. reaction temperature for an unsteady propagation*
T_{mp}	*Melting temperature of nanomaterial*
T_{mb}	*Melting temperature of bulk material*
N	*No. of surface atom*
n	*No. of total atoms*
a	*Atom diameter*
h	*Film thickness*
C, X	*Composition*
D	*Coefficient of atomic diffusion*
t	*Time*
Q	*Total heat*
dQ/dt	*Heat generation rate*
C_p	*Specific heat capacity*
ρ	*Density*
λ	*Thermal diffusion coefficient / Thermal diffusivity*
E_a	*Activation energy for atomic diffusion*
R	*Gas constant*
v	*Reaction front velocity*
υ_{un}	*Reaction velocity for unsteady propagation*
w	*Thickness of premixed zone*
d	*Bilayer or periodic thickness*

d_1, d_2	*Dual bilayer spacing*
l	*Total film thickness*
δ	*1/4 of the bilayer thickness*
A, D_0	*Arrhenius pre-factor*
K_n	*Fourier eigenvalues*
α_n	*Fourier coefficient*
K	*Energy release rate constant*
n	*Fitting parameter*
ΔH	*Enthalpy of formation/ heat of formation / reaction heat*
ΔH_{rxn}	*Exothermic reaction heat considering premixed layer*
ΔH_{form}	*Heat of formation without premixed layer*
V	*Atomic molar ratio of reaction and premixed products*
ΔHo	*Reaction heat at adiabatic condition*
T_{fo}	*Maximum adiabatic temperature*
T_{ig}	*Ignition temperature*
m	*Atomic fraction of one of the reactants*
f	*Fractional concentration of product*
g	*Geometrical term*
G	*Gibbs energy*
G_i^{φ}	*Gibbs energy of phase i*
P	*Pressure*
T_c	*Curie temperature*
J	*Diffusion flux*
β_0	*Average magnetic moment per atom*
C_{Ti}	*Concentration of Titanium*
ε	*Emissivity*
σ	*Stephan-Boltzmann constant*

A_f	*Foil exposed area*
d_w	*Width of rectangular columnar grain*
d_g	*Width of grain boundary, columnar gap*
D_l	*Atomic or lattice diffusion coefficient*
D_g	*Grain boundary diffusion coefficient*
J_l	*Atomic diffusion flux*
J_g	*Grain boundary diffusion flux*
f	*Fraction of the grain boundary area*
D_{eff}	*Effective diffusion coefficient*
at.%	*Atom percent*

List of own publications in reviewed international journals

[1] Sen S., Lake M., Schaaf P.: Optimization of self-propagating reaction properties through Al-molar ratios in ternary Titanium-Silicon-Aluminum reactive multilayer films, *Vacuum,* 156 (2018) 205-211.

[2] Sen S., Lake M., Schaaf P.: Experimental investigation of high temperature oxidation during self-propagating reaction in Zr/Al reactive multilayer films, *Surf. Coat. Technol.,* 340 (2018) 66-73.

[3] Sen S., Lake M., Schaaf P.: Al-based binary reactive multilayer films: large area freestanding film synthesis and self-propagating reaction analysis, *Appl. Surf. Sci.,* 2018 (in press)

[4] Sen S., Lake M., Grieseler R., Schaaf P.: Effects of multilayer arrangements in ternary reactive films on self-propagating reaction, *Surf. Coat. Technol.,* 327 (2017) 25-31.

[5] Sen. S., Lake M., Kroppen N., Farber P., Wilden J., Schaaf P.: Self-propagating exothermic reaction analysis in Ti/Al reactive films using experiments and computational fluid dynamics simulation, *Appl. Surf. Sci.,* 396 (2017) 1490-1498.

[6] Sen S., Lake M., Wilden J., Schaaf P.: Synthesis and characterization of Ti-Al reactive multilayer films with various molar ratios, *Thin Solid Films*, 631 (2017) 99-105.

[7] Sen S., Babaei M., Lake M., Schaaf P.: Characterization of self-propagating exothermic reaction in bimetallic Zr/Al reactive multilayer nanofoil. In*: Symposium für Smarte Strukturen und Systeme.* De Gruyter Verlag., DOI 10.1515/9783110467130-028, pp. 305-314, April 2016.

[8] Sen S., Langels G., Lake M., Schaaf P.: Effects of melting layers on nanobonding using reactive multilayer nanofoil. In: *Euro Hybrid Materials and Structures- Conference proceedings*. ISBN 978-3-88355-414-3, pp. 257-261, April 2016

[9] Sen S. R., Durst K., Göken M.: Nanoindentation as a tool for strain measurements in TiAl alloys experiments and Finite Element Modeling, In: *Elitenetzwerk Bayern Forschungsbericht (scientific research report)*, Germany, September 2009.

[10] Rahman M. J., Sen S. R., Moniruzzaman M.: Morphology and properties of electrodeposited Zn-Ni alloy coatings on mild steel. *Journal of Mechanical Engineering*, vol. 40, No. 1, pp.1-6, 2009.

Conferences

[1] Sen S., Lake M., Schaaf P.: Al-based binary reactive multilayer films: large area freestanding film synthesis and self-propagating reaction analysis, *AEM 2017 conference series on energy materials*, oral presentation, England, 11-13 September 2017.

[2] Sen S., Lake M., Grieseler R., Schaaf P.: A comparative study of Al based reactive multilayer nanofoil as energetic material for storing chemical energy. *Materials Science and Engineering Congress (MSE)*, poster, Darmstadt, September 2016.

[3] Sen S., Langels G., Lake M., Schaaf P.: Effects of melting layers on nanobonding using reactive multilayer nanofoil. *Euro Hybrid Materials and Structures Congress*-poster, Kaiserslautern, April 2016.

[4] Sen S., Babaei M., Lake M., Schaaf P.: Characterization of self-propagating exothermic reaction in bimetallic Zr/Al reactive multilayer nanofoil. *Symposium für Smarte Strukturen und Systeme*, poster, Darmstadt, April 2016.

[5] Sen S. R., Scherm F., Bezold J., Glatzel U.: Hybrid Al / Mg alloy joints with Zn-Al fillers. *FEMS-Junior Euromat Conference*, oral presentation and poster, no. 310, Switzerland, July 2012.

[6] Sen S., Armstrong. P.: Investigation of the Hertzian contact theory and adhesion forces for the spherical Si particles with molecular dynamics simulation and AFM experiment. *3rd International conference on Structure, Processing and Properties of Materials, proceeding*. Bangladesh, pp.116, February 2010.

Scientific presentations

[1] Chairing a session at a scientific conference '*AEM2017 conference series on energy materials'*, Guildford, England, 2017.

[2] Attending '*12. Aachener Tagung Wassertechnologie'* conference, Aachen, 2017.

[3] Oral and poster presentation 'Nanoskalige reaktive Multilagen-schichten: Herstellung und Charakterisierung' *Promotionskolleg*, Krefeld, Germany, 2015.

[4] Oral presentation 'Atomic site location by channeling enhanced microanalysis (ALCHEMI/TEM) in Ni-basis model super alloys', *Graduiertenkolleg 1229 seminar of stable and metastable multi-phase systems for elevated service temperatures*, DFG Research Training Group - 1229, Pommersfelden, Germany, 2011.

[5] Oral presentation 'Long range interaction in Molecular dynamics simulation', *Bavarian Grade School of Computational Engineering*, Algorithms of Computational Science and Engineering, Ferienakademie, Sarntal/Südtirol, Italy, 2009.

[6] Oral presentation 'Hertzian contact theory of Si particles and wafer with molecular dynamics simulation and AFM experiment', Doktorandenkolleg '*Structure, Reactivity and Properties of Oxide Materials*', Thurnau - Frankish Schweiz, Germany, 2009.

[7] Attending '*11. Jülicher Werkstoffsymposium for Processes and Materials for tomorrow's Thermal Barrier Coatings*', Jülich, Germany, 2009.

[8] Oral presentation 'Nanoindentation and FEM simulation for strain measurements in TiAl alloys', '*Advanced Materials Science (AMS)*', Kleinwalsertal, Austria, 2009.

Patent registration

[1] Sen S., Lake M., Schaaf P.: Methods of optimizing self-propagating reaction via distinct reaction interfaces in multicomponent reactive materials systems, PROvendis Deutschland, Patentanmeldung No. 5417 18 RMS-REAC-Interface, 07.06.2018.

[2] Sen S., Lake M.: Zr/Al, Ti/Al reactive multilayer particles for medical applications, PROvendis Deutschland, Patentanmeldung No. 447215, 01.07.2015.

[3] Sen S., Lake M.: Efficient freestanding PVD foil Production, PROvendis Deutschland, Patentanmeldung No. 435115, 10.02.2015.

Lectureship and teaching

[1] Lecture on '*Corrosion and corrosion protection'*, conducting practical class on '*Coating technology*', Department of Mechanical and Process Engineering, Niederrhein university of Applied Science, Germany, 2013-2017.

[2] Conducting practical class on '*Forming and shaping processes*', Department of Metals and Alloys, Bayreuth University, Germany, 2010-2012.